BEDFORM MIGRATION IN RIVERS

by

Chan-Yi Martin Lin
B.Sc., University of Victoria, 2006

THESIS SUBMITTED IN PARTIAL FULFILLMENT OF
THE REQUIREMENTS FOR THE DEGREE OF

MASTER OF SCIENCE

In the
Department of Geography
Faculty of Environment

SIMON FRASER UNIVERSITY

Summer 2011

APPROVAL

Name: **Chan-Yi Martin Lin**

Degree: **Master of Science**

Title of Thesis: **Bedform migration in rivers**

Examining Committee:

Chair: **Dr. Owen Hertzman**
Senior Lecturer
Department of Geography
Simon Fraser University

Dr. Jeremy Venditti
Senior Supervisor
Assistant Professor
Department of Geography
Simon Fraser University

Dr. Edward Hickin
Committee Member
Professor Emeritus
Department of Geography
Simon Fraser University

Dr. Michael Church
External Examiner
Professor Emeritus
Department of Geography
University of British Columbia

Date Defended/Approved: June 30th, 2011

ABSTRACT

Bedform migration rate is important for estimating sediment transport in rivers. Migration rate is difficult to estimate because current theoretical approaches have limited practical use and empirical relations between migration rate and various flow parameters are not well defined. I examine field and flume data that contain information on migration rate and other flow and sediment parameters. I demonstrate an empirical relation between bedform migration rate and transport stage defined by the Shields number. I also report an investigation of the mechanisms of bedform migration in a laboratory experiment in which bed and water-surface topography data were collected under controlled conditions at different transport stages. The experiment shows migration is dominated by translation under bedload-dominated conditions, but bedform shape deformation increases with transport stage, which leads to greater variability in migration rate and bedform geometry. In addition, migration rate is conditioned by suspended-sediment transport mechanisms.

Keywords: bedform; river; migration; transport stage; bedload; suspension

To my Parents

To Venerable Ajahn Brahmavamso Mahathera

ACKNOWLEDGEMENTS

I would like to thank my senior supervisor, Dr. Jeremy Venditti, who helped me tremendously. Your time and effort were very much appreciated. I would also like to thank Dr. Edward Hickin for being my on supervisory committee and all his helpful comments and suggestions. Dr. Michael Church offered many insightful critiques and recommendations.

I would like to thank Robert Humphries and Natalia Domarad for helping at my experiment and providing intellectual support. I would also like to thank Moslem Kazemi for sharing his knowledge on programming and Dr. Brandon McElroy for providing MATLAB® codes for my data analysis. Lastly, I would like to thank Dr. Tracy Brennand for providing access to the Sedimentary Analysis Laboratory and Dr. Owen Hertzman for many insightful recommendations.

I would like to thank all the faculty, staff and fellow students in the Department of Geography. I would especially like to thank, Megan Hendarshot, Elizabeth Baird, Liliana Hill, Marion Walter, Jessica Nelson, Joyce Chen, Chris Au-Yeung, B-Jae Kelly, John Ng, and Justin Song, for their support.

TABLE OF CONTENTS

LIST OF FIGURES

LIST OF TABLES

LIST OF NOTATIONS

A	Amplitude of a waveform
a	Regression analysis intercept
C	Suspended-sediment concentration at z
$\overline{C}$	Depth-averaged suspended-sediment concentration
C_α	Suspended-sediment concentration at α
d	Flow depth
d_{bl}	Thickness of bedload layer
D	Sediment grain size
D_{50}	Median sediment grain size
$\overline{D}_{10}$	Mean sediment grain size under 10°C-water
$\overline{D}_{20}$	Mean sediment grain size under 20°C-water
Fr	Froude number
g	Gravitational acceleration
H	Bedform height
H_c	Characteristic bedform height
L	Bedform length
L_c	Characteristic bedform length
L_{sat}	Saturation bedform length
H/L	Bedform aspect ratio

m	Regression analysis slope
n	Number of data population
P	Porosity of sand
Q	Discharge of water
q_s	Total sediment flux per unit width
q_{sb}	Bedload transport per unit width
q_{ss}	Suspended load transport per unit width
q_{st}	Translation load per unit width
R^2	Coefficient of determination
R_{sat}	Saturation bedform height
Re^*	Grain Reynolds number
S	Slope of the water surface
U	Downstream velocity
$\overline{U}$	Mean downstream velocity
U_0	Non-eroding mean velocity
$\overline{U}_{10}$	Mean flow velocity under 10°C-water
$\overline{U}_{20}$	Mean flow velocity under 20°C-water
u^*	Shear velocity
V_b	Bedform migration rate
W	Bed roughness
w	Width of flume channel
w_s	Grain settling velocity

X	Coordinate in stream-wise direction
Y	Coordinate in cross-stream direction
Z	Coordinate in vertical direction
z	Height above the sediment bed
z_b	Thickness of bedload layer
α	Distance from the bed of the reference concentration
β	Coefficient that describes the difference in diffusion between a sediment particle and a fluid particle
β_s	Bedform shape factor
η	Bed elevation
κ	Von Karman constant
μ_{10}	Molecular viscosity of water at 10°C
μ_{20}	Molecular viscosity of water at 20°C
ν	Kinematic viscosity of water
ξ	Relative depth
ρ	Water densities
ρ_s	Sediment densities
τ	Boundary shear stress
τ_c	Critical boundary shear stree
τ^*	Shields number
τ^*_c	Critical Shields number
ω	Angular frequency of a waveform

1: CHAPTER 1

1.1 Introduction

Bedforms are geometric elements, such as ripples or dunes, formed on sediment beds as a result of interaction of the bed with the overlying fluid flow. They are important to sedimentary geologists because they are common sedimentary structures found in stratigraphy and are thus widely used for interpreting paleo-flow conditions [*Bridge*, 2003]. Their length and height, which are important for calculating flow resistance [*Bridge*, 2003], can be empirically predicted from flow parameters [*Yalin,* 1972*; Yalin and Karahan,* 1979*; Allen,* 1982; *Bridge*, 2003]. Migration rate is important for estimating bed-material load [*Simons et al.*, 1965; *Bridge*, 2003; *Church*, 2006; *Nittrouer et al.*, 2008], but empirical relations between migration rate and flow are not well defined. This is because migration is heavily conditioned by the dominant sediment transport mechanism (traction, saltation, suspension). Here, I investigate the relations between bedform migration and transport mechanisms.

1.2 Background

1.2.1 Bedforms in river channels

Many types of bedforms are observed in river channels. Figure 1-1 shows bedform morphology developed under unidirectional flow over a sand bed [*Simons and Richardson*, 1966]. Ripples (Figure 1-1A) form when flow velocity is 10-20% larger than the critical velocity for initiation of motion [*Van Rijn*, 1993], and as flow velocity increases, dunes (Figure 1-1B) start to form. As flow velocity continues to increase, dunes increase in size (Figure 1-1C) and are eventually washed away (Figure 1-1D-F). At even higher flow velocity, antidunes, which are sandwaves that can migrate upstream, (Figure 1-1F-G) and chute-and-pools (Figure 1-1H) develop [*Simons and Richardson*, 1966].

Bedforms can be classified into lower flow regime and upper flow regime based on the Froude number (Fr)

$$\mathrm{Fr} = \frac{\mathrm{U}}{[\mathrm{gd}]^{0.5}} \tag{1-1}$$

where U is downstream velocity, g is acceleration due to gravity and d is flow depth. Ripples and dunes (Figure 1-1 A-D) are classified as lower flow regime bedforms for which the Froude number is less than 1. Plane bed, antidunes and chute-and-pools (Figure 1-1 E-H) are upper flow regime bedforms for which the Froude number is greater than 1 [*Bridge*, 2003].

When the bedform crest is perpendicular to the main flow direction, it is called a transverse bedform, such as a ripple, dune or anti-dune; when the bedform crest is parallel to the flow, it is called longitudinal bedform, such as

sand ribbon [*Van Rijn*, 1993]. Many researchers have attempted to explain the types of bedform generated under given flow conditions and to classify bedforms using various criteria [*Allen*, 1982; *Simons and Richardson*, 1966; *Southard and Boguchwal*, 1990; *Van Rijn*, 1993; *Venditti et al.*, 2005b]. Ripples and dunes are the most common bedforms in nature and are the most studied. Here, I focus on lower regime, transverse bedform geometry and its relation to transport stage.

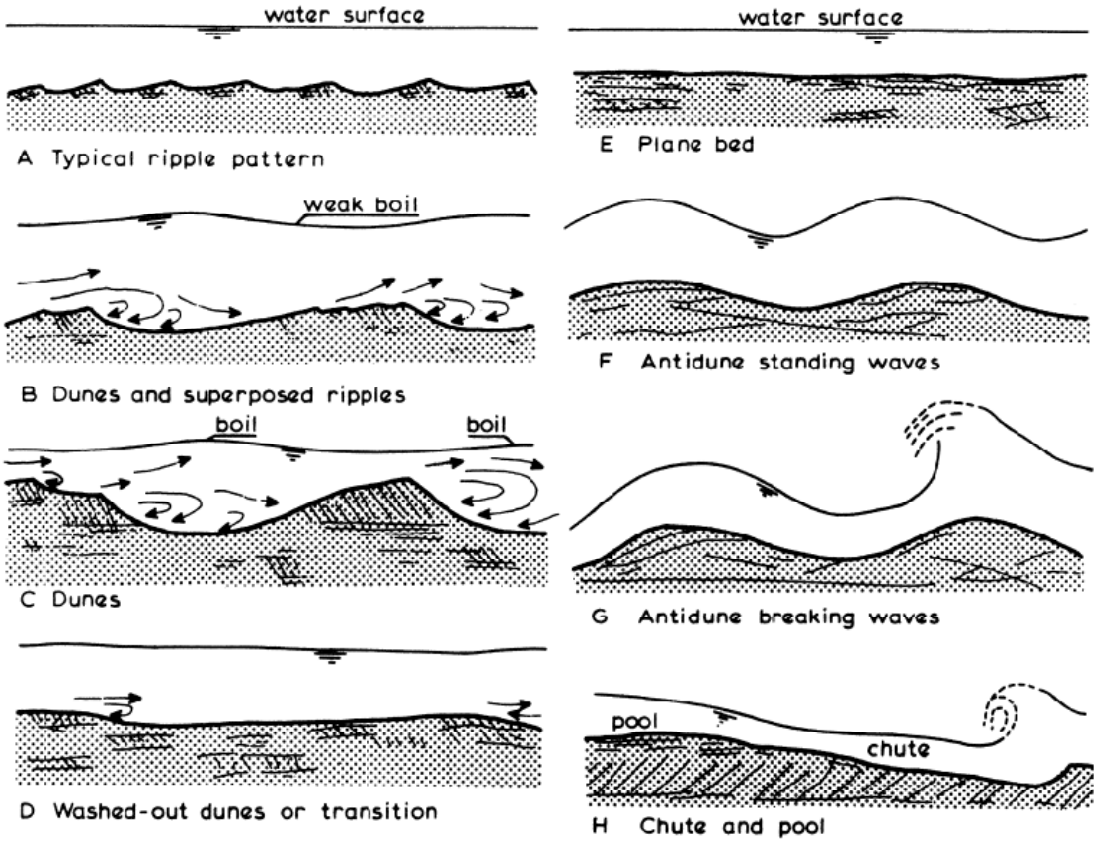

Figure 1-1. Bedform types under increasing Froude number (A to H) [Van Rijn, 1993; adopted from *Simons and Richardson*, 1966].

1.2.2 Bedform geometry and relation to transport stage

Bedform height (H) is defined as the vertical distance from the crest to the trough of a bedform (Figure 1-2); bedform length (L) is the horizontal distance between the trough of a bedform to the trough of the adjacent bedform [*Simons et al.*, 1965; *Stein*, 1965]. Bedforms are often highly asymmetrical with an upstream (stoss) slope averaging 2° to 6° and a downstream (lee) slope near the angle of repose (approximately 30°) [*McLean*, 1990]. A simple empirical relation, proposed by *Flemming* [1988] on the basis of several thousand laboratory and field measurements, relates bedform height and length

$$H = 0.0677\ L^{0.81} \qquad (1\text{-}2)$$

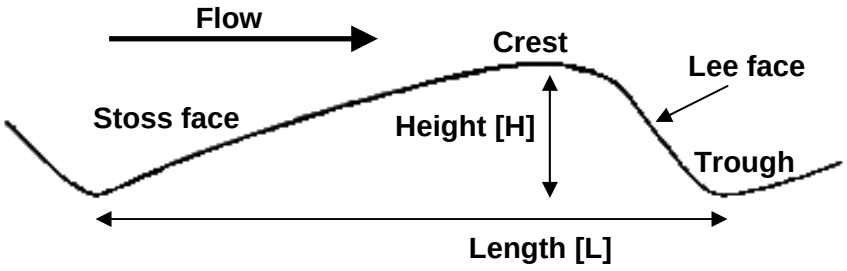

Figure 1-2. Bedform dimensions.

Bedform geometry is shown to be influenced by transport stage [*Simons and Richardson*, 1966; *Guy et al.*, 1966; *Van Rijn*, 1993]. Geometry may also be influenced by flow depth. Bedform height typically scales as H = d/6 and length scales as L = 5d [*Alle*n, 1982]. In addition, bedform geometry is also influenced by sediment concentration in flow [*Simons et al.*, 1963; *Wan*, 1982], suggesting bedform geometry is dependent on how sediment is transported by flow [*Kostaschuk and Villard*, 1996; *Best*, 2005].

Sediment transport mechanisms are often classified as suspended load or bedload. Suspended sediment is supported in the water column and may travel a long way before being deposited. Bedload progresses downstream by rolling, sliding or bouncing over the channel bed, and often only travels a short distance in one movement [*Ritter et al.*, 2002]. Saltation is a third type of sediment transport in which a particle is launched into the water column and returns relatively quickly to the bed in a ballistic trajectory. This mode of transport mechanism is rarely discussed because it is difficult to separate from sediment transported as suspended or bedload in practice [*Church*, 2006]. The relative importance of certain transport mechanisms in a flow can be classified as bedload-dominated transport stage, suspension-dominated transport stage and mixed transport stage, in which both bedload and suspended load are important contributors to the total flux.

Dade and Friend [1998] use the ratio of grain settling velocity (w_s) over shear velocity (u*) and its relation to the fraction of total load travelling as bedload (Figure 1-3) to define different transport stages. The relation varies with relative depth $\xi = d/z_b$, in which d is flow depth and z_b is the thickness of bedload layer. They define $w_s/u^* \geq 3$ for predominantly bedload transport, $0.3 < w_s/u^* < 3$ for predominantly mixed-load transport, and $w_s/u^* \leq 0.3$ for predominantly suspended-load transport. Bedload-dominated transport stage occurs when more than 80-90% of the total sediment load is bedload and suspension-dominated transport stage occurs when less than 10-20% of the total sediment load is bedload [*Dade and Friend*, 1998].

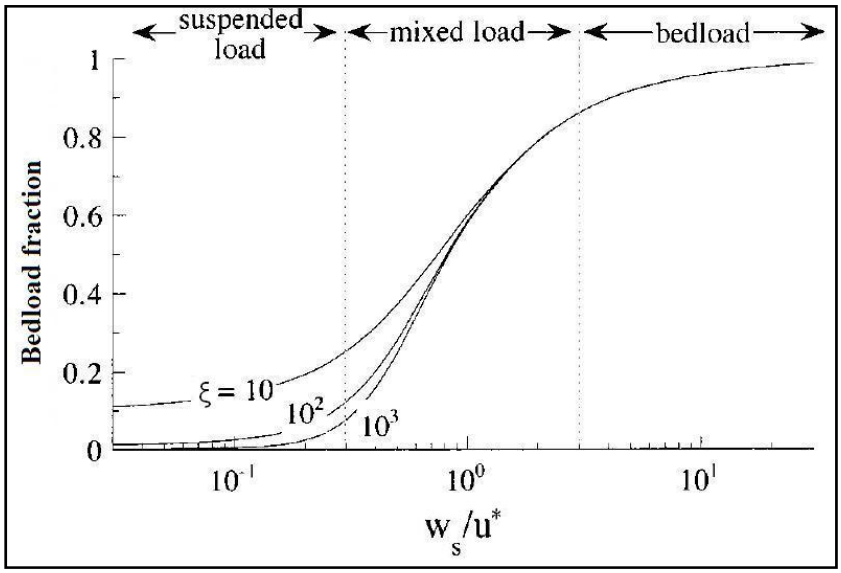

Figure 1-3. Fraction of total load travelling as bedload as a function to w_s/u^* and relative depth [*Dade and Friend*, 1998].

Different transport stages can also be also defined by the Shields number [*Church*, 2006], which is a dimensionless measure of the shear stress exerted by the flow on the bed [*Shields*, 1936] and is calculated as

$$\tau^* = \frac{\rho g d S}{g(\rho_s - \rho)D} \tag{1-3}$$

where ρ and ρ_s are fluid and sediment densities, respectively; g is the acceleration due to gravity, S is the slope of the water surface, and D is the grain size of the sediment, which is usually taken to be D_{50} [*Raudkivi*, 1967]. When τ^* is plotted versus grain Reynolds number (Re*)(Figure 1-4), different transport stages can be distinguished. Grain Reynolds number is defined as

$$Re^* = \frac{u^* D}{\nu} \tag{1-4}$$

where ν is kinematic viscosity of water. For 500μm sand in 10°C water, the grain Reynolds number is approximately 100. Suspended load, mixed load and bedload are characterized by $1 < \tau^*$, $0.1 < \tau^* < 1$, and $0.01 < \tau^* < 0.1$, respectively. *Dade and Friend* [1998] define the transport stage in terms of the total sediment load, so flow with large wash load may inflate the suspended fraction [*Church*, 2006]. Variables used to calculate the Shields number are generally easier to obtain than for the *Dade and Friend* [1998] criteria. Thus, I use the Shields number to define the transport stage throughout this work.

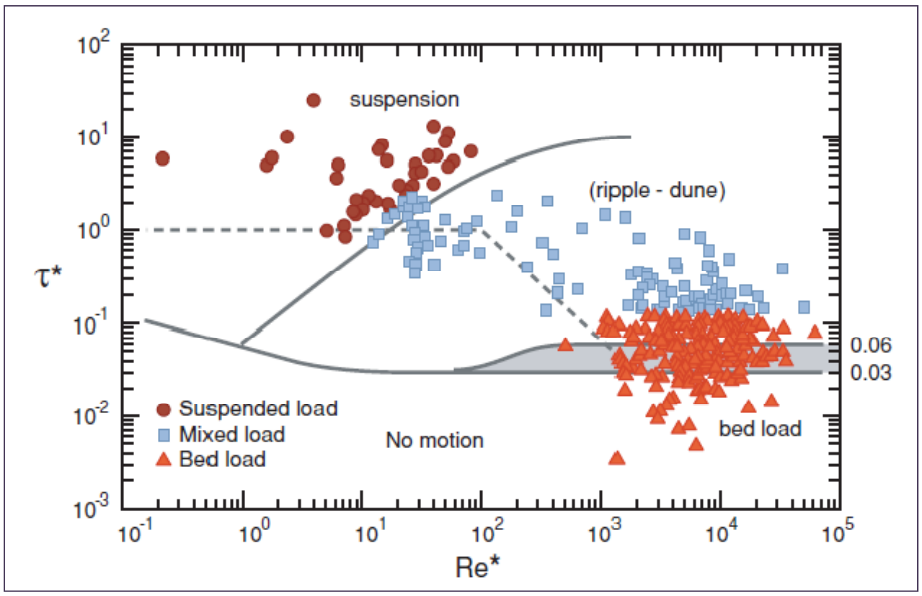

Figure 1-4. The Shields diagram with data for bedload, mixed load, and suspended load dominance superimposed [*Church*, 2006].

The Shields number can be used to predict bedform geometry. The aspect ratio of bedforms (H/L) is shown (Figure 1-5) to be dependent on the

Shields number (τ^*) over the critical Shields number (τ_c^*) [*Yalin*, 1972], which is the threshold of sediment entrainment. The aspect ratio for ripples is represented by the crescent shape. The aspect ratio for dunes is represented by the arc. To maintain continuity with *Church* [2006], I use the dimensionless version of the Shields number ratio, which is equivalent to the ratio of the dimensional variables.

When $\tau^*/\tau_c^* = 1$, shear stress equals the critical shear stress for entrainment and bedforms start to develop. At this stage, suspended load is minimal, bedforms are small and bedload dominates sediment transport. The bedload-dominated transport stage occurs when $0.01 < \tau^* < 0.1$ (Figure 1-4), and with $\tau_c^* = 0.03$, bedload in Figure 1-5 can be defined as $1 < \tau^*/\tau_c^* < 3.3$. As shear stress increases, more sediment is entrained, and bedforms become taller relative to their length. Eventually bedload and suspended load become equal contributors to the sediment flux and both ripples and dunes reach their maximum height relative to length (Figure 1-5). Mixed transport stage occurs when $0.1 < \tau^* < 1$ (Figure 1-4) or $3.3 < \tau^*/\tau_c^* < 33$ (Figure 1-5)(assuming $\tau_c^* = 0.03$). As shear stress increases further, more sediment is entrained into the flow and suspended load dominates the sediment transport. Suspension-dominated transport stage occurs when $\tau^* > 1$ (Figure 1-4) or $\tau^*/\tau_c^* > 33$ (Figure 1-5) (assuming $\tau_c^* = 0.03$).

Ripples reach their maximum height at a lower transport stage than dunes. They are washed out or turn into dunes at a higher transport stage and do not

exist at the suspension-dominated transport stage [*Bridge*, 2003]. Dunes reach their maximum height at the mixed transport stage and start to decrease at the suspension- dominated transport stage. The maximum aspect ratio for ripples is 0.2, which is greater than the maximum aspect ratio for dunes, which is 0.06. Ripples are completely washed out at $\tau^*/\tau_c^* = 14$ whereas dunes are completely washed out at $\tau^*/\tau_c^* = 65$.

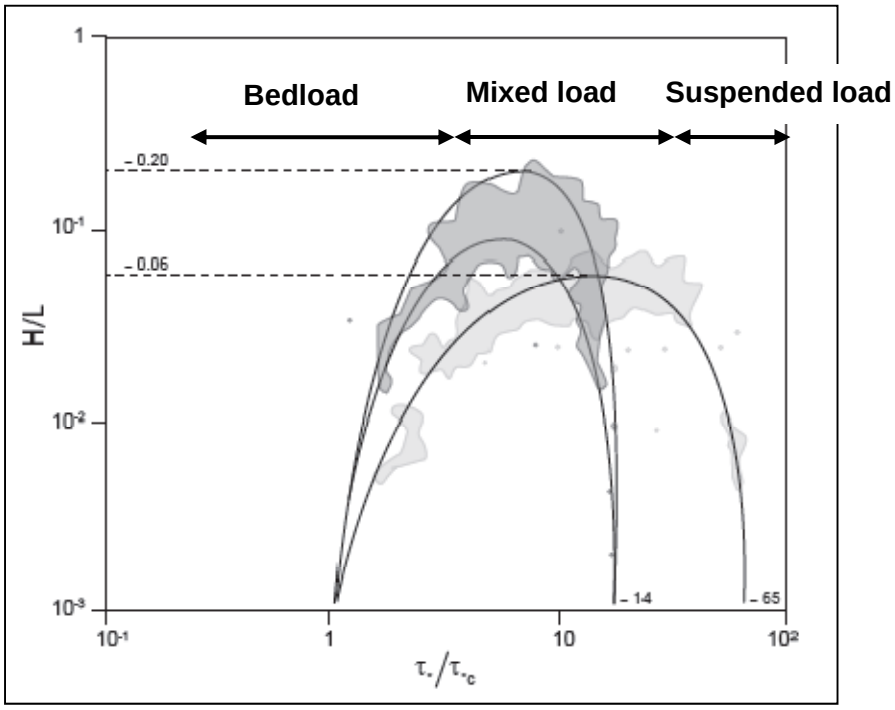

Figure 1-5. The aspect ratio of equilibrium ripples and dunes versus the ratio of Shields number over critical Shields number [*Venditti*, in press; adapted from *Yalin*, 1972]. The dark and light shaded areas represent the data clouds for ripples and dunes presented in *Yalin* [1972].

1.2.3 Bedform migration and relation to transport stage

While we can predict bedform height and length from measures of transport stage there are not comparable relations that link migration rate and flow. *Simons et al.* [1965] present a bedload transport equation to calculate bedload sediment flux, assumed to be the total sediment flux per unit width (q_s), from average bedform migration rate (V_b) as

$$q_s = (1 - p)V_b \left(\frac{H}{2}\right) + K \tag{1-5}$$

where P is the porosity of the sand bed, and K is the part of load that does not contribute to the propagation of dunes or ripples. *Simons et al.* [1965] used the equation to calculate sediment flux using 101 flume experiments and found the calculated values agreed well with observations for coarser sand, but underestimated total load for finer sand (Figure 1-6). The model also failed at higher flows where the bed is in transition to a plane bed.

Simons et al. [1965] also attempt to calculate bedform migration rate from measured flow parameters using empirical equations by *Znamenskaya* [1962]

$$V_b = \frac{K_1 [\bar{U} - U_0]d}{H} \tag{1-6}$$

and *Barekyan* [1962]

$$V_b = \frac{K_2 \overline{U^3}}{gd} \tag{1-7}$$

where d is flow depth, $\bar{U}$ is mean flow velocity, U_0 is noneroding mean velocity, K_1 and K_2 are constants. Solid lines in Figure 1-7 and Figure 1-8 are the migration rate calculated from equation 1-6 and 1-7, respectively. Equation 1-6

shows poor agreement with laboratory data obtained by *Simons et al.* [1965]. Equation 1-7 shows good agreement with laboratory data, but overestimates ripple migration for medium and fine sand. The results suggest that the bedform migration rate is difficult to be predict strictly from flow variables. This highlights a need for investigations of bedform kinematics.

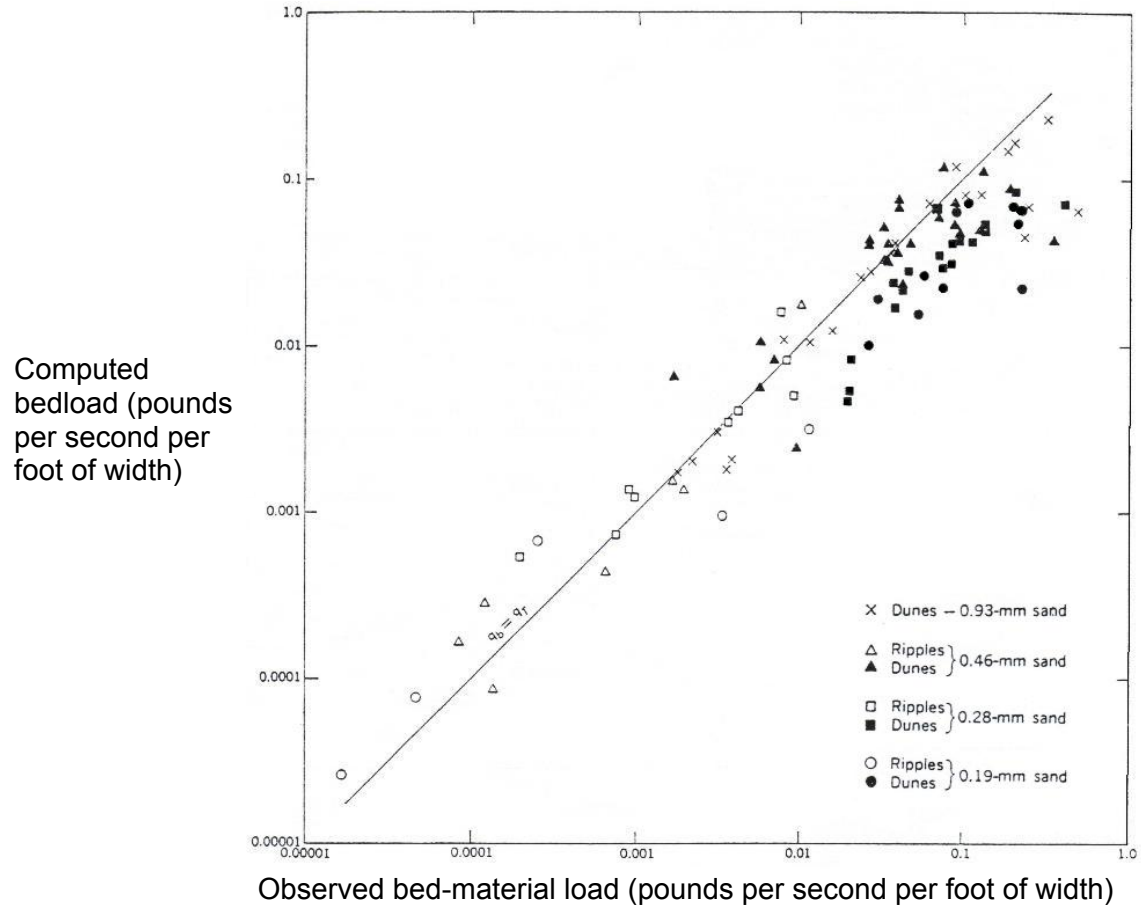

Figure 1-6. Comparison between computed bedload and observed bed-material load [*Simons et al.*, 1965].

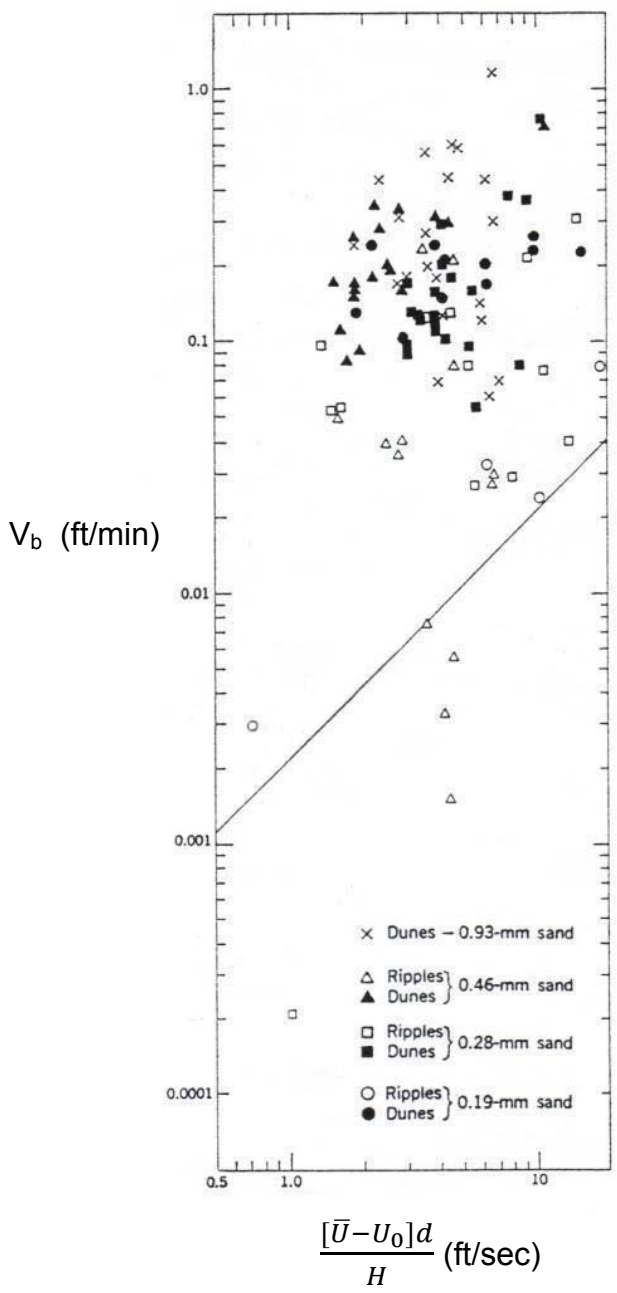

Figure 1-7. Migration rate derived from equation 1-6 compared to laboratory data [*Simons et al.*, 1965].

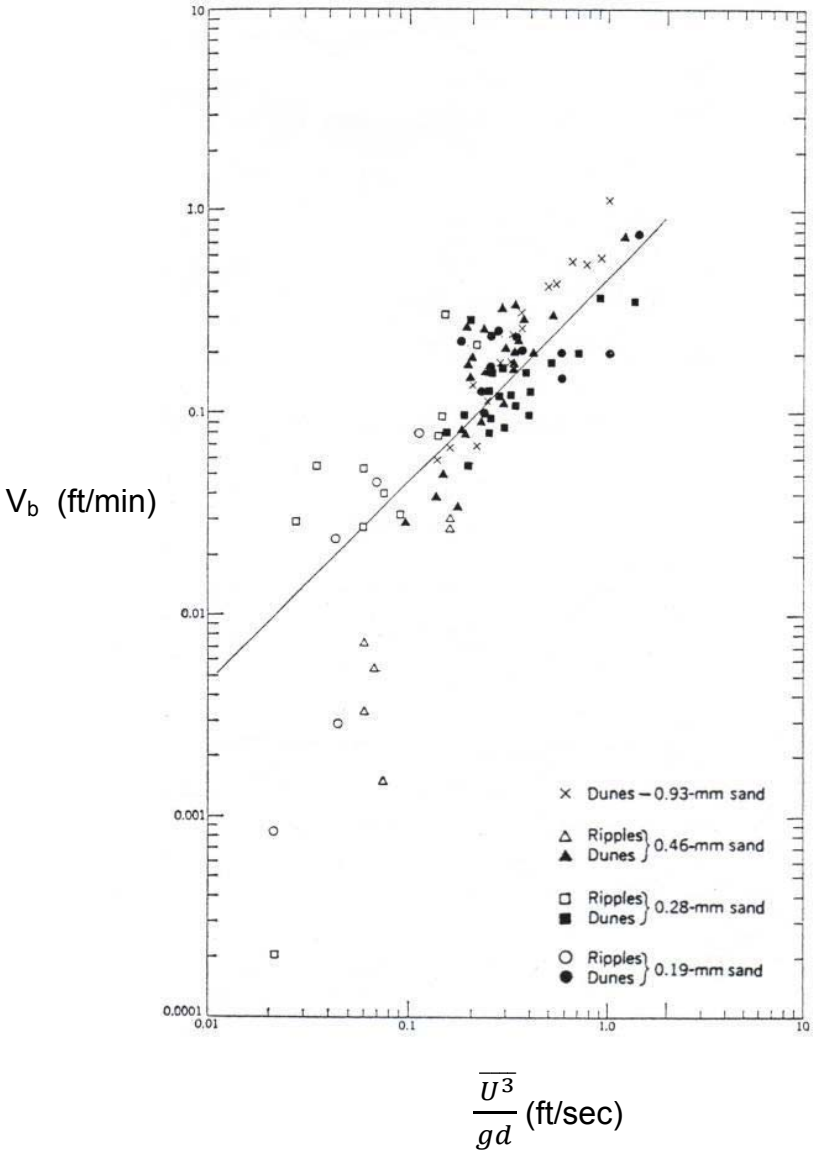

V_b (ft/min)

$\frac{\overline{U^3}}{gd}$ (ft/sec)

Figure 1-8. Migration rate derived from equation 1-7 compared to laboratory data [*Simons et al.*, 1965].

1.2.4 Bedform kinematics

Since the bedform migration rate cannot be predicted strictly from flow variables, studying the mechanisms of bedform movement would improve our understanding of what controls bedform migration rate. Bedforms move downstream by erosion at the upstream face (stoss side) and deposition at the downstream face (lee side)(Figure 1-9)[*Van Rijn*, 1993]. The length and height of an individual dune in a bed may increase or decrease in space and time as it moves downstream under steady and uniform flow conditions [*Allen*, 1973; *Gabel*, 1993; *Bridge*, 2003; *Jerolmack and Mohrig*, 2005ab; *Leclair,* 2002*; Venditti et al.*, 2005a]. In addition, a population of bedforms can change by constant creation and destruction of individual bedforms [*Gabel*, 1993]. The most common mechanisms that change bedform geometry are overtaking (combining), splitting, trough-scouring [*Coleman and Melville*, 1994; *Gabel*, 2003; *Leclair*, 2002; *Bridge*, 2003] and spontaneous formation of new dunes [*Venditti et al.*, 2005b].

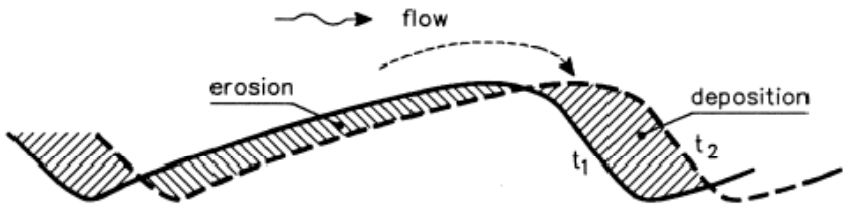

Figure 1-9. Bedform migration in lower regime [*Van Rijn*, 1993].

Increase in the height of individual dunes is commonly accomplished by trough scouring and/or by a fast upstream bedform overtaking and adding to the height of a downstream bedform [*Allen*, 1973; *Leclair*, 2002]. The length of the downstream bedform decreases as it is being overtaken, and the length of the combined bedform increases. The speed of the combined dune normally decreases as its height increases [*Allen*, 1973; *Coleman and Melville*, 1994], if sediment transport rate is constant in space and time [*Bridge*, 2003].

A bedform decreases in height as it splits into two or more smaller bedforms. Bedforms that superimpose or spontaneously form on the back of a dune are smaller than the host [*Venditti et al.*, 2005b]. The small-scale superimposing bedforms move faster than the large bedform and the addition of new bedforms decreases the length of the host bedform [*Bridge*, 2003]. On the other hand, a bedform being overtaken by an upstream bedform may decrease in height or be destroyed when trapped in the flow separation zone of the upstream bedform [*Gabel*, 2003].

Growth and diminution of an individual bedform is also commonly observed without interaction with other bedforms. *Smith* [1970] proposed that when the shear stress is maximum at a bedform crest and minimum over bedform trough, sediment flux follows the same pattern. In this case, erosion occurs on the stoss side and deposition occurs on the lee side resulting in bedform migration downstream without growth and decay (Figure 1-10a) [*McLean*, 1990]. When maximum shear stress shifts upstream of the crest, maximum sediment flux also occurs upstream of the crest resulting in deposition

on the crest and hence growth of the bedform (Figure 1-10b). On the other hand, when maximum shear stress shifts downstream of the crest, maximum sediment flux also occurs downstream of the crest resulting in erosion of the crest and hence destruction of the bedform (Figure 1-10c) [*Smith*, 1970; *McLean and Smith*, 1986; *McLean, 1990*; *Jerolmack and Mohrig*, 2005ab]. These shifts in the maximum shear stress and changes in bedform morphology can be linked to changes in transport stage.

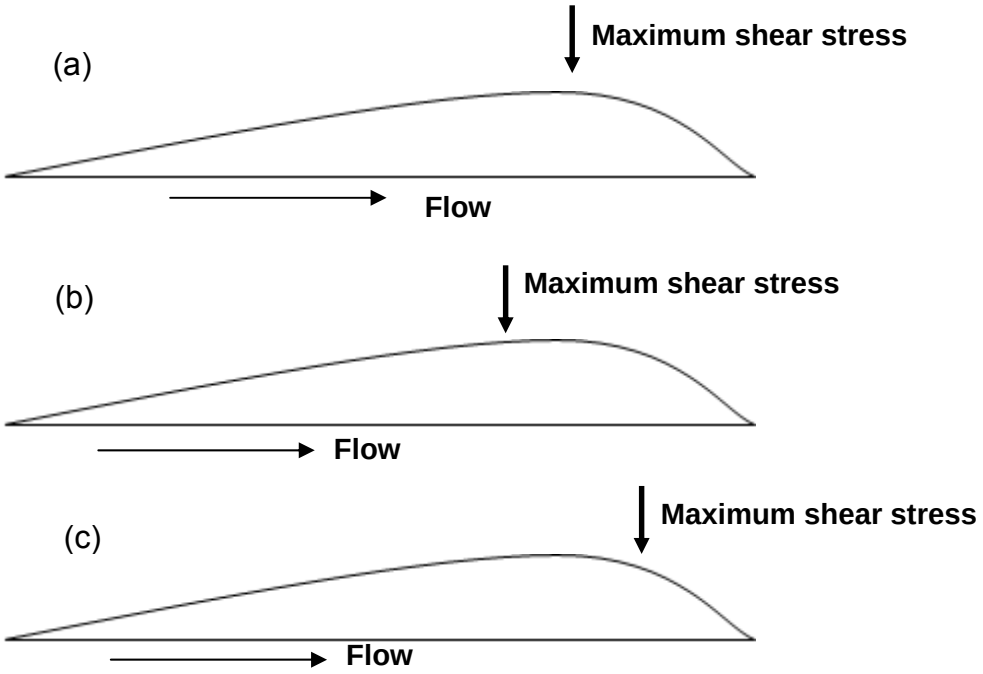

Figure 1-10. Bedform morphology changes corresponds to change location of the maximum shear stress. (a) Bedform migrates downstream without changing its size. (b) Bedform grows in height when maximum shear stress shifts to upstream of crest. (c) Bedform decays when maximum shear stress shifts to downstream of crest.

1.2.5 Linkage between migration rate and transport stage

The dependence of migration rate on transport stage is highlighted by a number of previous works. *Venditti et al*. [2005b] examined the kinematics and morphodynamics of low-amplitude, small-scale bedforms, which they referred to as ‘sand sheets’, superimposed on migrating dunes in a bedload-dominated transport stage. The mean sand sheet length and migration rate was constant along the dune. Sand sheets were one-tenth the size of dunes and migrated ten times faster than the dunes. The sediment transport rate from sand sheet migration and dune migration were identical demonstrating that the bedforms were indeed formed in a bedload-dominated transport stage.

Mohrig and Smith [1996] developed a model to calculate bedform migration rate in a mixed transport stage by estimating the fraction of sediment moving over the crests of bedforms that bypasses the lee face. The bypass fraction was found by calculating a characteristic excursion length for every grain size making up the bedforms (Figure 1-11). Particles with excursion lengths greater than the length of the bedform lee face were assumed not to contribute to bedform migration. The model results are highlighted in Figure 1-12. The solid line in Figure 1-12b represents the agreement between predicted and measured values and it shows the model agreed with field and laboratory data. If it was assumed in the model that all sediment that bypassed the dune crest deposited on the lee face, the model overestimated dune migration rates (Figure 1-12a). If the opposite was assumed in the model, that is, no sediment suspended at the dune crest dropped back on lee face), the model underestimated dune migration

rates (Figure 1-12c). Results from *Mohrig and Smith* [1996] show bedform migration in a mixed transport stage is achieved by a constant exchange between suspended load and bedload.

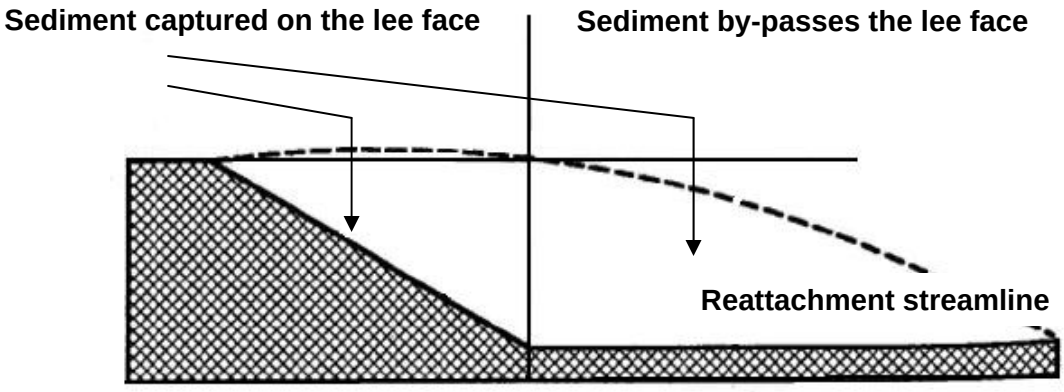

Figure 1-11. Characteristics excursion length for every grain size making up the bedforms [*Mohrig and Smith*, 1996].

Wan and Wang [1994] showed that under a suspension-dominated transport stage, the stability field of dunes was influenced by clay concentration, with dunes being replaced by upper stage plane beds at higher volumetric clay concentrations. Laboratory experiments also indicate that at certain clay concentrations the dune morphology may be significantly modified [*Simons et al.*, 1963] depending on the clay concentration, clay type and applied shear stress [*Wan*, 1982]. In natural rivers, bedforms are documented to change from asymmetrical to symmetrical with greater rates of suspension [*Kostaschuk and Villard*, 1996].

All the above shows that bedform migration is controlled by how sediment is transported. In other words, bedform migration is controlled by transport stage.

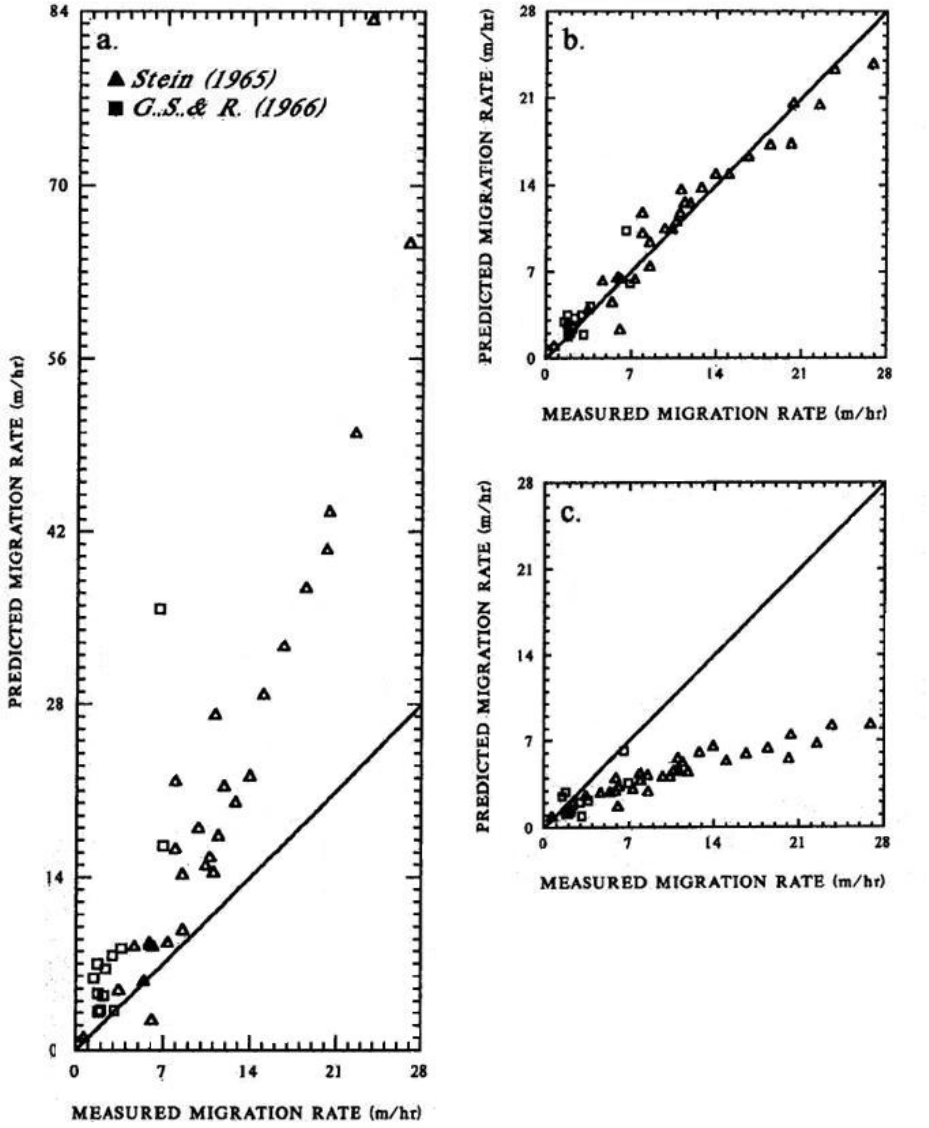

Figure 1-12. Predicted average rates of dune migration plotted versus the migration rates reported by *Stein* [1965] and *Guy et al.* [1966]. The solid lines represent agreement between predicted and measured values. (a) Predicted rates calculated assuming all sediments that pass dune crest deposit at the lee face. (b) Predicted rate calculated from the bypass fraction derived from characteristics excursion length. (c) Predicted rate calculated assuming all sediments being suspended at the dune crest do not drop back on lee face [*Mohrig and Smith*, 1996].

1.2.6 Perspective

The ability to predict the migration rate of bedforms is important for studying sediment transport because we can relate the rate of dune advance to the volume flux of sediment and vice versa [*Simons et al.*, 1965; *Mohrig and Smith*, 1996; *Nittrouer et al.*, 2008]. Transport stages, which can be represented by the Shields number, are shown to control the morphology of bedforms [*Bridge, 2003*; *Wan*, 1982; *Wan and Wang*, 1994]. In addition, studies suggest bedform morphology can control the rate and mode of migration [*Allen*, 1973; *Coleman and Melville*, 1994; *Jerolmack and Mohrig*, 2005ab; *Venditti et al.*, 2005ab]. The known relations between transport stage, bedform geometry and bedform migration rate are illustrated in Figure 1-13 as solid line between circles. As a result, one may expect to find a relation between migration rate and transport stages, represented by dashed line in Figure 1-13.

Figure 1-13. Summary of the relations among bedform migration rate, bedform geometry, and shear stress/Shields number.

1.3 Objectives

The objectives of this research are to answer the following questions:

Do laboratory and field data from the literature reveal a relation between transport stage and bedform migration? What is the relation? What is the process of bedform migration under each transport stage that leads to such a relation?

The specific objectives of the research are as follows:

1. To determine the nature of the relation between transport stage and bedform migration from published data sets.
2. To obtain a detailed set of observations in a controlled laboratory experiment of the processes that lead to bedform migration under different transport stages.

1.4 Thesis format

Chapter 2 is based on analysis of data sets from the literature and includes a discussion. Chapter 3 is based on a lab experiment and contains experiment design, methods, results and discussion of the laboratory data. Chapter 4 is a short discussion and conclusion chapter that also highlights further research directions. Chapters 2 and 3 are designed to be submitted to journals as separate papers, which leads to some minor repetition in their introductions.

2: CHAPTER 2

2.1 Introduction

Bedform migration rate (V_b) is important for estimating sediment transport in sand-bedded rivers. Migration rate is difficult to estimate because empirical relations between V_b and various flow parameters (e.g. mean velocity, Froude number, velocity head) are not well defined [*Simons et al.*, 1965]. Models of bedform migration require a great deal of input information to produce predictions [*Mohrig and Smith*, 1996]. Methods of estimating sediment transport associated with bedform migration using time-lapsed observations of bed topography are improving [*Van den Berg*, 1987; *Ten Brinke et al*., 1999; *Villard and Church*, 2003; *McElroy and Mohrig*, 2009], but require observational data which are often difficult to acquire and labour intensive to analyze. As such, empirical relations between fluid forcing and bedform migration could be quite useful for predicting sediment transport.

There are well-defined relations between the transport stage in a river and bedform geometry (Figure 1-13). *Yalin* [1972] demonstrates an empirical relation exists between the ratio of Shields number (τ^*) over the critical Shields number (τ^*_c) and bedform geometry, which is expressed in terms of height/length ratio (aspect ratio)(Figure 1-5).

Bedforms are smaller when τ^* is just above the level of sediment entrainment and then they grow in height as τ^* increases [*Yalin*, 1972]. The aspect ratio then reaches a maximum then decreases at high τ^* (Figure 1-5). Ripples and dunes show the same trend. Ripples reach maximum aspect ratio at a lower τ^*/τ^*_c than dunes and the maximum aspect ratio for ripples is higher than for dunes. *Yalin and Karahan* [1979a] further demonstrate that the aspect ratio of dunes show multiple curve patterns when stratified by the ratio of flow depth (d) to grain size (D).

Bedform geometry (height, length, aspect ratio) has been shown to directly influence migration rate [*Allen*, 1973; *Coleman and Melville*, 1994; *Venditti et al.*, 2005b](Figure 1-13). The length and height of individual dunes in a bed configuration vary in space and time as they migrate under steady and uniform flow conditions [*Allen*, 1973; *Leclair*, 2002; *Bridge*, 2003; *Venditti et al.*, 2005b; *McElroy and Mohrig*, 2009]. If the sediment transport rate is constant, the speed of a bedform is controlled by its size. Bedform migration rate normally decreases as its height increases to maintain constant sediment transport rate [*Allen*, 1973; *Gabel*, 1993; *Coleman and Melville*, 1994; *Leclair*, 2002; *Bridge*, 2003; *Venditti et al.*, 2005b]. However, how migration rate varies at different transport stages is not clearly defined in the literature.

Given the relations between transport stage and bedform geometry, and bedform geometry and migration rate, it seems likely that there is a relation between bedform migration rate and transport stage that has remained relatively unexplored (Figure 1-13). Here, I explore the relation between bedform migration

rate and transport stage using a variety of laboratory and field data from the literature.

2.2 Methods

In order to explore the empirical relation between migration rate and transport stage, I re-examined data available in the literature where the following conditions were met: 1) bedform height (H), length (L) and migration rate (V_b) were reported; (2) information required to calculate the Shields number were reported; (3) the flow was unidirectional; (4) data were collected when bedforms were in equilibrium with flow. Data sets used in this study are listed in Table 2-1. Bedform type (ripple or dune) was classified according to the original authors' classification. *Guy et al.* [1966] is the only data set that separates ripples and dunes. Unclassified bedform data were assumed to be dunes.

Table 2-1. Data source for analysis.

Source	Data type	Channel width (m)	D_{50} (mm)	Number of data	Number of data used
Stein [1965]	Flume experiment	1.22 (4ft)	0.4	59	40
Guy et al. [1966]	Flume experiment	2.43 (8ft)	0.19, 0.27, 0.28, 0.47, 0.93	339	125
		0.61 (2ft)	0.32, 0.33, 0.54		
Williams [1967]	Flume experiment	0.3 (1ft)	1.35	37	26
Gabel [1993]	Field data	23	0.31 – 0.41	27	18
Leclair [2002]	Flume experiment	0.6	0.43	34	21
		2.7	0.81		
Venditti et al. [2005b]	Flume experiment	1	0.5	5	5

The data required to calculate the relative quantities of bedload and suspended load are not available in the literature, so I quantified the transport stage following *Church* [2006] as the ratio of the Shields number (τ^*; Equation 1-3) to its critical value for entrainment of bed material. The ratio of the non-

dimensional shear stress (Shields number) to the critical non-dimensional shear stress is the same as the ratio of the dimensional shear stress values. I use the dimensionless version to maintain continuity with the original work of *Yalin* [1972] that showed the dependence of bedform geometry on transport stage.

The critical Shields number (τ^*_c) was chosen to be 0.03 for the analysis [*Shields*, 1936; *Raudkivi*, 1967; *Yalin and Karahan*, 1979b]. The shear stress (τ) was calculated as

$$\tau = \rho g d S \tag{2-1}$$

where ρ is the density of water, g is gravitational acceleration, d is flow depth and S is the slope of bed and water surface. The density of water is assumed to be 1000 kg/m^3 and the density of sediment is assumed to be 2650 kg/m^3. Sidewall corrections were implemented for flume data to calculate shear stress applied to the bed using the empirical equation of *Williams* [1970]:

$$\tau_{(\text{corrected})} = \tau \frac{1}{1+0.18(\frac{d}{w^2})} \tag{2-2}$$

where w is the width of flume. Shields number is calculated from $\tau_{(\text{corrected})}$ using Equation 1-3.

There are two statistical methods for deriving relations between two variables – least-square regression analysis and functional regression analysis. Least-square regression analysis assumes all errors reside in the dependent variable and there is none in the independent variable [*Mark and Church*, 1977]. It is most appropriate for predictive purpose where the independent variables is

known. Functional regression analysis assumes that the data are normally distributed and that errors are the same in the independent and the dependent variables. Functional regression analysis is more appropriate to investigate the underlying function between two variables. The data used in this analysis are not normally distributed (Figure 2-1) and I do not know the errors in either the independent or dependent variables. As a result, I did not use functional regression analysis to analyze my data.

In light of this and because I am deriving relations for predictive purpose, I used least-square regression analysis. In doing so, I must decide which variable has smaller associated errors for use as the independent variable. I suspect migration rate has a larger associated error than the Shields number in the mostly flume data I examine. Water surface slopes and flow depths are easier to measure in flumes than bedform movement.

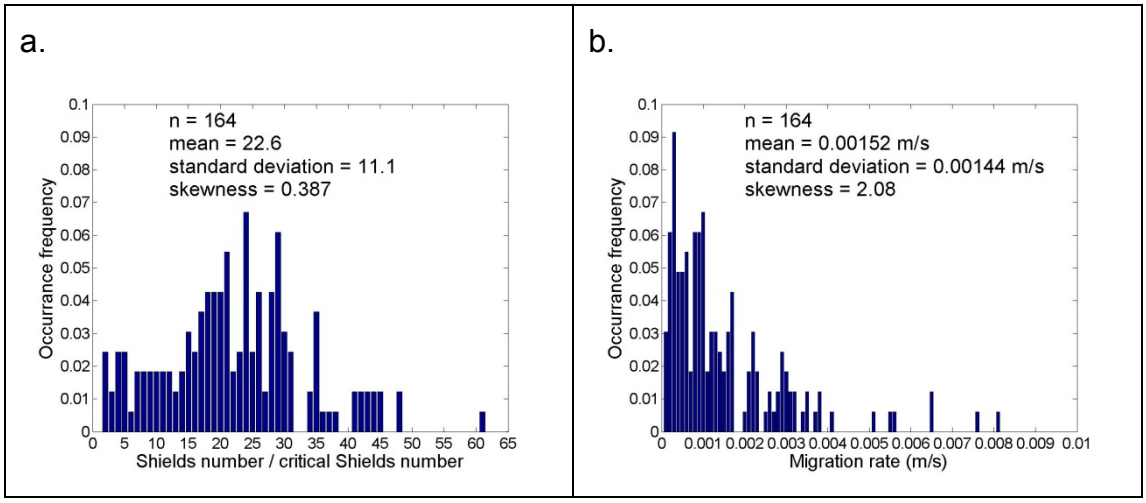

Figure 2-1. Distributions of (a) τ^*/τ^*_c and (b) migration rate from the data in Figure 2-5.

2.3 Results

2.3.1 Data assessment

The aspect ratio (H/L) of bedforms was plotted as a function of τ^*/τ^*_c in Figure 2-2 and the bedform migration rate was plotted as a function of τ^*/τ^*_c in Figure 2-4. Several eccentric data points were removed from the analysis to avoid biasing the results.

1) Data from *Williams* [1967] are observations of bedforms developed in very coarse (D_{50} = 1.35mm) sand. The data have high migration rates for a given τ^*/τ^*_c compared to data from other sources (Figure 2-2; Figure 2-4). I suspect that the large grain-size inhibits suspension and impacts the response of these bedforms to higher flows. These data were excluded in all the analysis except in section 2.3.5 where *Williams* [1967] data formed their own category when all the data were stratified.

2) The data circled in red (Figure 2-4) were collected in flows with high bentonite concentrations by *Guy et al.* [1966]. They were excluded from all the analysis because they have low V_b compared to data from other sources for a given τ^*/τ^*_c.

3) Runs 25, 26, 31, 32 from *Stein* [1965] were excluded from all the analysis because they have higher V_b compared to other data points in the same category when stratified (Figure 2-9). I did not know what is different about these data, but decided to exclude them as anomalous.

2.3.2 Bedform geometry and its relation to the Shields number

The aspect ratio (H/L) of ripples and dunes was plotted as a function of τ^*/τ^*_c in Figure 2-2 and Figure 2-3. Data points that represent ripples have black edges around them whereas points that represent dunes do not. Ripple data range from 1.69 to 19.2 in τ^*/τ^*_c and from 0.0172 to 0.117 in H/L. Dune data range from 2.45 to 61.5 in τ^*/τ^*_c and from 0.00690 to 0.119 in H/L. Dune data points have wider range in τ^*/τ^*_c than ripple data because ripples are unstable and washout at higher transport stages. The red crescent represents the relation between H/L and τ^*/τ^*_c for ripples and the black curve represents the relation for dunes from *Yalin* [1972]. It is clear that the dune data conform to *Yalin* [1972]'s relation, but ripple data do not. The mismatch between the ripple data from *Guy et al.* [1966] and *Yalin* [1972]'s relation is because *Yalin* [1972]'s relation for the ripples was derived from the *Guy et al.* [1966] data and 14 other data sets. However, I only have the *Guy et al.* [1966] data to compare to *Yalin* [1972]'s relation for the ripples.

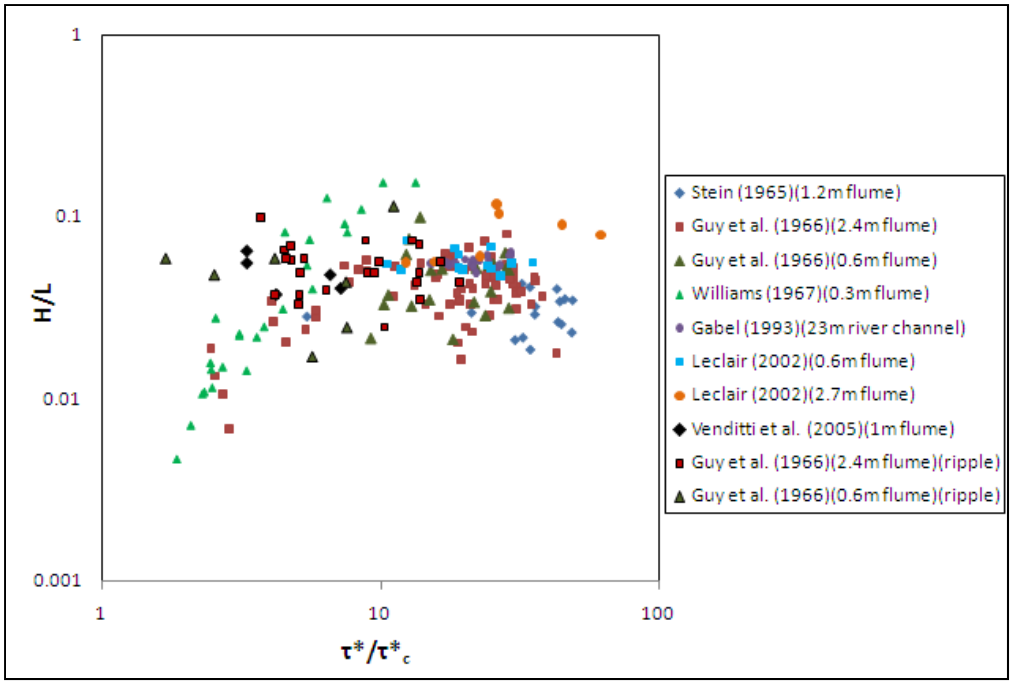

Figure 2-2. Aspect ratio (H/L) versus transport strength for all the data.

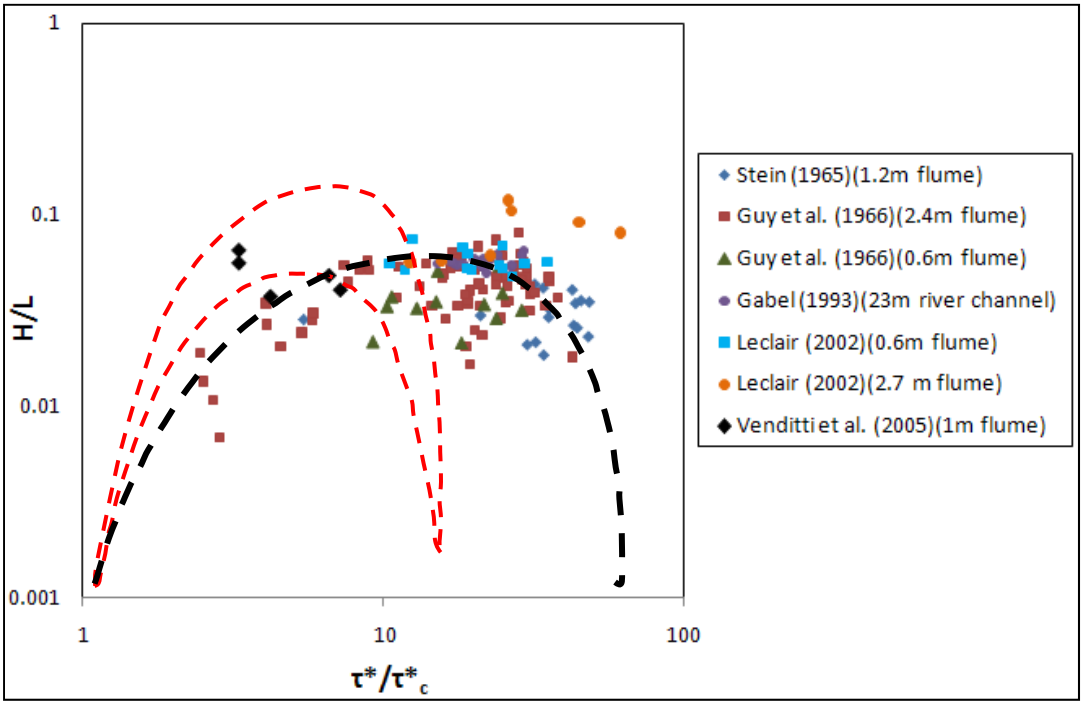

Figure 2-3. Aspect ratio (H/L) versus transport strength with eccentric data removed.

2.3.3 Regression analysis of all the dune and ripple data

Migration rate shows a positive correlation with τ^*/τ^*_c for both ripples and dunes (Figure 2-4). Migration rates range from 5.08×10^{-7} to 1.58×10^{-3} m/s for ripples and 1.52×10^{-4} to 8.13×10^{-3} m/s for dunes. The ripple data have a wider range of migration rates than the dune data. The slopes of the relation between V_b and τ^*/τ^*_c vary considerably between ripples and dunes and amongst different data sets (Figure 2-4).

The regression analysis on the dune and ripple data yields a trend line that has the form of

$$V_b = a\left(\frac{\tau^*}{\tau^*_c}\right)^m \qquad (2\text{-}3)$$

where a and m are intercept and slope, respectively. The values of a, m, R^2 and P-value are summarized in Table 2-2.

The dune migration rate shows a positive correlation with τ^*/τ^*_c (Figure 2-5 black line). While the relation is statistically significant at the 99% confidence level, less than 19% of the variation in V_b is explained by τ^*/τ^*_c. The ripple migration rate also shows a positive correlation with τ^*/τ^*_c (Figure 2-6 black line). The relation is statistically significant at the 99% confidence interval and a greater amount of the variance (61%) in V_b is explained by τ^*/τ^*_c than for dunes.

These results suggest that statistically significant relations exist between V_b and τ^*/τ^*_c, but for dunes, the strength of the relation is poor. So the data were stratified by two measures of relative roughness: H/d and d/D because H is

dependent on τ^*/τ^*_c (Figure 1-5; Figure 2-2) and the latter was used by *Yalin and Karahan* [1979a].

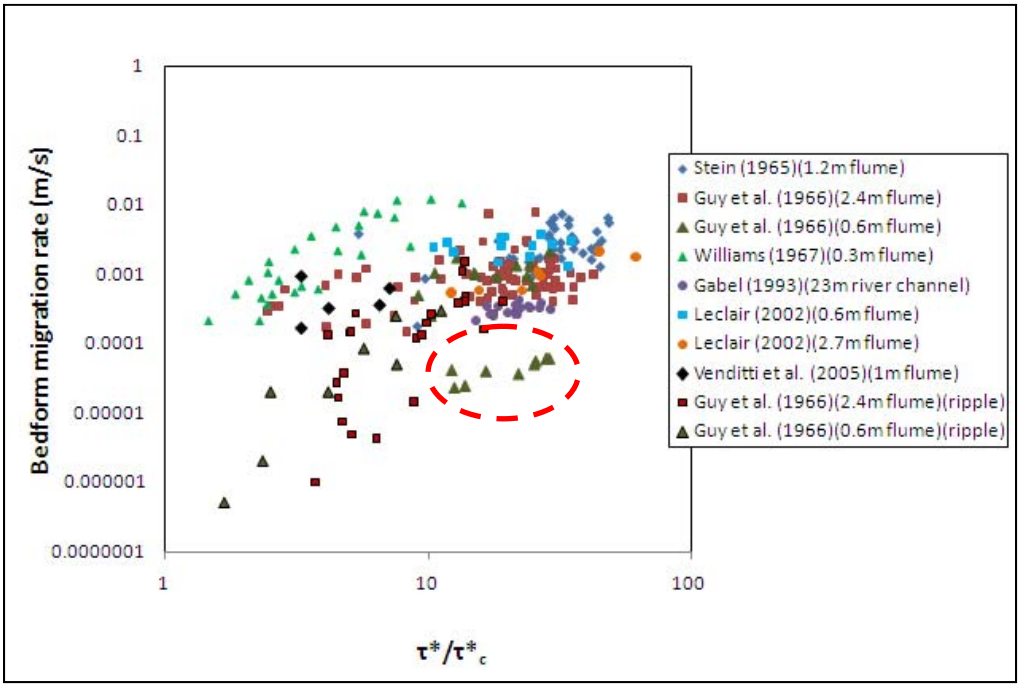

Figure 2-4. Bedform migration rate versus transport strength for all the data.

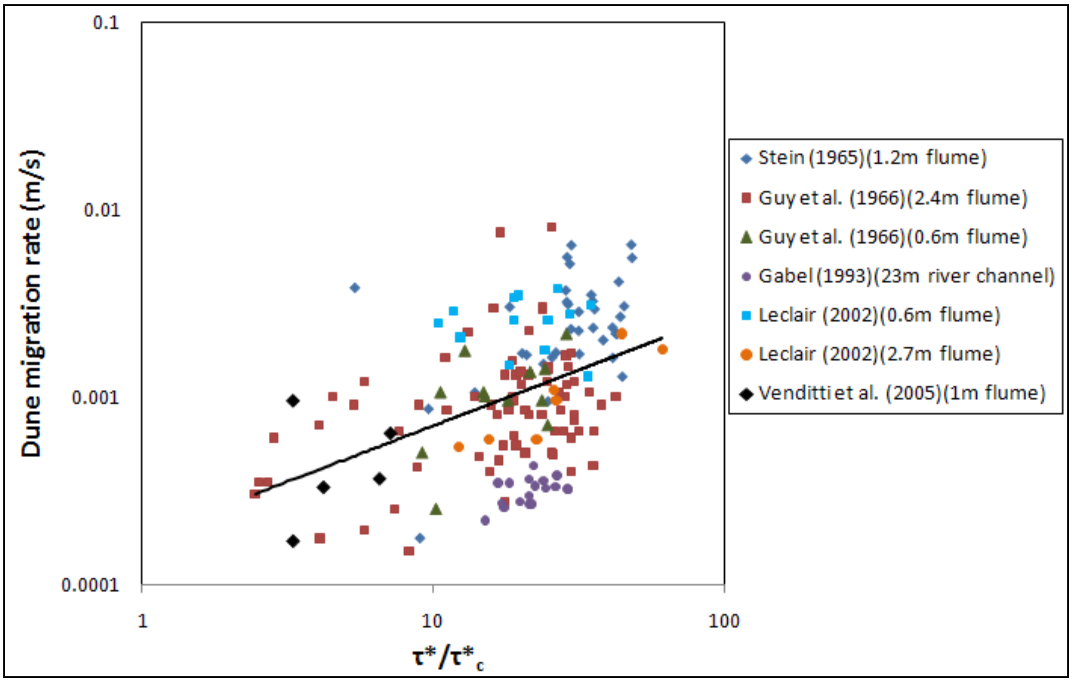

Figure 2-5. Dune migration rate versus transport strength. Eccentric data were removed. Black line was generated with regression analysis.

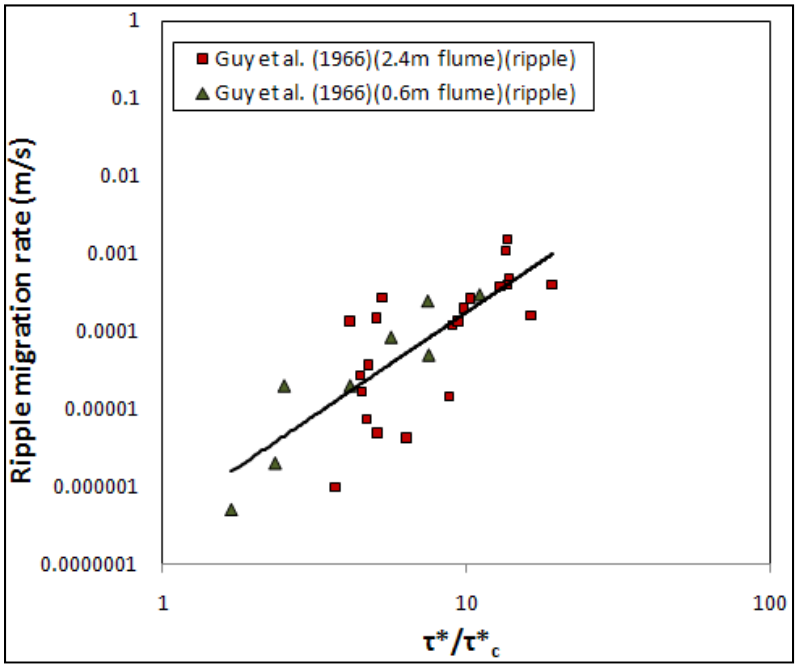

Figure 2-6. Ripple migration rate versus transport strength. Black line was generated with regression analysis.

2.3.4 Regression analysis for dune data stratified by H/d

Figure 2-7 shows dune migration data stratified by H/d. These categories have boundaries that are easy to distinguish and similar number of data (Table 2-3). Small H/d represents low-amplitude bedforms compared to flow depth; large H/d represent high-amplitude bedforms compared to flow depth. Each category yields a trend line that shares the same form as Equation 2-3. The values of a, m, R^2 and P-value for each category are summarized in Table 2-3.

The intercept and slope vary greatly among the categories and only one category has a relation between V_b and τ^*/τ^*_c that is statistically significant at the 99% confidence interval. The low R^2 values imply that it is highly likely that fitted trends based on regression analysis are within the error bands of each curve (ie, there is no statistical difference between the two). The results indicate stratification of the data by H/d does not improve the explanatory power of V_b by τ^*/τ^*_c.

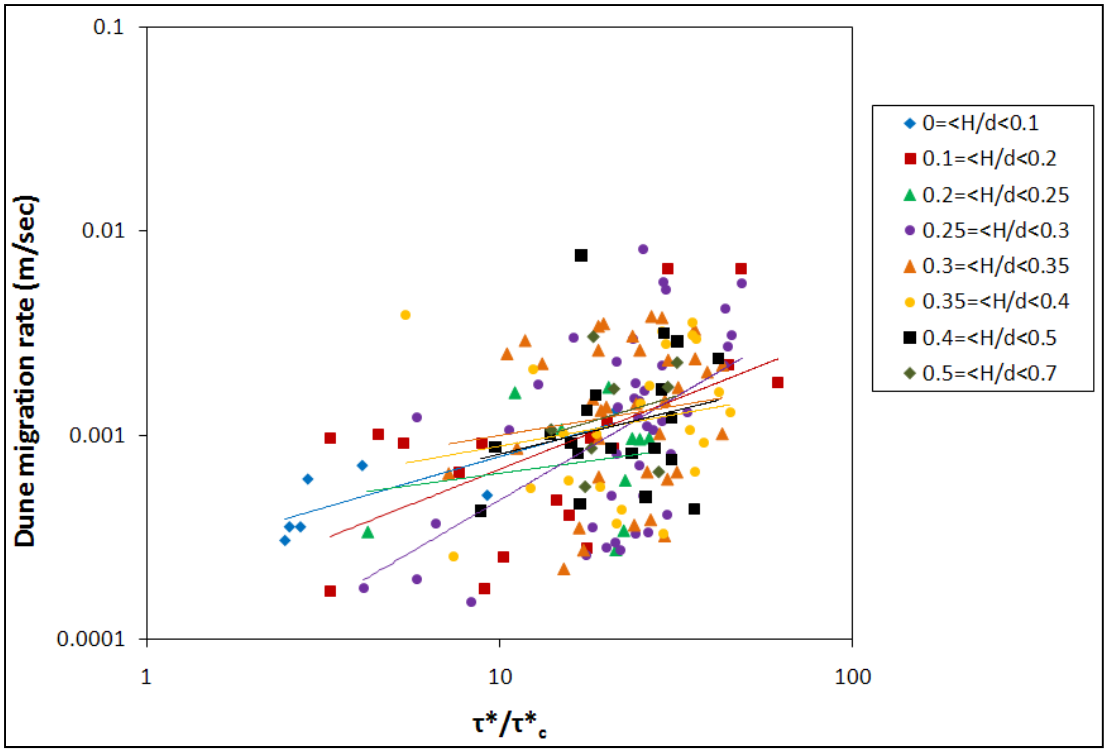

Figure 2-7. Dune migration rate versus transport strength stratified by H/d.

Table 2-2. Summary of a, m, R^2 and P-value for dune and ripple.

Bedform type	(n)	Regression analysis intercept (a)	Regression analysis slope (m)	R^2	P-value
Dune	164	1.80×10^{-4}	0.594	0.189	5.74×10^{-9}
Ripple	31	3.96×10^{-7}	2.65	0.613	2.85×10^{-4}

Table 2-3. Summary of a, m, R^2 and P-value for each stratified category of Figure 2-7.

Category (H/d)	(n)	Regression analysis intercept (a)	Regression analysis slope (m)	R^2	P-value
$0 \leq H/d < 0.1$	7	2.47×10^{-4}	0.503	0.662	2.59×10^{-2}
$0.1 \leq H/d < 0.2$	18	1.40×10^{-4}	0.686	0.336	1.18×10^{-2}
$0.2 \leq H/d < 0.25$	10	3.76×10^{-4}	0.237	0.0406	5.77×10^{-1}
$0.25 \leq H/d < 0.3$	42	4.66×10^{-5}	1.01	0.301	1.67×10^{-4}
$0.3 \leq H/d < 0.35$	36	5.12×10^{-4}	0.289	0.0202	4.09×10^{-1}
$0.35 \leq H/d < 0.4$	23	4.32×10^{-4}	0.311	0.0428	3.43×10^{-1}
$0.4 \leq H/d < 0.5$	20	3.02×10^{-4}	0.427	0.0583	3.05×10^{-1}
$0.5 \leq H/d < 0.7$	8	2.58×10^{-4}	0.520	0.0651	5.42×10^{-1}
Mean	21	2.89×10^{-4}	0.498	0.191	2.77×10^{-1}
Maximum	42	5.12×10^{-4}	1.01	0.662	5.77×10^{-1}
Minimum	7	4.66×10^{-5}	0.237	0.0202	1.67×10^{-4}

2.3.5 Regression analysis for dune data stratified by d/D

Figure 2-8 shows dune migration data stratified by d/D. These categories have boundaries that are easy to distinguish and similar number of data points. Small d/D represents large grain size relative to flow depth and vice versa. Each category yields a trend line that shares the same form as Equation 2-3. The values of a, m, R^2 and P-value for each category are summarized in Table 2-4.

The relation between V_b and τ^*/τ^*_c are statistically significant at the 99% confidence interval, except the last category where the boundary is the largest. The last category contains a wider range of data including river and flume data. The mixture of unlike data may be the reason that the relation is insignificant.

The slope of the relations vary between 0.9 and 1.9 with a mean value of 1.4 (Table 2-4). A greater percentage of the variation in V_b is explained by τ^*/τ^*_c when data were stratified by d/D in comparison to the H/d stratification and the unstratified relation.

Figure 2-9 shows a comparison between the relations derived using all the data in the category 600<d/D<700 and with the four anomalous data from *Stein* [1965] removed. The anomalous data have much higher migration rate compares to other data with similar τ^*/τ^*_c values. With the anomalous data included, the relation yields a slope of 2.5, which is more than 100% greater than the average slope of all the other relations. With the anomalous removed, the relation yields a slope that is within the range of other categories and has a higher R-square.

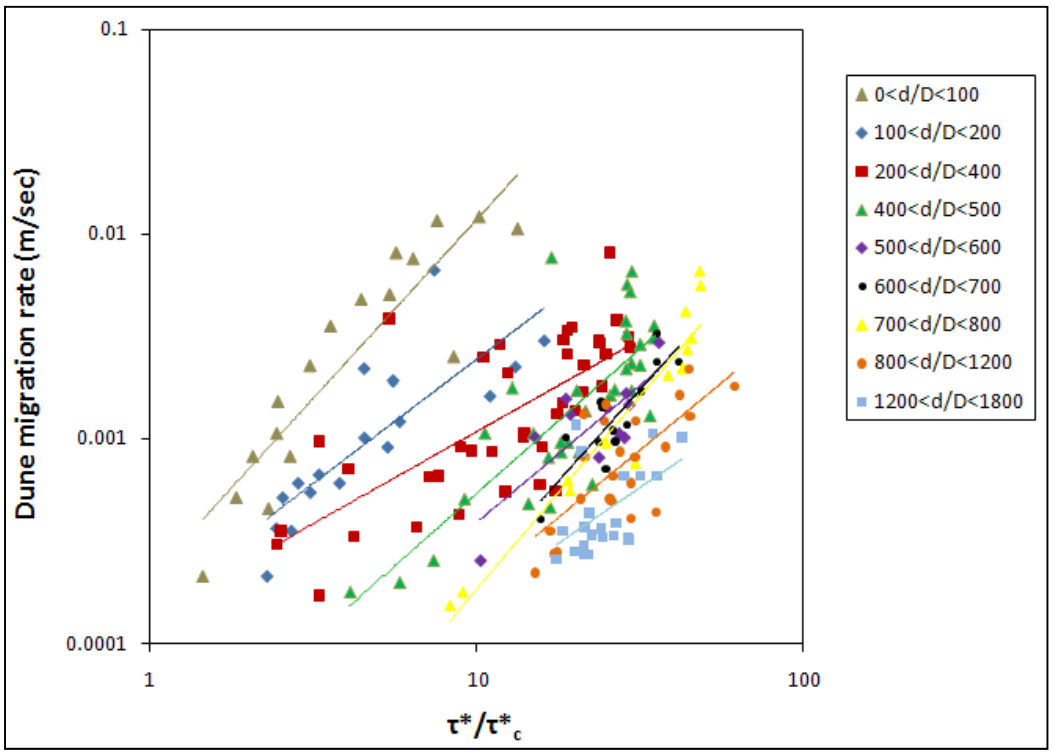

Figure 2-8. Dune migration rate versus transport stage stratified by d/D.

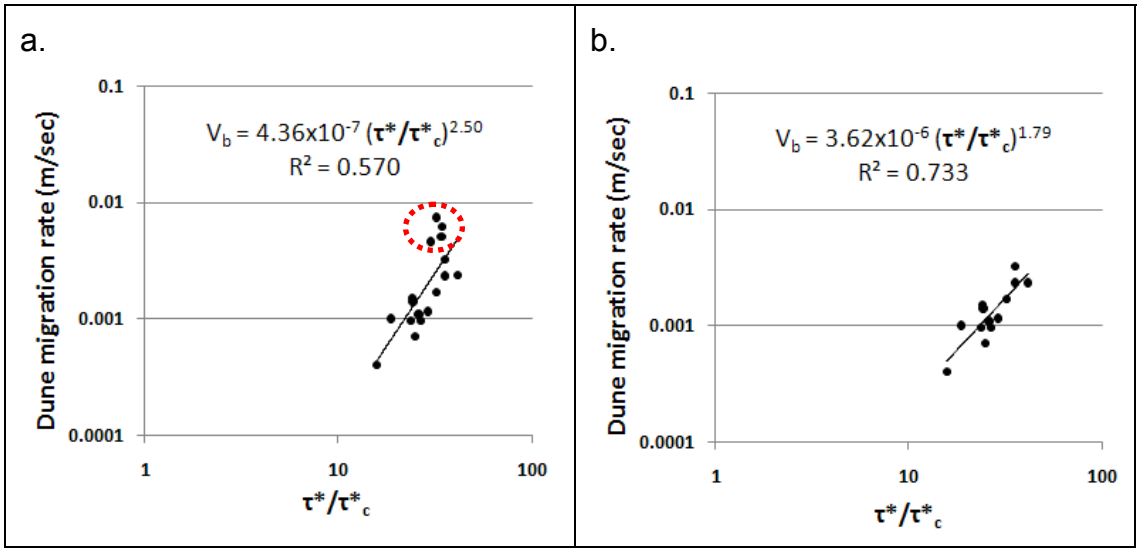

Figure 2-9. Comparison between plotting (a) all the data in category (600<d/D<700) and (b) having four eccentric data (red-circled) from *Stein* [1965] removed.

Table 2-4. Summary of a, m, and R^2 for each stratified category of Figure 2-6.

Category (d/D)	(n)	Regression analysis intercept (a)	Regression analysis slope (m)	R^2	P-value
0<d/D<100	17	2.10×10^{-4}	1.75	0.813	7.55×10^{-7}
100<d/D<200	17	1.50×10^{-4}	1.21	0.676	5.17×10^{-6}
200<d/D<400	40	1.36×10^{-4}	0.90	0.515	1.85×10^{-7}
400<d/D<500	33	2.08×10^{-5}	1.41	0.618	5.84×10^{-8}
500<d/D<600	11	1.77×10^{-5}	1.34	0.624	3.83×10^{-3}
600<d/D<700	13	3.62×10^{-6}	1.79	0.733	1.87×10^{-4}
700<d/D<800	14	2.40×10^{-6}	1.88	0.923	4.72×10^{-8}
800<d/D<1200	23	9.28×10^{-6}	1.32	0.510	1.3×10^{-4}
1200<d/D<1800	22	1.33×10^{-5}	1.09	0.262	0.0148
Mean	21	6.26×10^{-5}	1.41	0.630	2.11×10^{-3}
Maximum	40	2.10×10^{-4}	1.88	0.923	1.48×10^{-2}
Minimum	11	4.36×10^{-7}	0.90	0.262	4.72×10^{-8}

2.3.6 Regression intercepts and slopes

The regression slopes and intercepts from Table 2-4 were plotted in Figure 2-10. There does not appear to be any trend in slope across the groupings (Figure 2-10a blue line). However, the intercept, illustrated in Figure 2-10b as a blue line, declines with increasing d/D, meaning that as grain-size gets smaller relative to flow depth, the intercept declines.

The dependence of the intercept on d/D suggests a threshold exists. The most obvious threshold to examine is the sediment entrainment threshold. The critical Shields number (τ^*_c) is dependent on grain size of sediment [*Buffington and Montgomer*y, 1997]. The decrease in the intercept with increasing grain size (Figure 2-10b) may be caused by using constant $\tau^*_c = 0.03$ in calculating the Shields numbers. I attempted to vary τ^*_c by calculating it for each observation using the *Brownlie* [1981] fit to the Shields diagram

$$\tau_c^* = 0.22\,\mathrm{Re}^{*-0.6} + 0.06 \times 10^{(-7.7\mathrm{Re}^{*-0.6})} \qquad (2\text{-}4)$$

where Re* is the grain Reynold's number. A new set of slope, R^2 and intercept were generated from regression analysis illustrated in Figure 2-10 as red lines. These values are similar to those using a constant τ^*_c in the calculation. However, the last group (1200<d/D<1800) where grain size was small compare to flow depth, was influenced by the choice of τ^*_c. This observation suggests assuming $\tau^*_c = 0.03$ for all data was valid except for very fine grain size relative to flow depth.

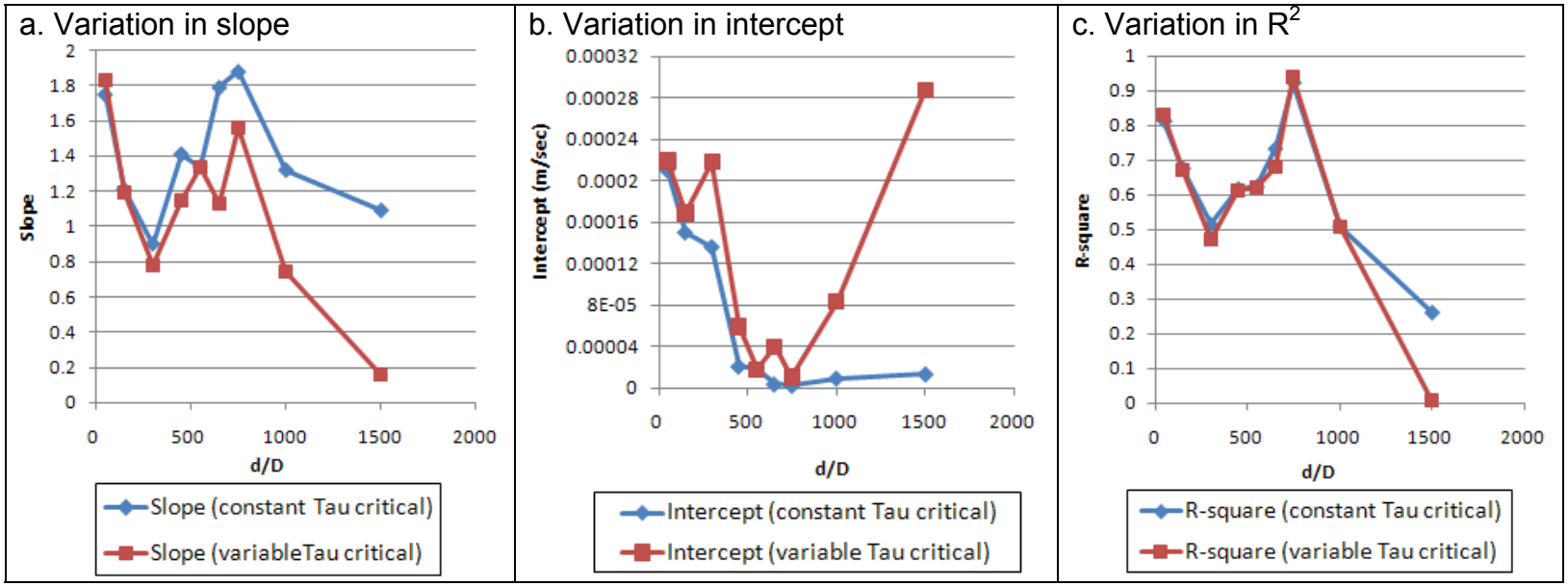

Figure 2-10. Variation in (a) slope, (b) intercept and (c) R^2 using constant and variable critical Shields numbers. All values are generated from regression analysis.

2.4 Discussion

2.4.1 Bedform migration and its relation to sediment grain size

Dune (Figure 2-5) and ripple (Figure 2-6) migration rates show statistically significant positive correlation with transport stage, defined as τ^*/τ^*_c. Ripple migration rate shows a higher correlation with τ^*/τ^*_c than dunes. However, a weaker relation is expected for ripples because the data are from a much smaller pool (n = 31) than dunes (n = 164). The weaker relation for dunes reflects the greater scatter in the dune data set.

Dune migration data were stratified by two measures of relative roughness (H/d and d/D) to determine if bedform height or grain-size influences the relations. Results show dune migration rate is not influenced by dune geometry; instead, it is controlled by grain size.

Research has shown bedform migration rate normally decreases as bedform height increases to maintain constant sediment transport rate [*Allen*, 1973; *Gabel*, 1993; *Coleman and Melville*, 1994; *Leclair*, 2002; *Bridge*, 2003; *Venditti et al.*, 2005b]. Such a relation between bedform height and migration rate is true when a train of bedforms migrate under the same flow because it takes longer to move a larger pile of sediment (larger bedform) than a smaller pile of sediment (small bedform). Bedforms also propagate more slowly with an increase in height when they are developing from a flat bed [*Coleman and Melville*, 1994]. Small bedforms that grow on the back of a larger bedform move faster than their host to accommodate the flux [*Venditti et al.*, 2005b]. This is

because the group of dunes move as a whole package of sediment, so each part of the system has to move proportional to its size. However, migration data presented here span a range of transport stages, so the bedform size has little explanatory power in the derived relation.

Grain size is an important control for bedform migration because as the shear stress increases, more sediment is moved in suspension. In fact, transport stage can be defined by the percentage of total load moved in suspension [*Dade and Friend*, 1998] and the amount of sediment carried in suspension is directly controlled by grain size. For a given flow depth and strength (τ^*/τ^*_c), the migration rate declines with grain-size because finer particles are more likely to be suspended.

The important role of suspension implied by the analysis suggests that the data may be collapsed onto a single curve if an appropriate scale can be found to make the bedform migration rate dimensionless. Figure 2-11 shows the dune migration made dimensionless by the grain fall velocity calculated using the relations of *Dietrich* [1982]. I also tried to make V_b dimensionless with the mean velocity and shear velocity and found they did not influence the grouping seen in Figure 2-6.

The regression analysis of the data in Figure 2-11 yields a relation

$$\frac{V_b}{w_s} = 1.52 \times 10^{-3}\left(\frac{\tau^*}{\tau^*_c}\right)^{0.940} \quad (2\text{-}5)$$

Dimensionless dune migration rate shows a positive correlation with τ^*/τ^*_c (Figure 2-11). The relation is statistically significant at the 99% confidence level

(P-value = 2.12×10^{-18}) and 38% of the variation in V_b/w_s is explained by τ^*/τ^*_c. While the amount of variability in V_b/w_s explained by τ^*/τ^*_c is not great, the form of the relation is encouraging. The partial collapse when the migration rate is scaled by the settling velocity highlights the role sediment suspension plays in moderating the migration rate.

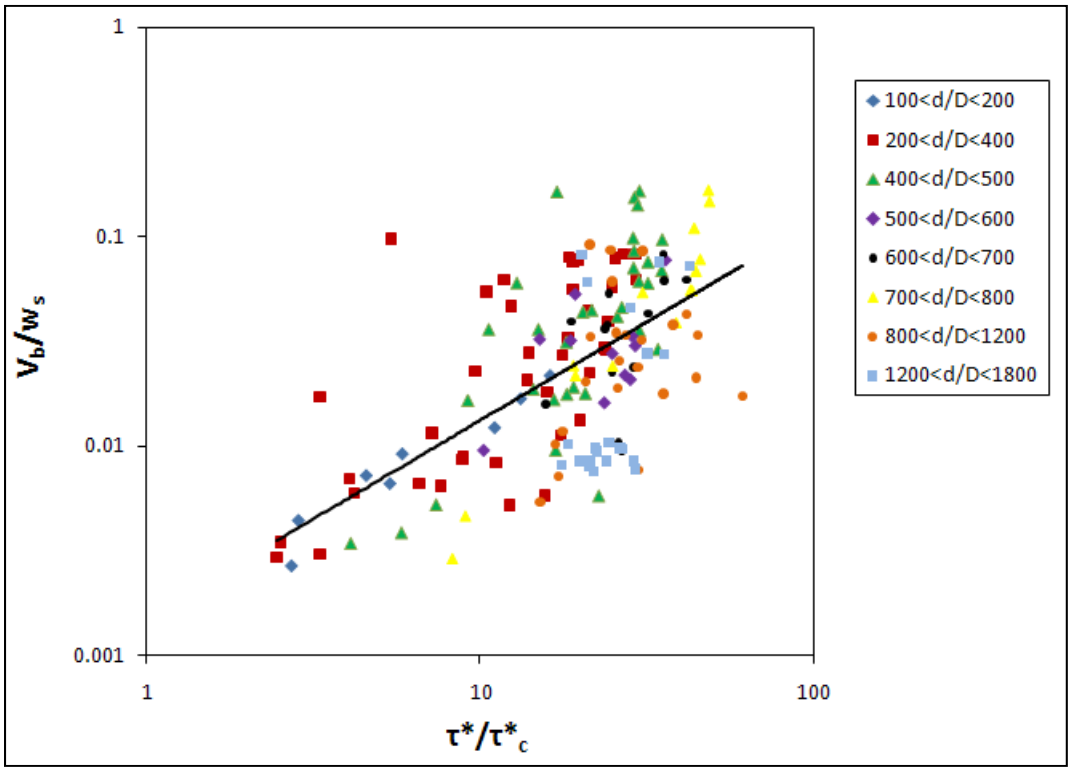

Figure 2-11. Dimensionless migration rate versus transport strength stratified by d/D.

2.4.2 Application in natural river channels

Application of models derived from laboratory data to natural channels should always be pursued with caution. The data sets examined here are all derived from laboratory channels except one that comes from a small channel [*Gabel*, 1993]. Data from large channels are absent in the analysis here because the information required to calculate various parameters is not available or because the flows are variable and are influenced by hysteresis effects [*Allen*, 1974, 1982] which would certainly impact the relations.

One potential concern with the model presented is that it represents a very small range of suspended-sediment concentrations. Natural river channels often have higher suspended-sediment concentrations of fine material than laboratory flume channels [*Best*, 2005]. Research shows dunes in flows with high suspended-sediment concentration have lower heights and migration rates relative to flow with low suspended-sediment concentrations [*Simons et al.*, 1963; *Wan*, 1982]. *Simons et al*. [1963] demonstrate that dunes show a distinguishable decreases in flow resistance, height and migration rate under flow with bentonite concentration greater than 5,000 to 10,000ppm, which are uncommon in rivers. *Wan* [1982] also shows dune height decreases at bentonite concentrations greater than 7,600ppm.

Therefore, it is of interest to determine if sediment concentration affects migration rates throughout the data set. Figure 2-12 plots dune migration rates versus suspended-sediment concentrations. It is not clear that sediment concentration differentiates migration rates, but the ten points identified as

outliers do plot separately from the rest of the data. It seems likely that the reason these data are outliers is caused by the suspended clay-material streamlining bedforms, which then reduces near bed turbulence and resistance to flow [*Simons et al.*, 1963]. Resistance to flow is caused by the generation of turbulence at the bed. Sediment transport is driven by shear stress. When flow resistance goes down, shear stress also goes down, decreasing bed-material transport and ultimately, bedform migration rates.

In natural channels, sediment concentrations can vary widely. In the Fraser River in British Columbia, Canada, suspended-sediment concentration ranged from 283 to 1400mg/L in 10 days during moderate flow (June 19th-29th, 1989) near Steveston [*Kostaschuk and Villard*, 1996]. In the Río Paraná, Argentina, suspended-sediment concentration ranged from 30 to 90mg/L from the top to the bottom of the channel (in March, 2004) just upstream of its confluence with Río Paraguay [*Shugar et al*., 2010]. In the Colorado River near Andrade, CA, averaged annual suspended-sediment concentration was 85mg/L in 1996, 146mg/L in 1997 and 211mg/L in 1998 [*Horowitz et al.*, 2001]. On the other hand, rivers that drain old glacial lakebeds, such as the For Nelson River and the Muskwa River in the northeastern British Columbia, Canada, may have suspended-sediment concentration up to 10,000ppm [*Hickin*, 1986]. The Yellow River that drains the loess regions of central China has suspended-sediment concentration about 1500g/L [*Wan and Wang*, 1994]. We might expect bedform migration rates to be impacted by suspended-sediment concentrations in rivers such as the Muskwa River and the Yellow River. Future work is required to

understand how bedform migration is impacted by suspended sediment in rivers that have high suspended-sediment concentrations.

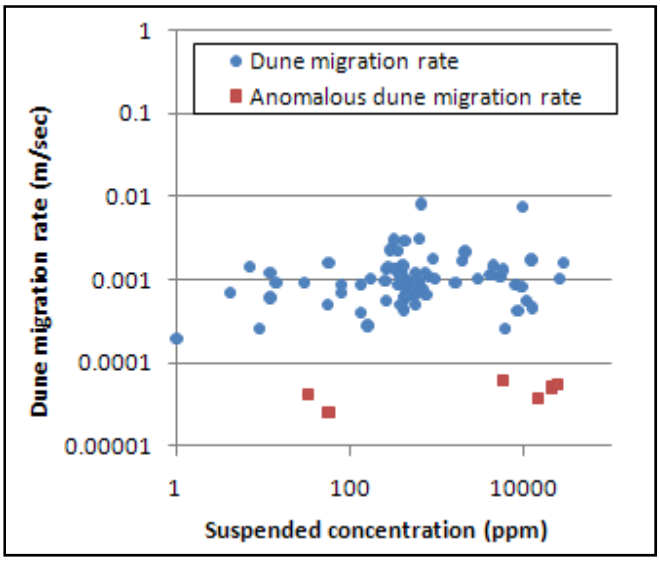

Figure 2-12. Dune migration rate from Guy et al. (1966) versus suspended concentration show no relation. Four points have suspended concentration of 0 ppm and cannot be plotted on a log-log plot.

2.5 Perspective

I examined the relation between migration rate (V_b) and transport stages using several field and flume data sets. These data sets (Table 2-1) contain information on migration rate and other flow and sediment parameters, which can be used to calculate the Shields number (τ^*), which I use as a measure of the transport stage. The data were stratified into dunes (Figure 2-5) and ripples (Figure 2-6), according to the original authors' classification. All data sets show positive correlations between V_b and τ^*. Ripple migration rates vary more than dune migration rates and are better correlated with τ^*. The dune migration data were further stratified by two measures of the relative roughness: the ratio of dune height H over flow depth (H/d) and the ratio of flow depth over median grain size D (d/D). Data stratified by H/d show positive relations between V_b and τ^* (Figure 2-7; Table 2-3) but only one category shows the relation is significant at 99% confidence level. On the other hand, stratification of the dune migration data by d/D yields a series of parallel positive relations between V_b and τ^* (Figure 2-8; Table 2-4). All categories, show V_b and τ^* are statistically significant at 99% confidence level except one that contains a mixture of field and flume data and is the largest category in the analysis.

The analysis highlights transport stage and grain size as important controls of bedform migration because as the flow velocity increases, more sediment is moved in suspension. I made the bedform migration rate dimensionless with the grain settling velocity and was able to partially collapse

data onto a single curve (Figure 2-11) that displayed a positive empirical relation between V_b and τ^*. This result further highlights the important role sediment suspension plays in moderating the migration rate.

In this chapter, I demonstrated an empirical relation exists between bedform migration and transport stage. In the next chapter, I will further explore the mechanisms of bedform migration under different transport stages by performing a flume experiment under bedload-dominated, mixed and suspension-dominated transport stages.

3: CHAPTER 3

3.1 Introduction

Bedform migration rate (V_b) is important for estimating bed-material sediment transport in sand-bedded rivers. Bed-material transport can be decomposed into translation and deformation in a river with bedforms [*McElroy and Mohrig*, 2009]. Translation is the mean downstream migration of bedforms where the shapes of the features are preserved. Bedform translation can be measured by tracking bedform crests as demonstrated in *Simons et al.* [1965]. Deformation is the sum of all changes to the bed's topographic profile that are not associated with the downstream translation of the bedforms. Deformation is difficult to quantify so it is usually not taken into account as part the bed material sediment flux in rivers. *McElroy and Mohrig* [2009] argued that the suspended bed-material flux is equivalent to the bedform deformation rate in rivers.

A common approach to estimating bed-material flux in rivers is to measure the bedform migration (translation) rate and to calculate the suspended bed-material flux from measured vertical profiles of suspended-sediment concentrations. A significant limitation of the approach is the heavy reliance on the measurement of bedform migration, which is often time consuming and expensive. There is a need for methods to estimate migration rates form simple hydraulic observations. However, migration rate is difficult to estimate because

empirical relations between V_b and various flow parameters (e.g. mean velocity, Froude number, velocity head) are not well defined.

Bedform height [*Simons and Richardson*, 1966] and aspect ratio [*Yalin*, 1972; *Yalin and Karahan*, 1979a] are known to increase from bedload-dominated to mixed transport stage then decrease from mixed to suspended transport stage. In Chapter 2, I demonstrated that bedform migration rate increased with transport stage, defined by the Shields number (τ^*) over the critical Shields number (τ^*_c). In addition, migration rate was shown to be controlled by sediment grain size and settling velocity, suggesting bedform migration is conditioned by suspended-sediment transport mechanisms.

Here, I used bed topography and bed-material transport measurements from a laboratory experiment to explore the mechanisms of bedform migration at different transport stages. I examined bedform height, length and migration rate at bedload-dominated, mixed and suspension-dominated transport stage. I used the measurements to examine the hypothesis of *McElroy and Mohrig* [2009] that suspended bed-material flux is equivalent to the bedform deformation rate in rivers.

3.2 Methods

Laboratory experiment was conducted in the Environmental Fluid and Sediment Dynamics Laboratory (EFSDL) at Simon Fraser University (Figure 3-1). The EFSDL flume is 15m long, 1m wide and 0.6m deep and is designed to study sediment dynamics in sand-bedded river channels. The flume has an adjustable slope (-0.5 to 2.0%) and accommodates flows up to 0.2 m^3/s. The open channel length is 12.5m. The flume re-circulates water and sediment.

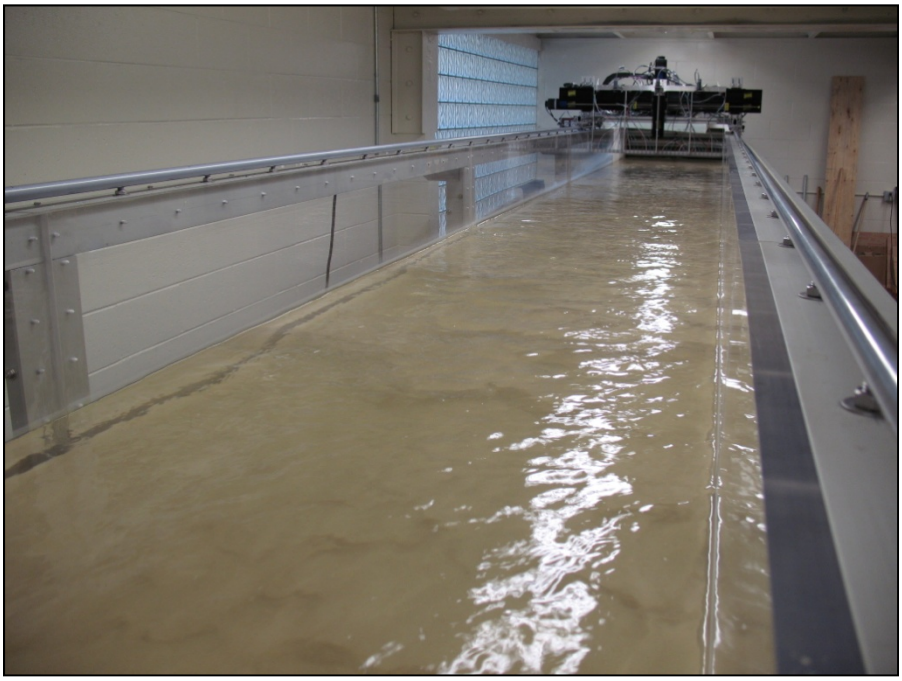

Figure 3-1. EFSDL flume (Photo taken by author).

Sediment used in the experiment was quartz sand and the median grain size was 550μm (Figure 3-2).

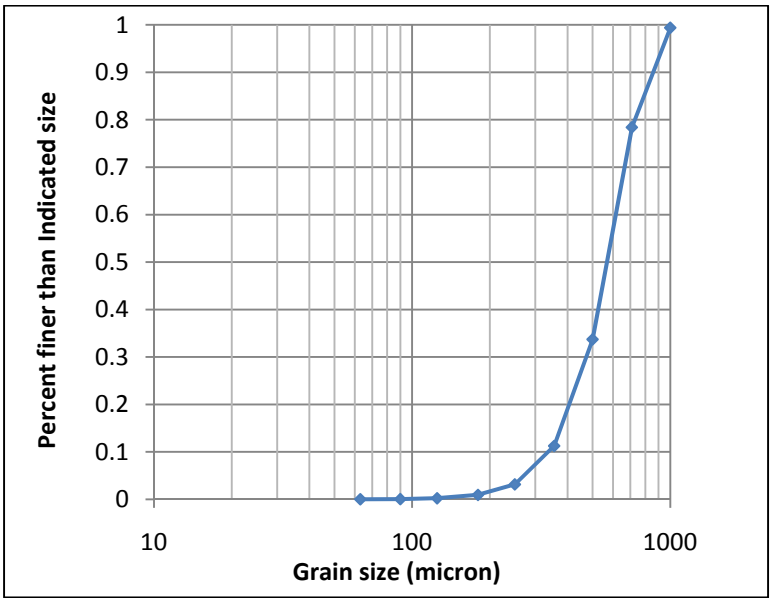

Figure 3-2. Grain size distribution of sand in the experiment.

3.2.1 Swath Mapping System

Observations of bed topography and bedform migration were made using a Swath Mapping System (SMS) (Figure 3-3) that was designed to measure bed topography and water surface elevation along the flume. The SMS consists of 1) a Seatek® transducer echo-sounding system, shown in Figure 3-3 mounted on a Plexiglas beam across the flume; 2) a MassaSonic® ultrasonic system (grey sensors in Figure 3-3); 3) a mechanical arm that moves sensors vertically; and 4) a mechanical system that moves the SMS in the stream-wise direction.

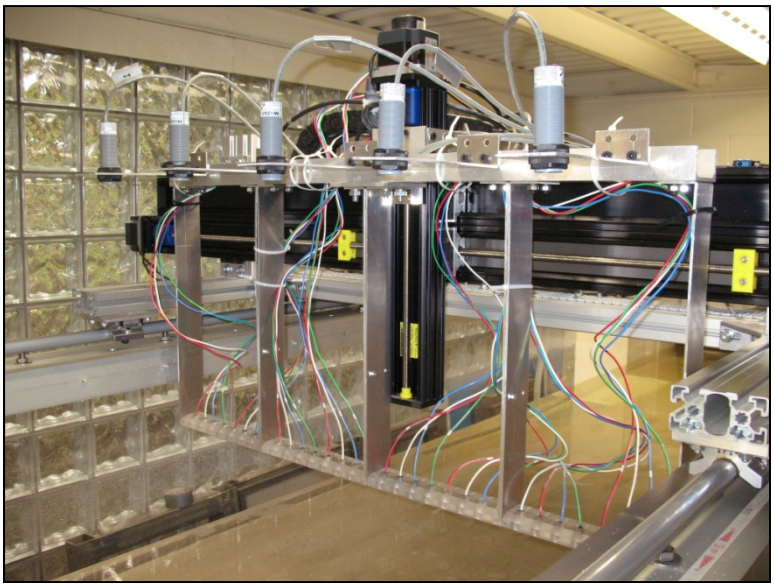

Figure 3-3. The Swath Mapping System (Photo taken by author).

The Seatek® echo-sounder consists of 32 sensors (Figure 3-4) that are submerged in the water, generate high frequency acoustic pulses, and capture subaqueous topography of actively deforming sand beds by measuring the distance between them and the channel bed. Sampling frequency of the sensors is dependent on the number of sensors sampled and when the SMS is moving at a given rate, sampling frequency determines measurement point density. In this

experiment, only 16 sensors (odd-numbered sensors) were used so data would have higher point densities in the along-stream direction. The sensors were positioned across the flume with sensor 1 closest to the right flume wall (Y = -0.9745m) and sensor 31 closest to the left flume wall (Y = -0.0583m). The positions of the 16 sensors are shown in

Table 3-1. Data collected from these sensors were analyzed to yield flow depth, bedform heights, bedform lengths and bedform migration rates.

Table 3-1. Seatek® sensors and their position in Y direction.

Seatek® sensor	Y (m)	Seatek® sensor	Y (m)
1	-0.9745	17	-0.4855
3	-0.9135	19	-0.4245
5	-0.8525	21	-0.3635
7	-0.7915	23	-0.3025
9	-0.7303	25	-0.2413
11	-0.669	27	-0.1805
13	-0.608	29	-0.1193
15	-0.547	31	-0.0583

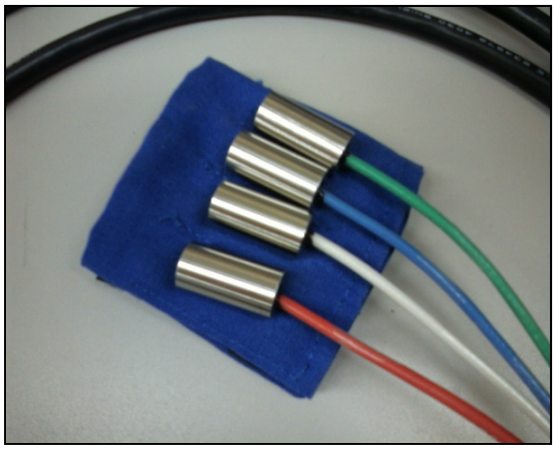

Figure 3-4. Four Seatek® echo-sounder sensors (Photo taken by author).

The MassaSonic® ultrasonic sensors (Figure 3-5) generate high frequency ultrasonic pulse directed at water-surface and measure the time it takes for the echo to return. The return time is used to calculate the distance to the water surface. The Massa® sensors were used in the experiment to determine water-surface slope and flow depth. Only Massa® sensor number 1, 3, and 5 were used in this experiment. They were positioned across the flume in approximately equal increments (Table 3-2). Number 1 was closest to the right flume wall and number 5 was closest to the left flume wall.

Table 3-2. Massa® sensors and their position in Y direction.

Massa® sensor	Y (m)
1	-0.805
3	-0.499
5	-0.206

Figure 3-5. A Massa® ultrasonic sensor (Photo taken by author).

The sensors were attached to a mechanical arm moved by a stepper motor and ball-screw mechanism (Figure 3-3) that lowered the Seatek® sensors into water during an along-stream scan and lifted the sensors up when the scan

was complete. The whole SMS was mounted on a mechanical assemblage that moved the SMS in the stream-wise direction using a stepper motor that was attached to the cart and a timing belt that was attached to the flume. The position of the instruments and all sensor signals were recorded to an onboard computer.

The coordinate system of the EFSDL flume follows a right-hand rule. The origin of stream-wise (X) position is at the beginning of the open channel, and increases positively downstream (Figure 3-6). The origin of the cross-stream (Y) position is the Plexiglas wall on the left side of the flume (looking downstream), and increases negatively across the channel. The origin of vertical position (Z) is at the top of rails, and increases negatively as it goes vertically downward.

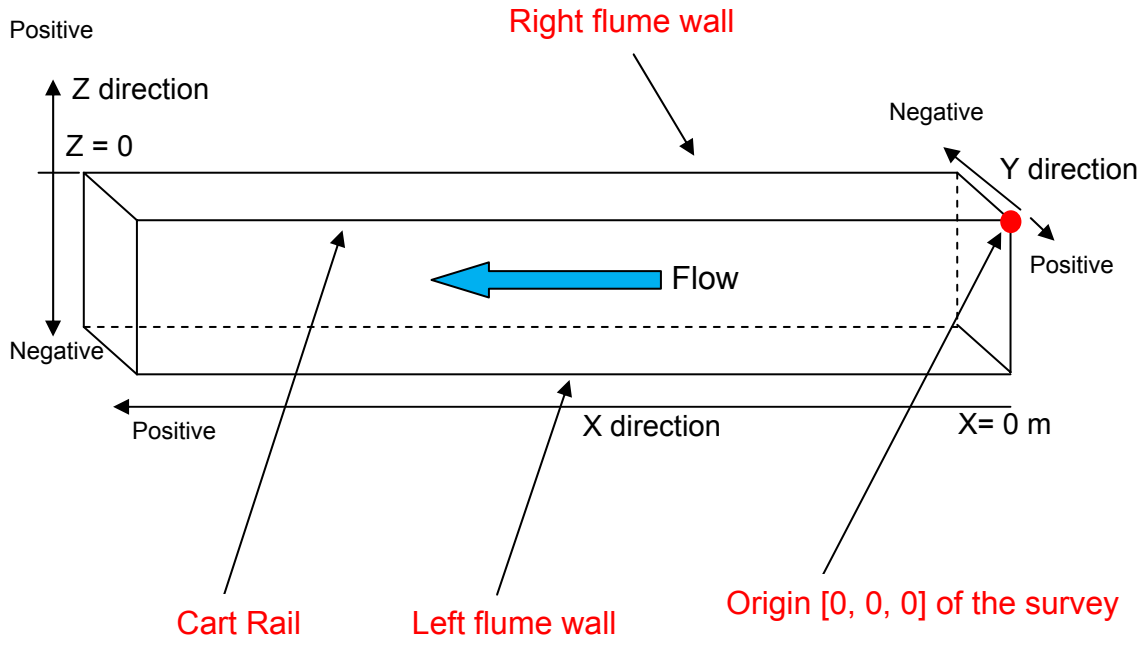

Figure 3-6. EFSDL flume coordinate system.

3.2.2 Experimental design

The experiment consisted of three runs that were designed to examine bedform kinematics under bedload-dominated, mixed and suspension-dominated conditions, which were defined using the Shields number (τ^*). Following *Church* [2006], ($0.01 < \tau^* < 0.1$) is a bedload-dominated transport stage, ($0.1 < \tau^* < 1$) is a mixed transport stage and ($1 < \tau^*$) is a suspension-dominated transport stage. The critical Shields number (τ^*_c) for 0.55mm sand is 0.03 [*Van Rijn*, 1993]. The corresponding ranges of τ^*/τ^*_c are 0 to 3.3 for the bedload-dominated transport stage, 3.3 to 33 for the mixed transport stage and > 33 for the suspension-dominated transport stage.

To calculate the Shields number, I first calculated shear stress (τ):

$$\tau = \rho g d S \tag{3-1}$$

where ρ is the density of water (1000 kg/m^3), g is acceleration due to gravity (9.81 m^2/sec) and S is the slope of the water surface. The experiment was designed so that flow depth (d) was held constant at 0.15m. Dune height and length are known to vary with flow depth, so by holding the depth constant, any observed variation is due to transport stage and not flow depth.

Shear stress was corrected for sidewall stress following *Williams* (1970),

$$\tau_{(\text{corrected})} = \tau \frac{1}{1+0.18(\frac{d}{w^2})} \tag{3-2}$$

where w is the flume width. Shields number (τ^*) was calculated from the sidewall-corrected shear stress as

$$\tau = \frac{\tau_{(\text{corrected})}}{g(\rho_s - \rho)D_{50}} \quad (3\text{-}3)$$

where ρ_s is the density of the sediment (2650 kg/m^3) and D_{50} is the median grain size (550μm).

Flow depth was held constant, so water-surface slope was an independent variable. The slope of the channel was measured with an electronic gauge mounted to the lab floor and the flume at X = 0.84 m that gave the vertical component of the slope. The resolution of the gauge is 0.01mm, but the practical resolution is on the order of 0.1mm. Water-surface slope relative to the channel was obtained along profiles measured using the Massa® sensor. The sum of the two slope measures were used to calculate the design shear stress (Table 3-3). Water-surface slope relative to the channel was not measured during the setup of the bedload-dominated transport stage and subsequent analysis of the data revealed that the observed τ^*/τ^*_c was 1.7 times greater than the design value. This placed the run in the lower end of the mixed transport stage, but my visual observations of sediment movement were consistent with a bedload-dominated transport stage. The observed τ^*/τ^*_c value for the suspension-dominated transport stage is 14% less than the design value and is at the high-end of the mixed-transport stage range according to *Church* [2006]. However, my visual observations of sediment movement were consistent with a suspension-dominated transport stage.

Table 3-3. Design slope and τ^*/τ^*_c values and observed τ^*/τ^*_c value.

Runs	Flume slope ($\times 10^{-4}$)	Water surface slope ($\times 10^{-4}$)	Slope (S) ($\times 10^{-4}$)	τ	τ (corrected)	τ^*	Design τ^*/τ^*_c (τ^*_c =0.03)	Observed τ^*/τ^*_c
Bedload-dominated	8.26	Did not measure	8.26	1.22	1.18	0.133	4.23	7.16
Mixed	13.3	25	38.0	5.59	5.45	0.612	20.4	18.3
Suspension-dominated	40.5	25	65.5	9.64	9.39	1.05	35.1	29.8

To ensure that the flow condition would produce dunes, I calculated mean velocities ($\overline{U}$) and compared the condition to the bedform phase diagrams of *Southard and Boguchwal* [1990](Figure 3-7).

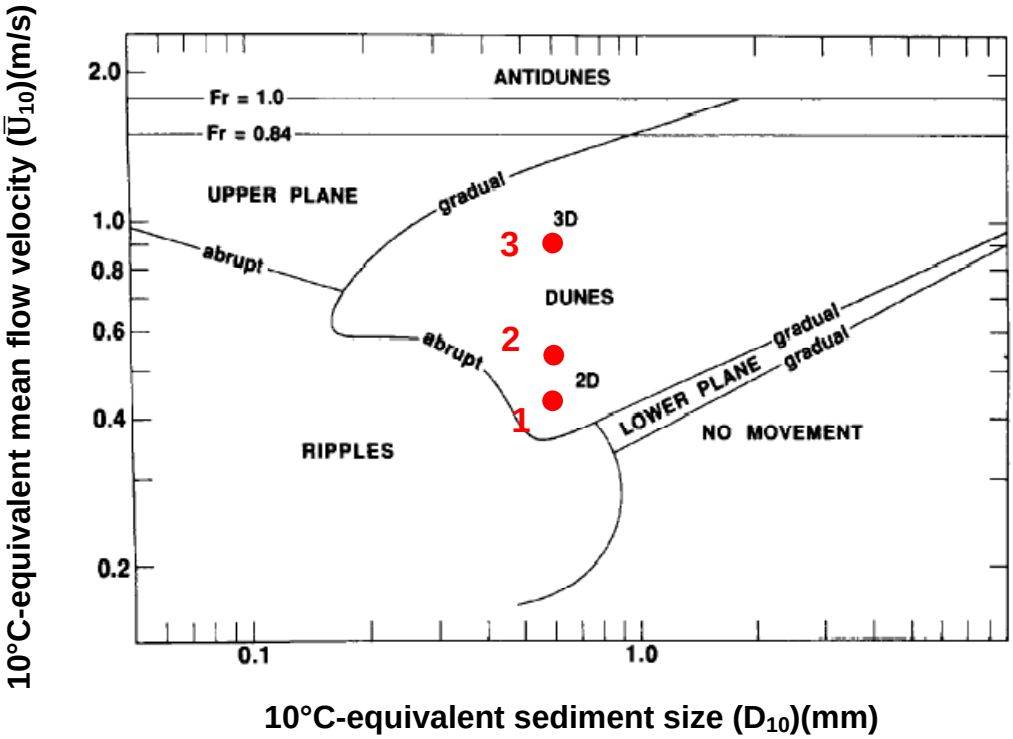

Figure 3-7. Phase diagram of bedforms generated at different mean flow velocity and sediment size [*Southard and Boguchwal*, 1990]. Number 1, 2 and 3 are runs of bedload-dominated, mixed and suspension-dominated transport stage, respectively.

Mean flow velocity was calculated as

$$\overline{U} = \frac{Q}{wd} \qquad (3\text{-}4)$$

where d is the design flow depth (0.15m). The discharge (Q) of the flow was measured by an acoustic transit time pipe flow-metre. The temperature of the water in the flume was assumed to be 20°C (air temperature) and flow velocity

was converted into 10°C-equivalent mean velocity ($\overline{U}_{10}$) to be displayed on Figure 3-7:

$$\overline{U}_{10} = \overline{U}_{20}(\frac{\mu_{10}}{\mu_{20}})^{1/3} \quad (3\text{-}5)$$

where $\overline{U}_{20}$ is the mean flow velocity at 20°C, μ_{10} is the molecular viscosity of water at 10°C, μ_{20} is the molecular viscosity of water at 20°C. Calculations for each run are displayed in Table 3-4.

Table 3-4. Conversion of mean flow velocity at 20°C to 10°C-equivalent velocity.

Runs	Q (m^3/sec)	w (m)	d (m)	$\overline{U}_{20}$ (m/s)	$\overline{U}_{10}$ (m/s)
Bedload	0.065	1	0.15	0.433	0.474
Mixed	0.088	1	0.15	0.587	0.641
Suspend	0.13	1	0.15	0.867	0.916

Mean grain size of sediment under 20°C-water ($\overline{D}_{20}$ = 550μm) was converted to 10°C-equivalent mean sediment size ($\overline{D}_{10}$) using the formula,

$$D_{10} = D_{20}\,(\frac{\mu_{10}}{\mu_{T20}})^{2/3} \quad (3\text{-}6)$$

where D_{10} was calculated to be 657μm. Bedload-dominated, mixed and suspension-dominated transport stages all fall into the dune occurrence field (Figure 3-7).

3.2.3 Experimental procedure

After the desired flow depth and slope were set for a transport stage, the flume was run until an equilibrium was reached where water-surface slope and flow depth became constant. The flume was run for 72 hours for the bedload-dominated and mixed transport stages and 30 hours for the suspension-dominated transport stage. After reaching equilibrium, flume slope, water-surface slope and flow depth were checked against design values. Qualitative observations of bed morphology and sediment transport were used to ensure the flow was generating the correct transport stage.

Each transport stage was run for approximately 18 hours after the equilibrium, over several days. The flume was shut down at the end of each day with the time recorded. Since the water was left standing in the channel, I assumed the effect caused by the interruption to the flow could be ignored and there is no evidence of an effect in the data.

At least 6m of the flume were surveyed repeatedly during each run with the SMS. The area covered by surveys, the speed of the SMS during surveys, and the periods between surveys were different among runs (Table 3-5).

The SMS was run at a faster speed on the second and third days of the bedload-dominated transport stage. Speed adjustment was made to minimize disturbance to the water surface. The SMS was run at a much faster speed during suspension-dominated transport stage. Since the data density was reduced at higher SMS speeds, surveys were collected every five minutes at the suspension-dominated transport stage.

Water temperature (Table 3-6) did not vary much during the course of a run, so was only measured at the beginning and the end on the same day of a run.

Table 3-5. Experiment time schedule and survey settings

Run	Bedload (survey 1-17)	Bedload (survey 24-144)	Mixed	Suspend
Number of surveys	114		94	193
Time span (hr)	20.3		16.9	16.0
Start survey position at X (m)	5	5	5	4
End survey position at X (m)	11	11	12	12
Speed of SMS (m/s)	0.02	0.04	0.05	0.2
Survey frequency (min)	Every 10	Every 10	Every 10	Every 5

Table 3-6. Water temperature at the start and end of a day

Experiment		Water temperature at the start of a day (°C)	Water temperature at the end of a day (°C)
Bedload	Day 1	10	10
	Day 2	15	16
	Day 3	16	16
Mixed	Day 1	11	11
	Day 2	16	17
Suspend	Day 1	11	11
	Day 2	11	11

Bedload transport was measured with miniaturized Helley-Smith samplers [*Helley and Smith*, 1971] that had a 0.02 by 0.02m mouth with the body of the sampler scaled to the mouth (Figure 3-8)[*Dietrich and Smith*, 1984; *Mohrig and Smith*, 1996]. A mesh bag with an opening of 310μm was attached to the back of a sampler. Each sampler was glued to a thin stainless steel plate and two samplers were attached to a holding rod. Samplers were placed on either side of the holding rod making it a sampler set (Figure 3-8a). The distance from the holding rod to the centre of each samplers' mouths is 0.065m. One sampler rested directly on the sediment surface while the other was placed 0.02m above the channel bed. As a result, one sampler collected sediment moving within the

bottom 0.02m of the flow and the other collected sediment between 0.02 and 0.04m above the bed. Three sampler sets were evenly spaced across the flume and mounted on a Plexiglas block positioned across the flume channel (Figure 3-8b).

Bedload samples were collected over bedform crests with one sampler set at a time for a set amount of time. After sampling with all three sampler sets, a sampling trial was completed. However, some sampling trials did not contain samples from all three sampler sets because sampling conditions were poor and samples taken were considered unrepresentative. Poor sampling conditions occurred when the bedform crest was washed out or when the operator could not identify a sampling spot. Samples were dried and weighed. The bedload data presented here are averages of all samples collected from the bottom sampler in a sampling trial. Observations from the top samplers are not presented here.

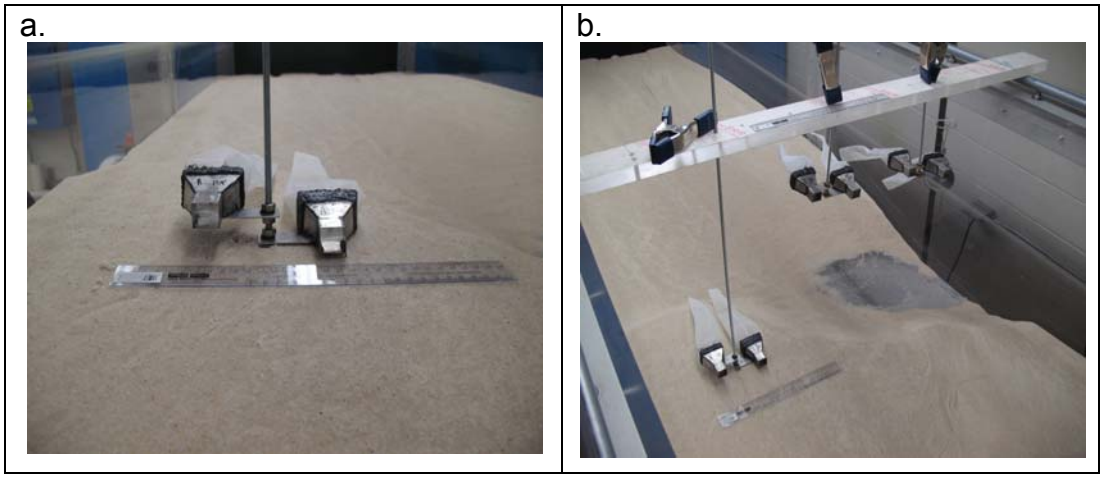

Figure 3-8. Miniaturized Helley-Smith samplers (Photos taken by author).

Suspended-sediment samples were collected with a siphon system composed of a copper tube, a nylon tube and a small variable speed pump (Figure 3-9). The copper tube had an outer diameter of 0.00635m (1/4 inch) and an inner diameter (I.D) of 0.005m. The tube was mounted on a point gauge with a Venier scale incremented at 0.3mm (0.001 feet). The nylon tube had an opening of 0.00635m (I.D.) and was connected to the copper tube at one end and to a one-litre-sample bottle at the other end through a small pump. A sampling trial is complete after a one-litre sample was taken at 0.04m from the bed in the centre of the channel. The pump rate was calibrated to the flow velocity at the intake calculated from the Law-of the-Wall to generate isokinetic flow. Water samples were filtered and the filters were dried and weighed to find sediment concentrations.

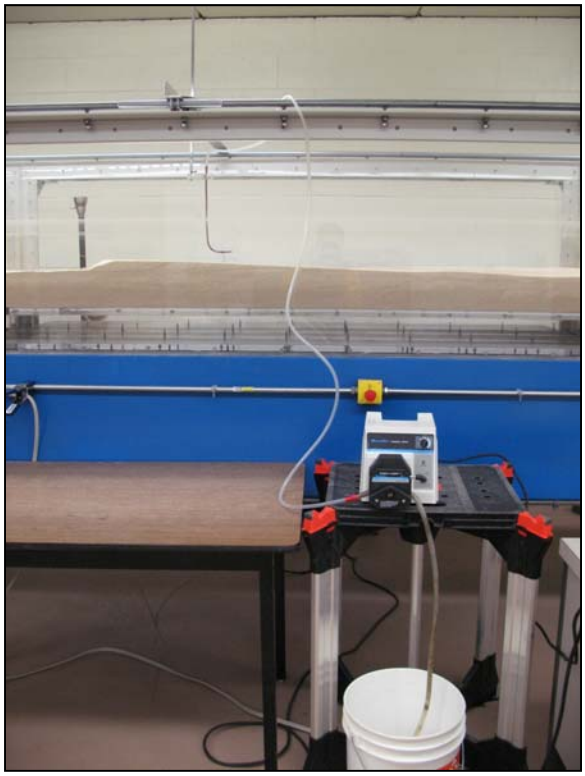

Figure 3-9. Apparatus for collecting suspended-sediment sample (Photo taken by author).

3.2.4 Data Processing

Acoustic noise was present in many of the Seatek® surveys and was removed with an algorithm written in MATLAB® that has three levels of filters. The first filter removed elevation readings that are obviously noise, which were 0.18m above the Plexiglas flume floor (Z > -0.46m) and below the Plexiglas bottom of the flume (Z < -0.64m). The second filter used a running average that removed data identified as noise. In the second filter, for every point (point *i*) elevation reading in each along stream profile, an average value was calculated from twenty points around this point (ten before point *i* and ten after). Elevation readings at point *i* were removed from the data set if value of point *i* exceeded the average value by 0.003m or was less than the average value by 0.001m.. These values were not replaced. The remaining data went through a third filter that ran the same running average to smooth the elevation profile by replacing 'noise' with the averaged value.

Figure 3-10 shows examples of original data (blue lines) and the filtered data (red lines) from a single Seatek® sensor at bedload-dominated (Figure 3-10a), mixed (Figure 3-10b), and suspension-dominated (Figure 3-10c) transport stage. Spikes in the blue profile are noise removed by the filtering process.

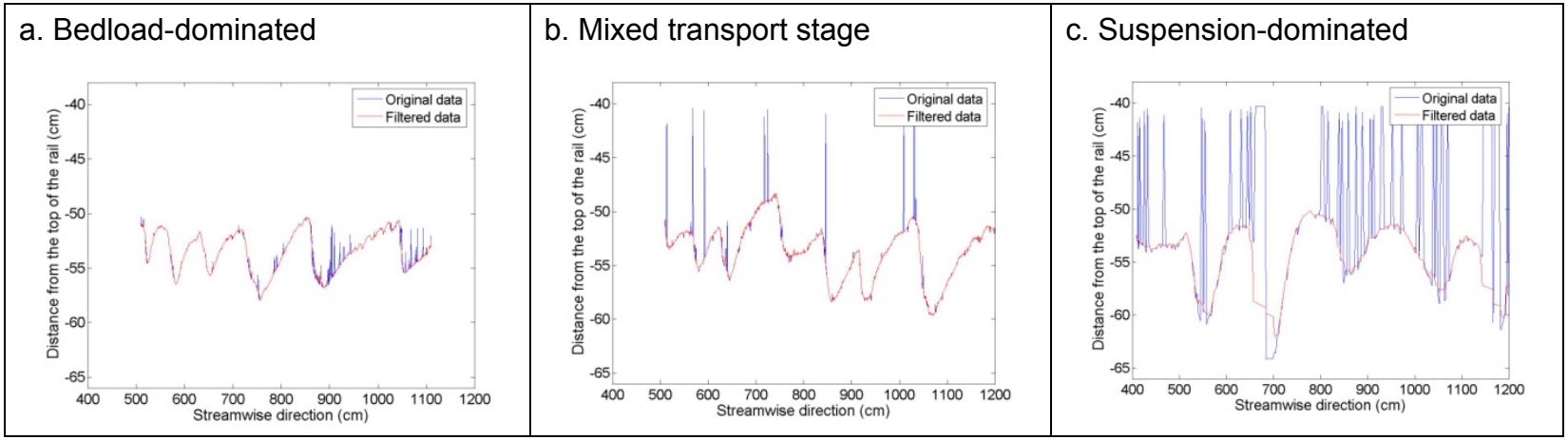

Figure 3-10. Examples of original data (blue lines) and the filtered data (red lines).

3.2.5 Data Analysis

3.2.5.1 Water surface and flow depth calculation

Water-surface data were filtered to remove noise using the algorithm that removed noise from the bed topography data. To calculate flow depth, water-surface data collected by Massa® sensor numbers one, three and five were compared against bed topography data collected by the Seatek® sensors that were closest: in the Y-direction number seven, seventeen, and twenty-seven, respectively (Table 3-7). Figure 3-11 shows the water-surface profile along the centre of the channel in one of the bedload-dominated transport stage surveys. A linear trend line was fitted through water-surface profile and bed topography profile. Water-surface slope was determined by the slope of the trend line. Flow depth was obtained by calculating the distance between the two trend lines at the middle of the survey window. Water-surface slope and flow depth were calculated from all three along-stream profiles and the values were averaged to produce a representative water-surface slope and flow depth for a single survey. The total slope of the survey was calculated by adding the flume slope on top of the water slope.

Table 3-7. Co-location scheme between Massa® and Seatek® sensors.

Massa® sensor	Y (m)	Seatek® sensor	Y (m)
1	-0.805	7	-0.7915
3	-0.499	17	-0.4855
5	-0.206	27	-0.1805

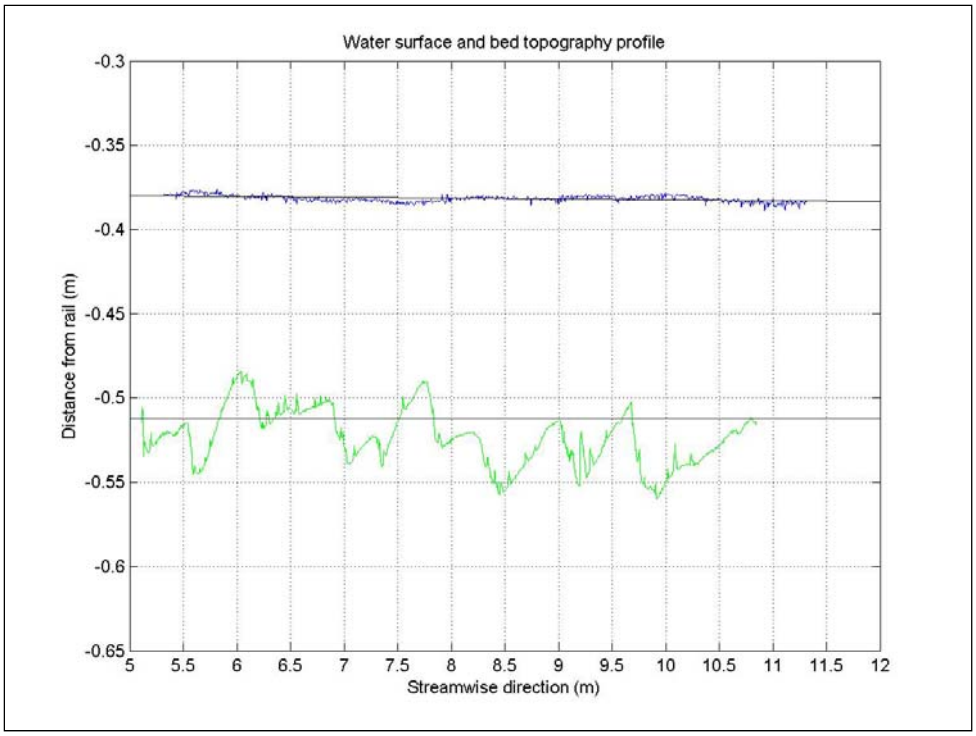

Figure 3-11. Example of a water-surface profile and bed elevation profile. The blue profile is the water surface collected by Massa® sensor 3 and the green profile is the bed topography collected by Seatek® sensor 17. The solid black lines are linear regressions.

3.2.5.2 Bedload and suspended-load transport measurement

The bedload sediment flux was calculated by dividing the weight of the sample by the sampling time and the width of the flume to give transport time per unit channel width.

The suspended-sediment flux was calculated using the Rouse equation [*Rouse*, 1939]

$$\frac{C}{C_\alpha} = \left(\frac{h-z}{z}\ \frac{\alpha}{h-\alpha}\right)^{\frac{w_s}{\beta\kappa u^*}} \tag{3-7}$$

where C is the concentration of suspended-sediment at height z above the sediment bed, α is the distance from the bed of the reference concentration C_α (measured at 0.04m), w_s is the grain settling velocity calculated using the relations of *Dietrich* [1982], β is a coefficient that describes the difference in diffusion between a sediment particle and a fluid particle (assumed to be 1), κ is the von Karman constant (0.41), and u* is the shear velocity ($u^* = (\tau/\rho)^{0.5}$). The reference concentration (C_α) was calculated from the suspended sediment samples by assuming the density of sediment (ρ_s) was 2650 kg/m^3. I calculated the suspended-load transport measurement as (q_{ss})

$$q_{ss} = \bar{C}\,\bar{U}\,\bar{d}\,\rho_s \tag{3-8}$$

where ($\bar{C}$) is the depth-averaged concentration, $\bar{d}$ is the average flow depth for the run, and $\bar{U}$ is the depth-averaged flow velocity for the run calculated by dividing the discharge by the averaged flow depth and the width of the flume.

3.2.5.3 Bed Mapping

The processed Seatek® data were used to generate a series of topographic maps of the bed. Grid files were generated using the settings shown in Table 3-8. Figure 3-12a shows bed topography generated from grid files with a 0.025×0.025m grid spacing at bedload-dominated transport stage. The colour scheme indicates the elevation of the bed relative to the top of the flume cart rail, which would be -0.64m for the bottom of the flume channel. Elevation change between surveys was obtained by subtracting one grid from another as in Figure 3-12b.

Table 3-8. Settings for creating surface grids from bed topography data.

Griding method: Kriging					
	Grid axis	Minimum (m)	Maximum (m)	Grid spacing (m)	Number of grid lines
Bedload	X-axis	5	11	0.025	240
	Y-axis	-1	0	0.025	40
Mixed	X-axis	5	12	0.025	280
	Y-axis	-1	0	0.025	40
Suspend	X-axis	4	12	0.025	320
	Y-axis	-1	0	0.025	40

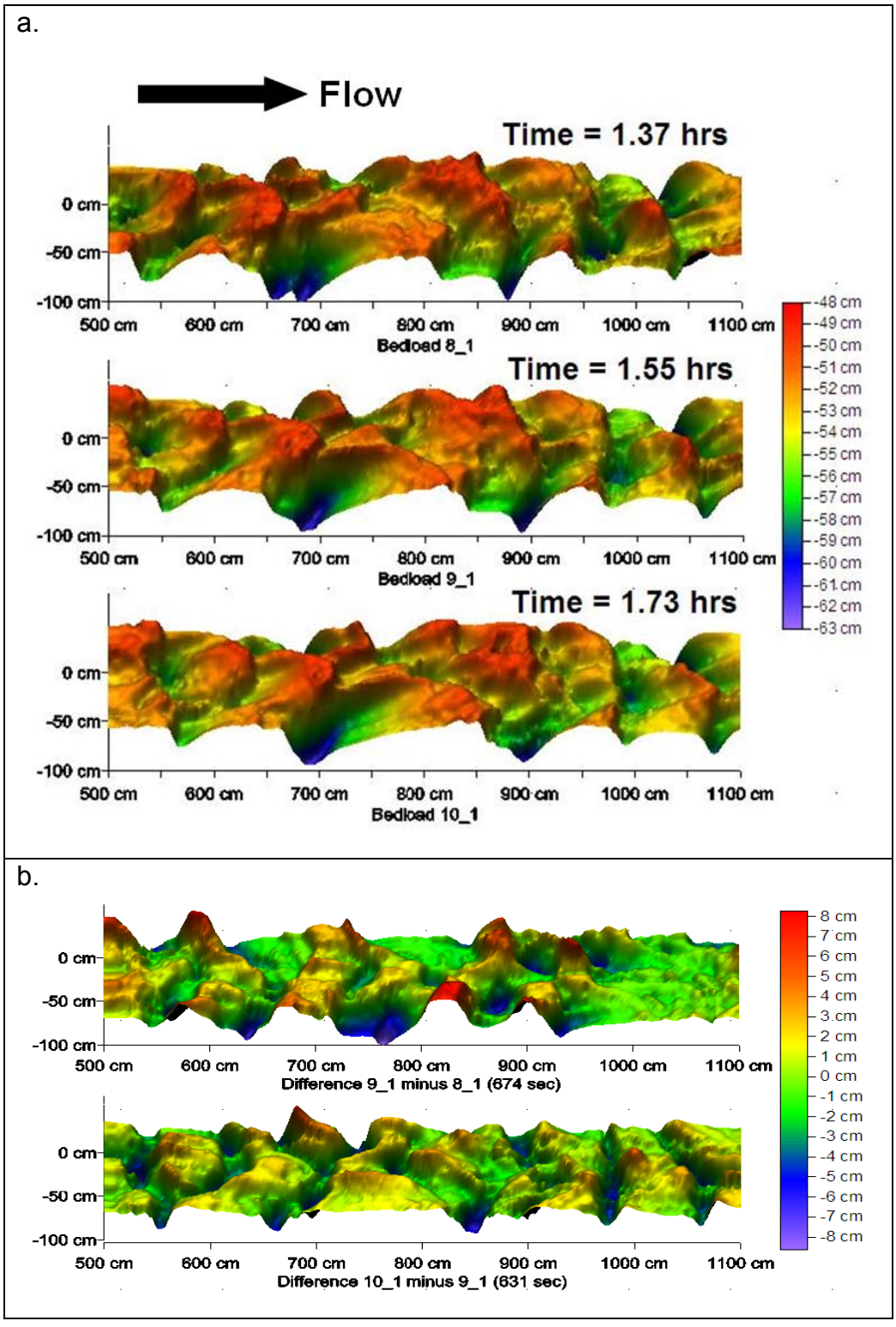

Figure 3-12. Bed topography and elevation change during bedload-dominated transport stage. Vertical axis on the diagram is the Y-direction of the flume.

3.2.5.4 Bedform dimensions calculation

Bedform dimensions were obtained with an automated method that was verified against conventional (manual) measurements. The conventional method used along-stream profiles obtained with Seatek® sensor 17, which was closest to the centre of the flume channel (Y = 0.-4855m). The profile was detrended and printed on paper (Figure 3-13). Bedforms that exceed a height of 0.01m and a length of 0.30m were measured manually with a ruler. Bedform heights were measured from the peak to the trough on the lee side of the bedform. Average height for each survey was obtained by summing all the heights from the profile and dividing by the number of measured bedforms in the profile. Bedform lengths were measured between two continuous troughs, and since bedforms were continuous, their average length was obtained by measuring the total distance of a train of bedforms, and divided by the number of the bedforms within the train. In bedload-dominated and mixed transport stage, incomplete bedforms were not included in the analysis. However, to reflect the fact that suspension-dominated transport stage frequently produced very long bedforms that extended beyond the boundary of survey window, the length of these long but 'incomplete' bedforms were also measured when they were greater than the average length of the other bedforms. Their height, however, could not be measured if their lee-side trough was beyond the survey window.

Examples of the conventional method of calculating bedform dimensions at bedload-dominated, mixed and suspension-dominated transport stage are shown in Figure 3-13ab, Figure 3-13cd and Figure 3-13ef, respectively.

Numbers shown in the figures are distances measured on paper in centimetres, which were later converted into real distance. For Figure 3-13e, the length of the bedform to the right (7.7cm on paper) is longer than the average length of the three bedforms to the left (1.97cm on paper), so it was included in the analysis. However, its height was not measured because its lee-side trough was beyond the survey boundary.

The conventional method was used for 114 surveys at bedload-dominated transport stage, 94 at mixed transport stage and 193 at suspension-dominated transport stage. This manual method produced statistics for the channel centreline, but was too labour intensive to pursue for all 16 along-stream profiles.

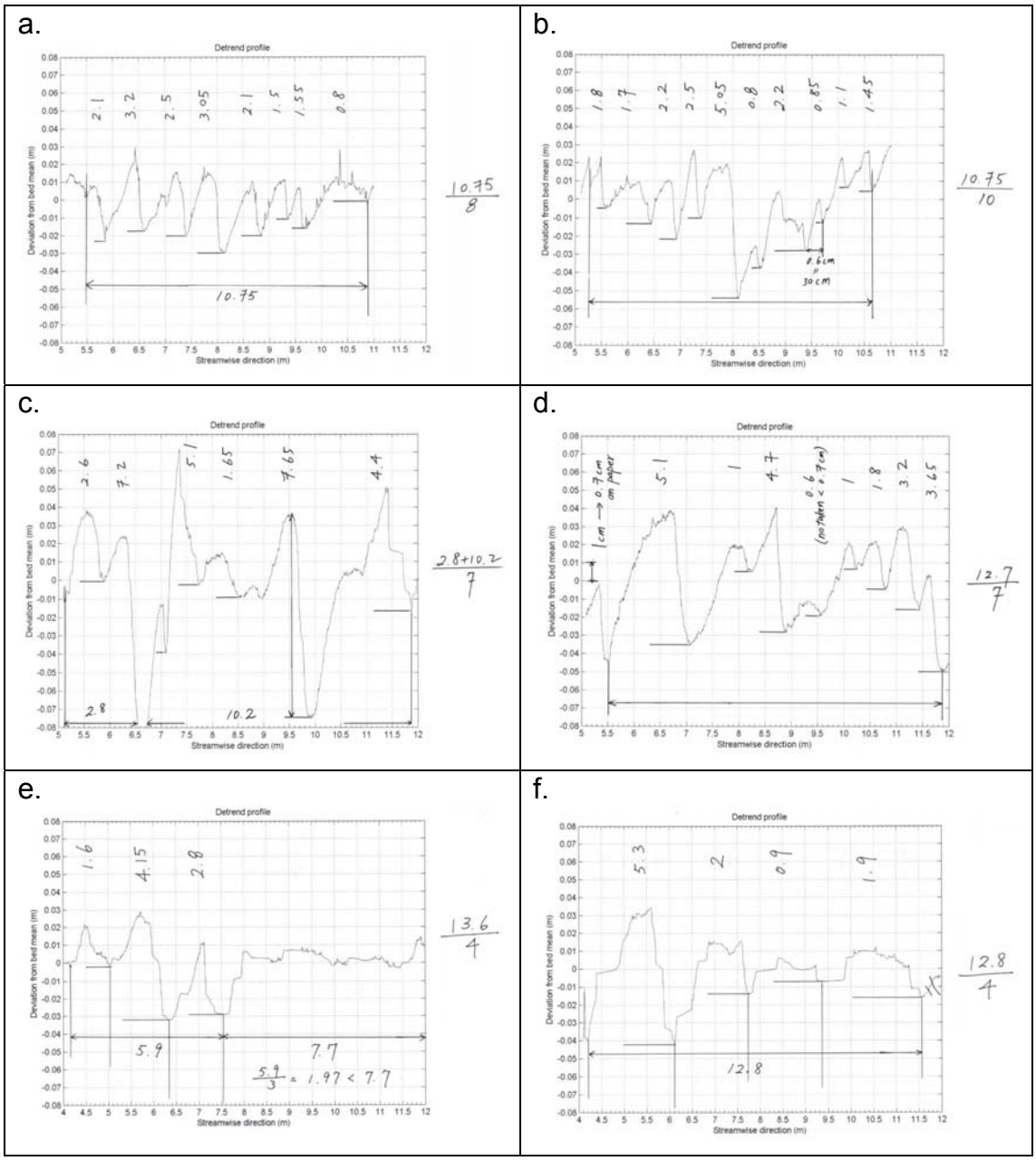

Figure 3-13. Examples of bedform dimensions calculation with conventional method.

In order to generate a more complete representation of bedform dimension variability with flow stage, measurements of bedform heights and lengths were automated using MATLAB® code developed by *McElroy* [2009]. The algorithm creates a 'roughness' function from an elevation profile that characterizes the variability of bed elevation over a certain length of the profile. Roughness (W) is calculated as the root mean square of elevation

$$W = \left[\frac{1}{n}\sum_{i=1}^{n}(\eta_i - \bar{\eta})^2\right]^{1/2} \quad (3\text{-}9)$$

where n is the number of data, η is the bed elevation, and the over bar represents an average over the length of the profile [*Jerolmack and Mohrig*, 2005a]. The algorithm calculates a roughness value for a given length of the profile and when the length of the profile incrementally increases, the algorithm is able to generate a continuous roughness function (Figure 3-14a). The roughness function slope is calculated for each point as in Figure 3-14b producing a slope curve. A saturation length (L_{sat}) is calculated where the logarithmic slope is half the maximum value. I modified the algorithm in order to ensure the half-maximum value is chosen from the first peak in the logarithmic slope when multiple curves existed. The relation between the saturation length of a waveform and its geometric length is $L_{sat} \approx 4/\omega$, where ω is the angular frequency of the waveform. Characteristic bedform length (L_c) is defined as $L_c = 2\pi/\omega$. The relation between characteristic length and saturation length would be

$$L_c = \frac{2\pi}{\omega} \cong \frac{2\pi}{4} L_{sat} \cong 1.57 L_{sat} \quad (3\text{-}10)$$

[*McElroy*, 2009].

The saturation height (R_{sat}) is calculated from the standard deviation of the elevations profile. In addition, $\mathrm{R_{sat}} = \mathrm{A}/\sqrt{\omega}$, where A is the amplitude of the waveform. Characteristic bedform height (H_c) is defined as $\mathrm{H_c} = 2\mathrm{A}$ because bedform height is the distance from the peak to the trough of a wave. The relation between characteristic height and saturation height is

$$\mathrm{H_c} = 2\mathrm{A} = 2\left(\sqrt{2}\mathrm{R_{sat}}\right) \cong 2.8\mathrm{R_{sat}} \tag{3-11}$$

[*McElroy*, 2009].

In order to use the algorithm, input data were linearly interpolated with even-spacing of 0.005m and were detrended. This method was used for 114 surveys at bedload-dominated transport stage, 94 at mixed transport stage and 193 at suspension-dominated transport stage. This automated method produced statistics for all 16 along-stream profiles.

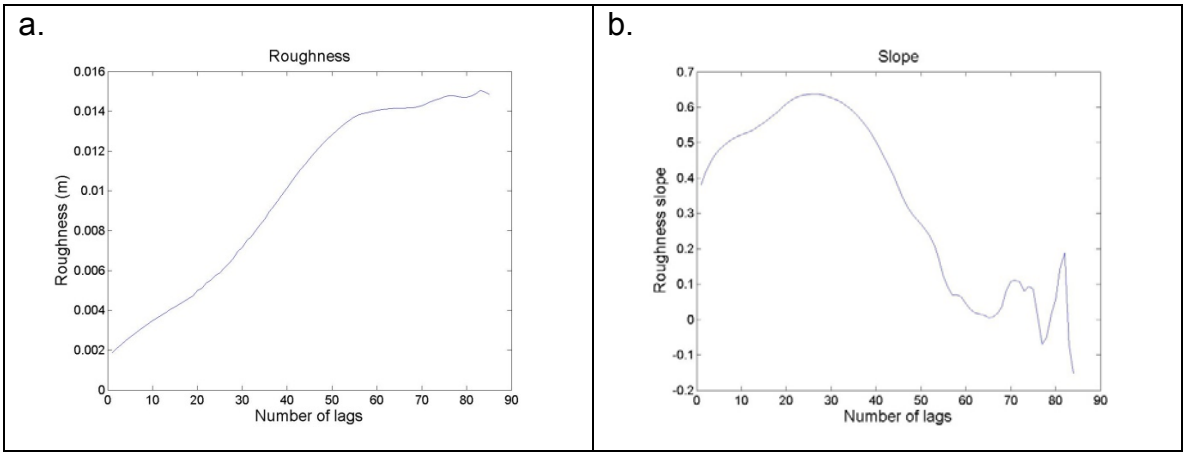

Figure 3-14. (a) Roughness function generated from a detrended elevation profile; (b) logarithmic gradient slope calculated from the roughness function.

3.2.5.5 Bedform translation calculation

Bedform translation was also obtained with an automated method that was verified against conventional (manual) measurements. Along-stream profiles from two surveys obtained with Seatek® sensor 17 were printed on paper as in Figure 3-15. Bedforms in the earlier survey that exceeded 0.01m in height were identified and the corresponding bedforms in the later survey were also identified. Translation distance of a bedform between two surveys was measured between peaks with a ruler. When a big bedform in the earlier survey split into two smaller bedforms in the later survey, I selected the nearest downstream crest in the later survey to calculate the translation distance. However, when two bedforms in the earlier survey merged into a single bedform in the later survey, I selected the crest further upstream in the earlier survey to calculate the translation distance. Some bedforms changed their geometry instead of changing in stream-wise position. These bedforms were interpreted to move 0 m. After average bedform translation distance and the time elapsed between two surveys was obtained, the average translation rate of bedforms between two surveys could be calculated.

Examples of the conventional method of calculating bedform translation distances at bedload-dominated and mixed transport stage are shown in Figure 3-15a and Figure 3-15b, respectively. Numbers shown are distances (in centimetres) of bedform translation between the two surveys. In Figure 3-15a, bedforms in the first two groups from the left moved downstream without much change in geometry. Bedforms in the third and sixth group from the left only changed their shapes. Bedforms in the fifth group from the left merged as they

moved. In Figure 3-15b, bedforms in the first group from the left merged as they moved while the bedform in the third group from the left split into two as it moved. Bedforms in the second and forth group from the left moved downstream without much change in geometry. Bedform in the fifth group only changed its geometry.

The manual method was used for 111 surveys at bedload-dominated transport stage and 92 at mixed transport stage. This method was not performed on profiles at suspension-dominated transport stage because bedform shapes changed so much between two surveys I could not identify and match them by eye. This manual method produced statistics for the channel centreline, but was too labour intensive to pursue for all 16 along-stream profiles.

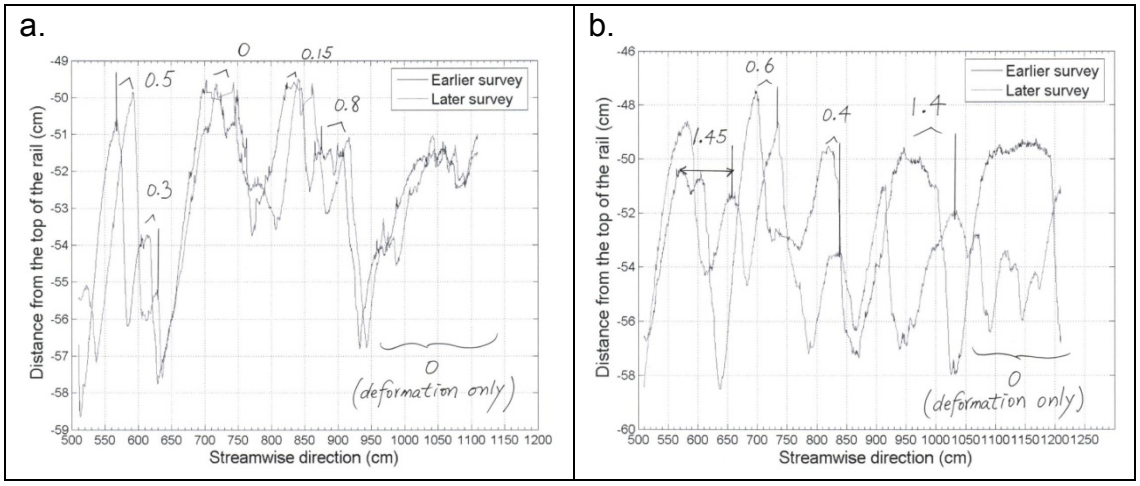

Figure 3-15. Bedform translation calculation with conventional method.

Bedform translation distance between two surveys was also obtained using a correlation technique between two survey profiles. This method computed the mean progression of a bedform profile by finding the optimum congruence between successive mappings of the bed.

Linear interpolations were performed on two consecutive survey profiles to produce an even-spacing of 0.001m. The profile from the later survey was moved forward against the other profile one spacing (0.001m) at a time, and the coefficient of determination (R-square) was calculated between the two profiles. The profiles were moved 1000 times for bedload-dominated transport stage, 1500 times for mixed transport stage, and 3000 times for suspension-dominated transport stage. The R-square value computed from each correlation was plotted against the distance moved. Translation distance between two surveys was the distance that corresponded to the maximum R-square value (Figure 3-16). This method was used for 111 surveys at bedload-dominated transport stage, 92 at mixed transport stage and 191 at suspension-dominated transport stage. This automated method produced statistics for all 16 along-stream profiles.

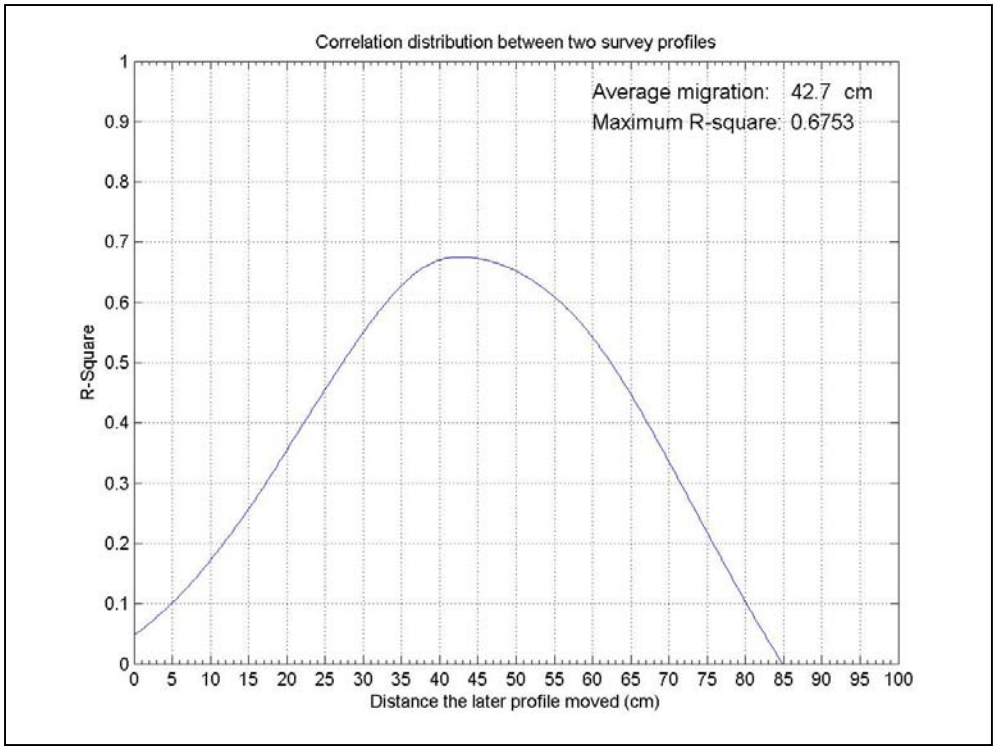

Figure 3-16. Example of correlation technique used to calculate bedform translation.

3.3 Results

3.3.1 Flow and sediment transport

Water-surface slope (Figure 3-17a) and τ^*/τ^*_c (Figure 3-17c) increased as transport stage increased. Variability in water-surface slope, flow depth (Table 3-9) and τ^*/τ^*_c, each represented by its coefficient of variation, all increased slightly from bedload-dominated to mixed transport stage, but increased dramatically from mixed to suspension-dominated transport stage (Table 3-9; Figure 3-18). The flow depth remained approximately constant at 0.15m for the bedload-dominated and mixed transport stages but dropped to 0.134m at the suspension-dominated transport stage.

Measurements of bedload and suspended-sediment transport (at 0.04m above the bed) both increased as transport stage increased (Table 3-10). At the bedload-dominated transport stage, nearly all suspended load was fine silt washload (Table 3-10). This material was derived from the bed sediment, but remained in suspension once entrained. Suspended bed-material load at the bedload-dominated transport stage was negligible. I attempted to account for this by assuming the washload for all the flows was equal to its value at the bedload-dominated stage (0.759 g/sec/m). I calculated the suspended bed-material load for mixed and suspension-dominated transport stage by subtracting the washload from the suspended load.

Bedload (Figure 3-19a) and suspended-sediment (Figure 3-19b) transport measurements increased as transport stage increased. The bedload transport was always greater than the depth-integrated suspended bed-material load. This

was because bedload was calculated from sediment collected between z = 0m and z = 0.02m and suspended bed-material load was calculated as sediment transported between z = 0.02m and z = d. If I restrict the bedload layer to a few grain diameters thick, suspended bed-material load greatly exceeded the bedload all transport stages. The bedload and suspended-load transport measurements in Table 3-10 is further discussed in section 3.3.5 (Bedform translation and deformation) and section 3.4.3 (Translation and deformation).

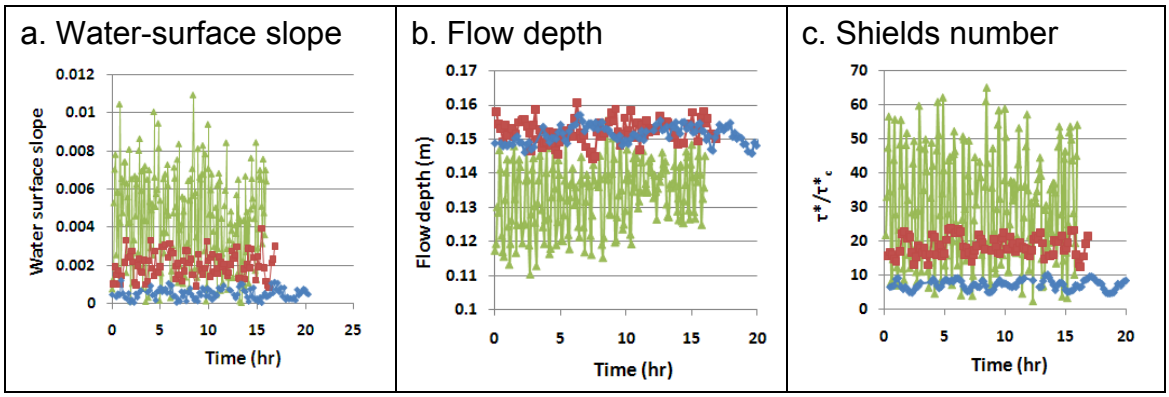

Figure 3-17. Time-series of water-surface slope, flow depth and Shields number at different transport stages. Bedload-dominated, mixed and suspension-dominated transport stages are represented by blue, red and green line, respectively.

Table 3-9. Mean values of Shields number, slope, flow depth, bedform height, bedform length, aspect ratio and translation rate at different transport stages. Bedform height, length, aspect ratio and translation rate were obtained from the automated methods.

Average	τ^*/τ^*_c	S	d (m)	H (m)	L (m)	H/L	Average translation rate (m/sec)
Bedload	7.16 (0.231)	1.32×10^{-3} (0.232)	0.151 (0.0169)	0.0565 (0.0717)	0.961 (0.0993)	0.0593 (0.101)	3.10×10^{-4} (0.151)
Mixed	18.3 (0.194)	3.37×10^{-3} (0.196)	0.152 (0.0226)	0.0828 (0.0912)	1.33 (0.123)	0.0628 (0.108)	11.7×10^{-4} (0.183)
Suspend	29.8 (0.657)	6.12×10^{-3} (0.647)	0.134 (0.0726)	0.0458 (0.205)	2.21 (0.223)	0.0215 (0.283)	44.0×10^{-4} (0.330)

Note: Values in brackets are the coefficient of variation

	Bedload-dominated	Mixed	Suspension-dominated
Water surface slope	a 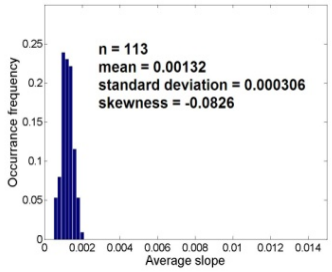	b 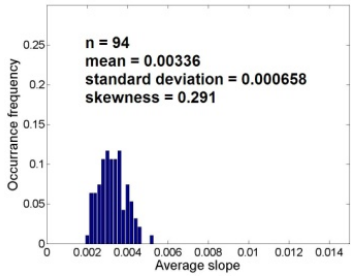	c 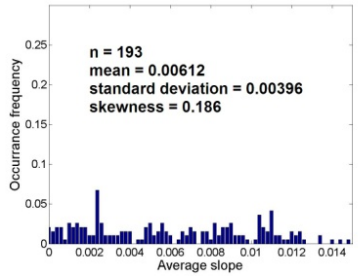
Flow depth	d 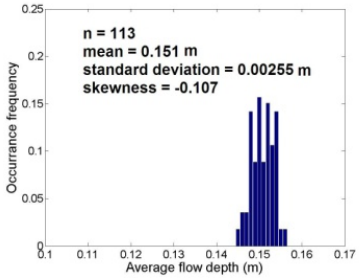	e 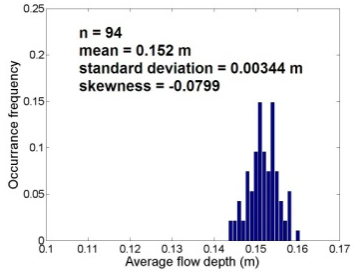	f 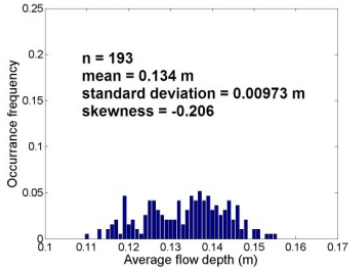
τ^*/τ^*_c	g 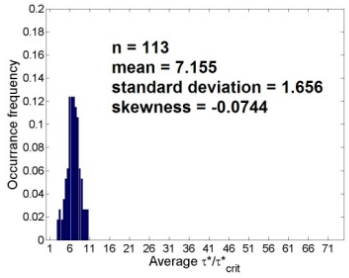	h 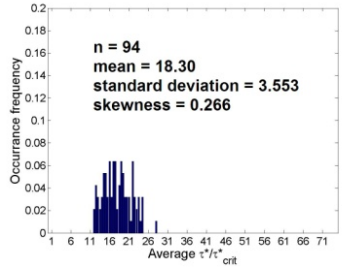	i 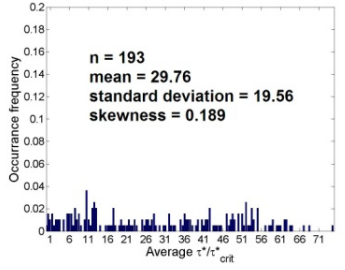

Figure 3-18. Histograms of slope ,flow depth and average τ^*/τ^*_c.

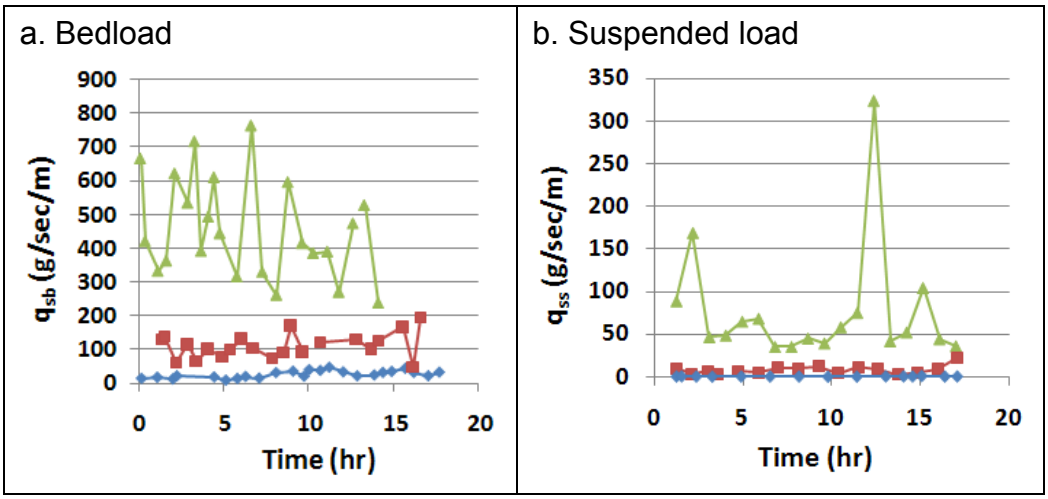

Figure 3-19. Bedload and suspended-sediment transport at different transport stages. Bedload-dominated, mixed and suspension-dominated transport stages are represented by blue, red and green line, respectively.

Table 3-10. Statistics derived from the distribution of measured sediment transport.

Transport stage	Bedload		Depth-integrated suspended load		Depth-integrated suspended bed material load (g/sec/m)
	n	Mean (g/sec/m)	n	Mean (g/sec/m)	
Bedload	24	25.8	15	0.759	0
Mixed	21	111	17	8.10	7.34
Suspended	23	459	18	76.7	75.9

Note: n = number of sampling trials

3.3.2 Bedform migration

3.3.2.1 Bedload-dominated transport stage

Sediment at this transport stage moved by rolling, sliding and bouncing on the bed and only some sand grains were mobile at a time. There was very little bed material measured in suspension. Bedforms moved mainly by translation where bedforms maintain their shapes as they move downstream (Figure 3-12). For example, bedform geometry in survey 8_1 was very similar to survey 10_1 in Figure 3-12a. The two panels in Figure 3-12b show elevation changed between the three surveys in Figure 3-12a also display similar near linear patterns of deposition. When the crest lee slope exceeded the angle of repose, sediment slumped down the slope and the bedform advanced. As a result, the bedform lee angle was sharp and angle of repose asymmetric bedforms dominated [*Kostaschuk and Villard*, 1996]. Most dunes were between 0.04 to 0.06m in height (Table 3-9).

It is clear from Figure 3-12a that the bed was populated by 3-D bedforms [*Venditti et al.*, 2005] where certain parts of the bedform crest lines moved faster and formed lobe-shaped portions of crest lines. Between the lobes were saddle-shaped portions of crest lines. Bedforms moved by having many lobe-shaped crest lines extending downstream at different speeds. Ridges that were parallel to the flow existed between two sinuous crest lines in front of a lobe. Ridges are shown in the survey 9_1 and 10_1 in Figure 3-11a from 0.7 to 0.8m. These plots indicate ridges shifted from side to side. A lobe may move and catch up with the

saddle in the downstream crest line forming a new lobe at the sides of the pre-existing lobe or saddle.

3.3.2.2 Mixed-dominated transport stage

Sediment was moved by bedload in thin sheets but more sediment was entrained and carried in the water column compared to the bedload-dominated case. Bedforms still moved by piling up sediment at crest and slumping down. However, more sediment was entrained from the stoss slope and bypassed the bedform crest. Bedform crest angle became rounder and the lee slope became less than an angle of repose (Figure 3-20). Bedforms deformed as sediment moved into suspension. Comparing bed configurations in Figure 3-20a to those in Figure 3-12a, bedforms at the mixed transport stage deformed more than at the bedload-dominated transport stage over the same period. In addition to shape deformation, bedforms merged and split more often at the mixed transport stage. For example, in Figure 3-20a, two bedforms (one at 0.7m and one at 0.8m) in survey 3_1 merged into one bedform in survey 4_1 that extended from 0.7m to 0.86m. On the other hand, the bedform at 1.08m in survey 3_1 moved to 1.14m in survey 4_1 without much change in its shape. Figure 3-20b shows more random erosion and deposition pattern than the more systematic deposition patterns in Figure 3-12b.

Mean bedform height increased from 0.565m during the bedload-dominated transport stage to 0.828m during the mixed transport stage (Table 3-9). Comparing Figure 3-12 and Figure 3-20, it appears that the bedforms

increased in height because of deeper scour in the trough, which may have been caused by stronger flow separation cells in the mixed load case relative to the bedload-dominated case. However, lower lee face angles were not consistent with stronger flow separation. Thus, increasing bedform height was caused by multiple flow mechanisms but it was unclear to know what these mechanisms were.

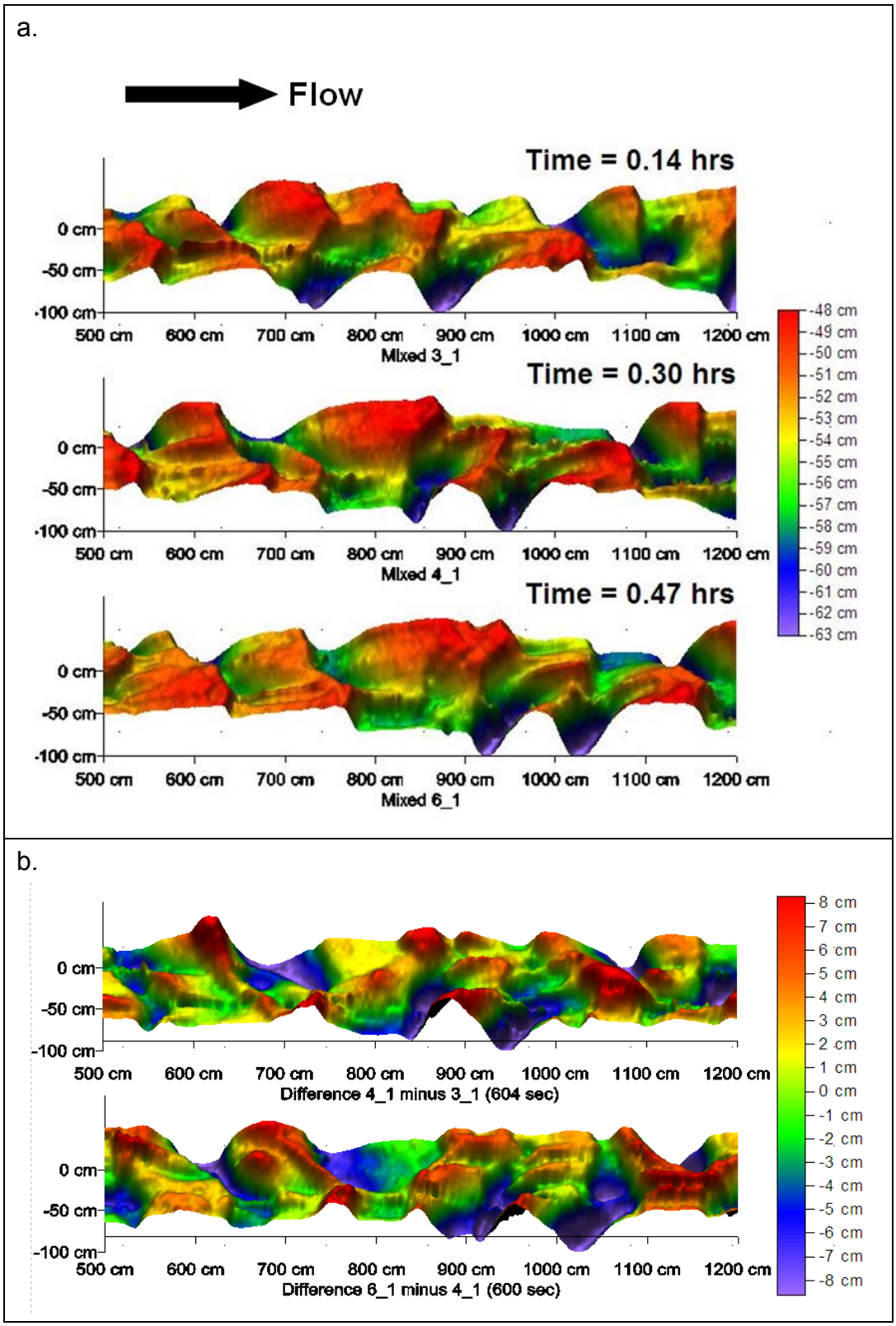

Figure 3-20. Bed topography and elevation change during mixed transport stage. Vertical axis on the diagram is the Y-direction of the flume.

3.3.2.3 Suspension-dominated transport stage

A lot more sediment was in suspension than at mixed transport stage and the water column was clouded with sediment. Sediment that was close to the bed (less than 0.01m) moved slower than sediment in the water column due to friction from the bed. This layer of sediment was dragged by flow across the bedform stoss sides and thrown over the crests. As a result, bedform crest angles were round and lee slope angles were low. However, angle of repose asymmetric bedforms existed but were quickly washed out after several seconds.

Bedforms in the suspension-dominated transport stage were unstable and constantly deforming. Bed configuration changed dramatically in a matter of 5 minutes (Figure 3-21a) and the erosion and deposition patterns differed between surveys (Figure 3-21b). The bed alternated between three phases: 1) plane bed and washed-out dunes (Figure 3-22a), 2) a train of large dunes (Figure 3-22b), and 3) a train of small dunes (Figure 3-21c). In phase one, the bed was mostly flat and most bedforms had lengths ranging from 1.5 to 2.5m and heights ranging from 0.02 to 0.05m. One or two bedforms grew as high as 0.08m. In phase two, the bed was populated by a train of large bedforms that grew up to 0.1m tall and 3m long. In phase three, the bed was populated by bedforms less than 1 m long and 0.02 to 0.04 m in height.

In phase one, flow separation and localized, intense erosion occurred on a plane bed and the back of dunes and split them into the large dunes formed in phase two (Figure 3-22a to b) or small dunes in phase three. Shortly after one localized erosion took place, two other erosion events would take place, one

upstream of the initial erosion and the other one downstream. The distance between the three erosion events were often evenly spaced. In phase two, large dunes may split into smaller dunes (Figure 3-22b to c) and smaller dunes may combine to form larger dunes. Dune fields in phase two or three may wash out into a plane bed (Figure 3-22c to d). A phase may exist from a few minutes to more than half an hour. Transformation between phases could occur over a few seconds or minutes. Plane beds and low-amplitude bedforms seemed to exist longer than the other two phases.

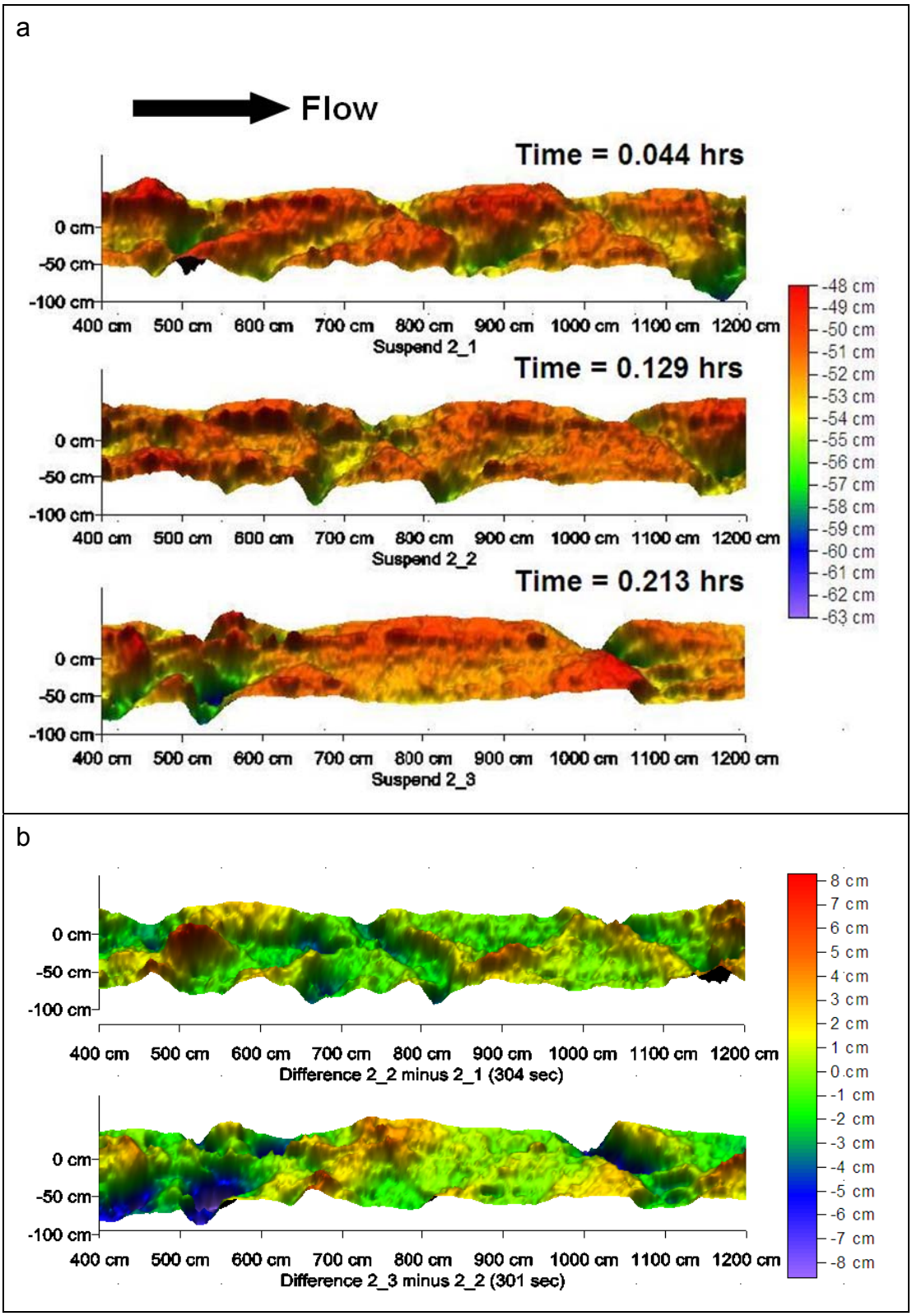

Figure 3-21. Bed topography and elevation change during suspension-dominated transport stage. Vertical axis on the diagram is the Y-direction of the flume. Data from Seatek® sensor 9 and 25 were removed because of excessive acoustic noise.

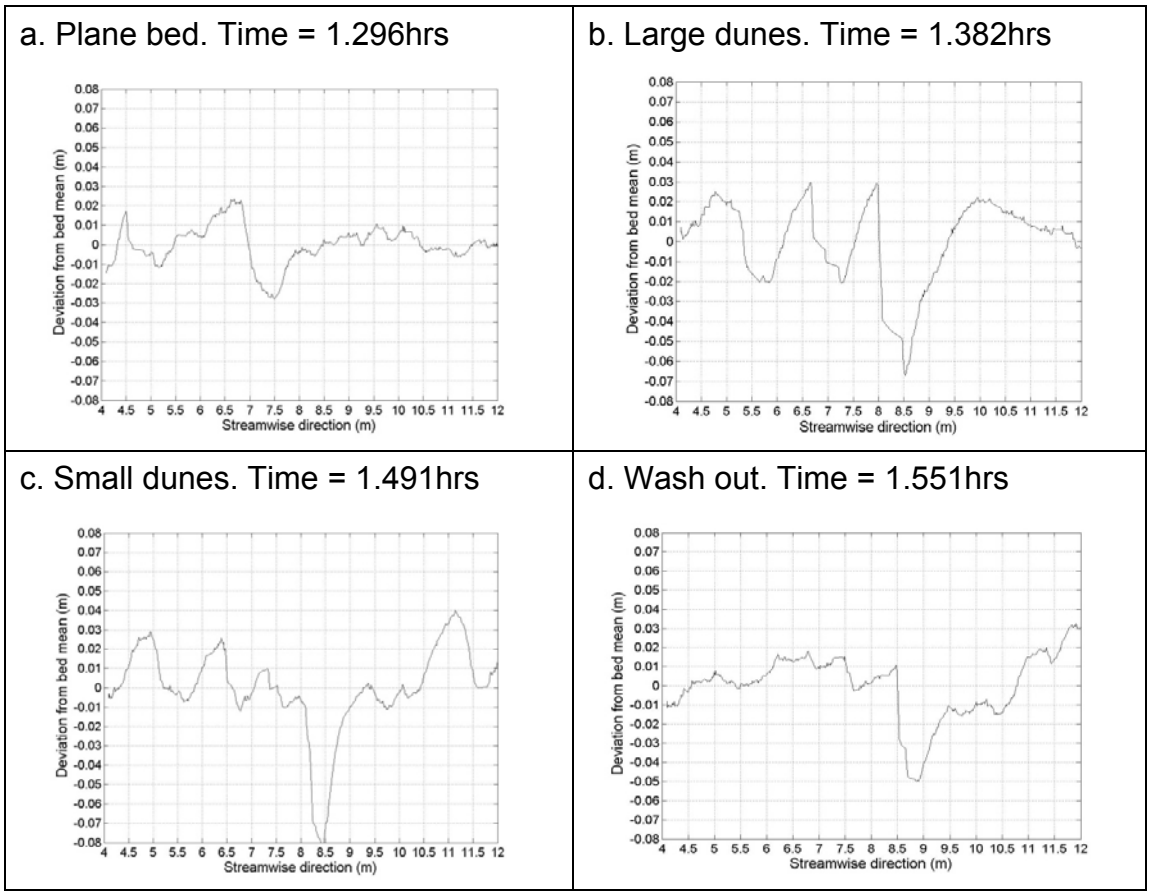

Figure 3-22. Detrended profiles of bed topography collected by Seatek® sensor 17 during suspension-dominated transport stage.

3.3.2.4 Bed erosion and deposition

Bed erosion and deposition are represented by the bed elevation change between two surveys (Figure 3-12b, Figure 3-20b, Figure 3-21b). The distribution of bed erosion and deposition shows increased variability in the order of bedload-dominated, suspension-dominated and mixed transport stage (Figure 3-23). Averaged bed-elevation change distribution at the suspension-dominated transport stage is misleading because the bed elevation change at suspension-dominated stage varied depending on the different phases of bed development

(Figure 3-23b). The most peaked distribution in Figure 3-23b corresponds to bed elevation change from a train of small bedform to mostly plane bed (Figure 3-22 c to d). The middle distribution is the average elevation change of all surveys and corresponds to elevation change from a mostly plane bed to a train of large bedforms (Figure 3-22 a to b). The broadest distribution corresponds to bed elevation change for a train of large bedforms into a train of smaller bedforms (Figure 3-22 b to c).

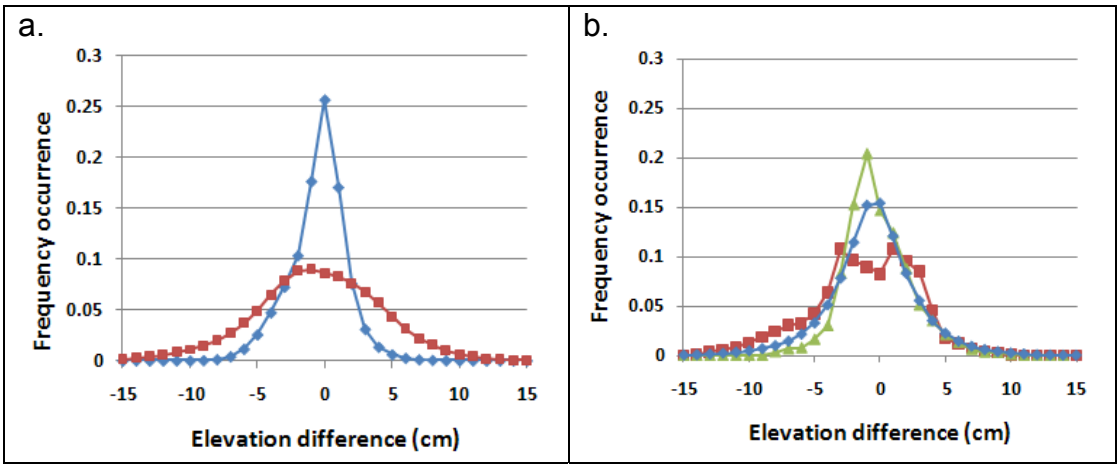

Figure 3-23. (a) Distributions of the average bed elevation change over all surveys. Bedload-dominated and mixed transport stages are represented by blue and red line, respectively. (b) The blue line represents the average elevation change at suspension-dominated transport stage; the red line represents bed elevation change from a train of large dunes to smaller dunes; the green line represents bed elevation change from a train of small dunes to mostly plane bed.

Topography grid files generated from Seatek® data were used to calculate the volume of sediment eroded and deposited between two surveys. Volumetric erosion and deposition rates between surveys were determined by dividing the change of sediment volume by time between surveys. Sediment erosion and deposition rate were balanced (Figure 3-24) and both the value and variability of sediment erosion and deposition increased with transport stage.

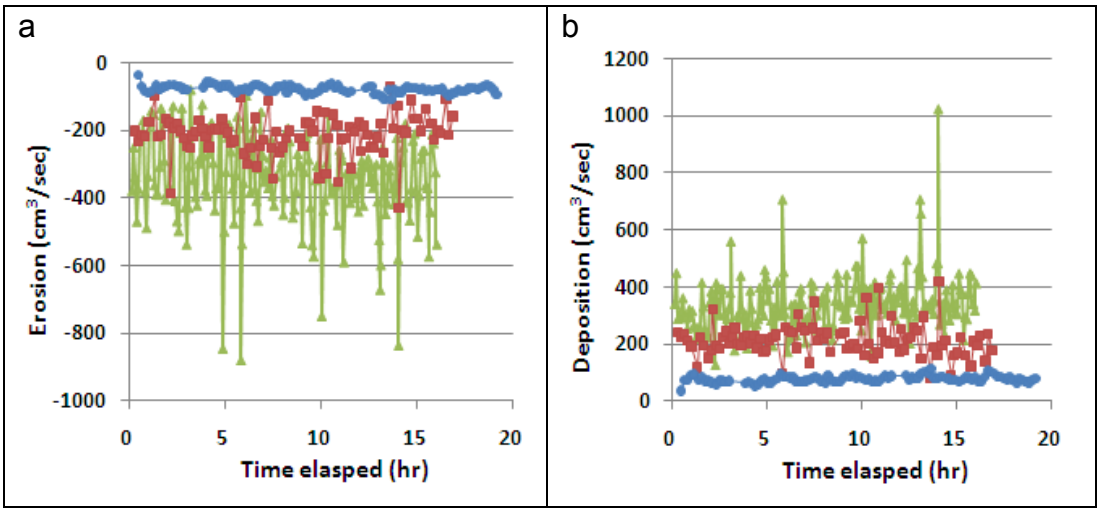

Figure 3-24. Sediment (a) erosion rate or (b) deposition rate between surveys at three transport stages versus time. Bedload-dominated, mixed and suspension-dominated transport stages are represented by blue, red and green line, respectively.

3.3.3 Bedform characteristics

3.3.3.1 Bedform height

The automated method tend to yield greater bedform heights than the conventional method (Figure 3-25). Comparing the two methods at sensor 17 (Figure 3-25 a,b,c), the automated method produced values 31%, 29% and 26% higher than the conventional method at bedload-dominated, mixed and suspension-dominated transport stage, respectively. The conventional method was only performed on Seatek® sensor 17(H_{m17}), so moving away from sensor 17 the difference between the two methods increased (Figure 3-25 d,e,f). However, comparison of bedform heights averaged over all sensors obtained using the automated method (H_{Avg}) to data from the conventional method at sensor 17 (Figure 3-25 g,h,i) shows the automated method has similar accuracy and better precision than comparing two methods at sensor 17 (Figure 3-25 a,b,c). The precision of the automated method decreased at higher transport stages but accuracy was maintained across all transport stages.

The observed difference between the two methods is a curious result. The roughness function method is a measure of all bed elevations, so it should be biased towards smaller heights assuming there is a continuous bed elevations below the largest dunes. It shows the roughness function is not a surrogate for the conventional manual method. Nevertheless, it is a well-defined, objective and consistent measure of bedform heights that I use below.

Bedform height had symmetrical pattern across the flume at all three transport stages (Figure 3-26a). Bedform height reached a maximum at the

flume walls and gradually decreased away from the walls. Maximum heights at the walls may be caused by wall-induced deep scour holes. Removing the two profiles closest to the walls may increase the homogeneity of the data. However, doing so requires that I know the distance into the flume where the bedforms are impacted by the wall. Selection of any particular distance is difficult to justify. Bedform height reached its minimum at 0.3m from flume walls and gradually increased toward the centre of the channel where bedform height reached a local maximum. At the mixed transport stage, bedform height did not have an obvious local maximum in the centre of the channel.

Bedform height (Figure 3-26b) varied through time, going through cycles of obvious increase and decrease at the bedload-dominated transport stage. Bedform height seemed to fluctuate randomly at the suspension-dominated transport stage. Bedform height at suspension-dominated transport stage increased through time. This trend may be part of a longer cycle or some non-equilibrium effect in the flume. The difference in trends shows that at low transport stage, bedforms were more stable and evolved gradually. Bedforms at high transport stage were unstable and deformed quickly and constantly. At the mixed transport stage, bedform height underwent cycles of obvious increase and decrease as well as seemingly random fluctuations because bedforms started to deform more rapidly.

In terms of relaxation time, which is the time required for bedforms to equilibrate to a change in flow [*Allen*, 1974], bedforms at higher transport stages have shorter relaxation times and react to flow more quickly. Thus, if the

temporal change of the bedform height is scaled by the relaxation time of the bed, the data series at mixed and suspension-dominated transport stages may look similar to the temporal change of the bedform height at bedload-dominated transport stage. The same assumption is applicable to temporal change in bedform length, aspect ratio and translation rate.

The mean bedform height increased from bedload-dominated to mixed transport stage and decreased from mixed to suspension-dominated transport stage (Figure 3-27). Height distributions had near-symmetrical distributions under mixed and suspension-dominated transport stage and positive skewness under the bedload-dominated transport stage, which showed bedforms under bedload-dominated transport stage were more stable. The likelihood of having higher bedforms at the bedload-dominated transport stage is much smaller. Increases in the coefficient of variation (Table 3-9) at higher transport stages show bedform were more unstable when suspension increased. The distribution became broader with an increase in transport stage because bedform were deforming more rapidly.

	Bedload-dominated	Mixed load	Suspension-dominated
Automated method on sensor 17 (H_{17})	a 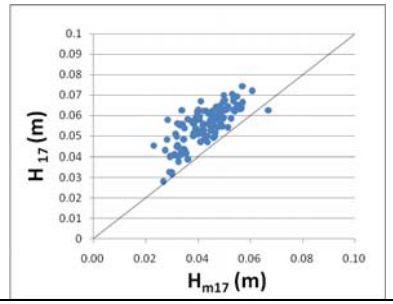	b 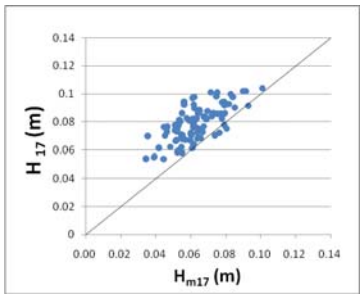	c 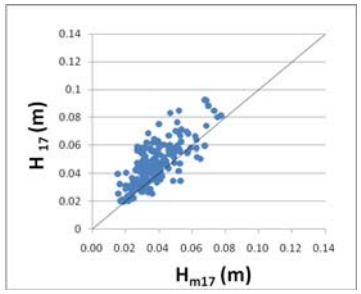
Automated method on sensor 1 (H_{1})	d 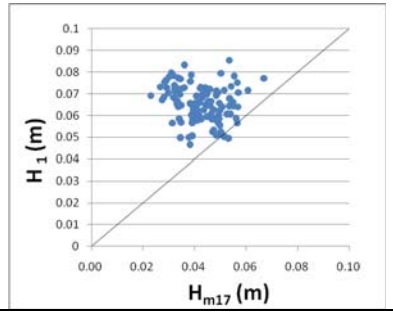	e 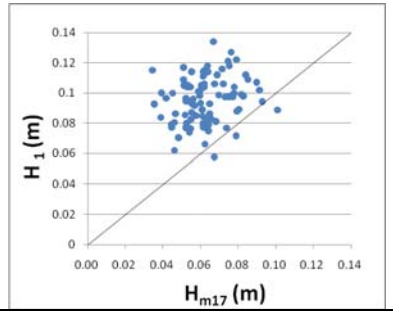	f 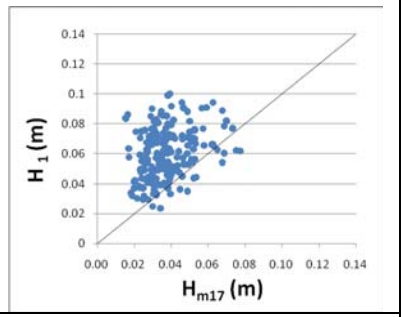
Automated method averaged over all sensors (H_{Avg})	g 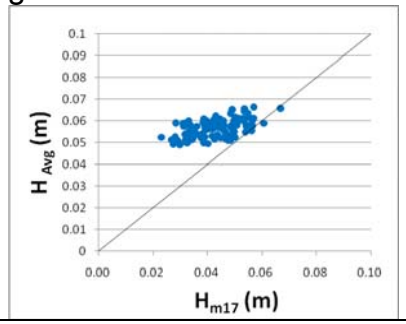	h 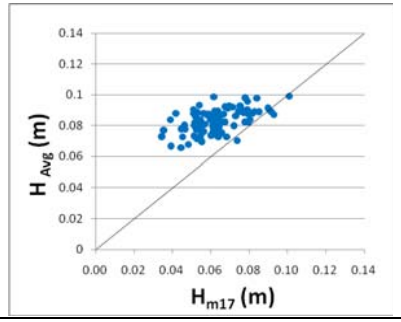	i 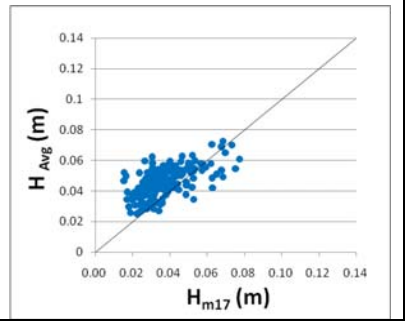

Figure 3-25. Bedform height obtained with conventional (H_{m17}) and automated method.

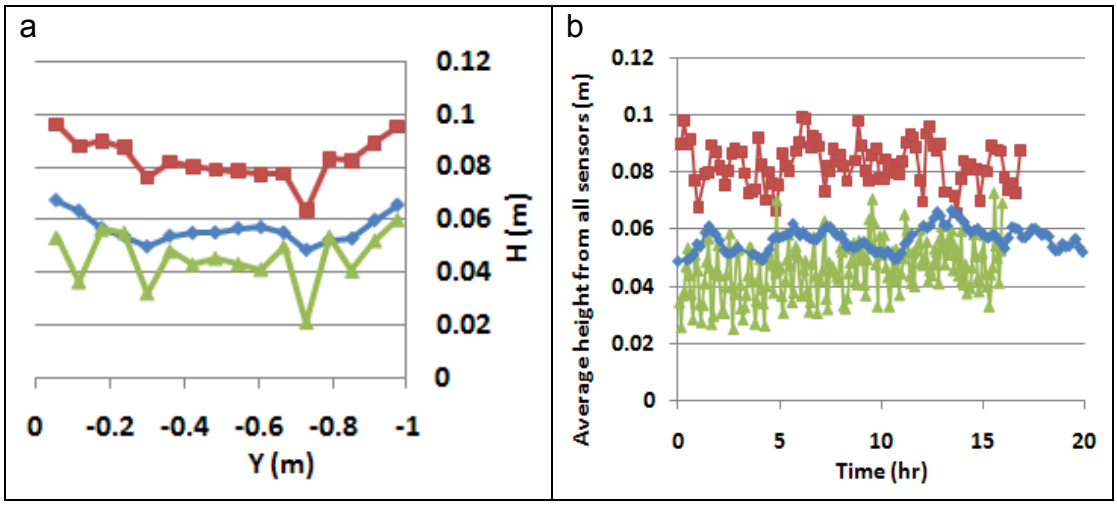

Figure 3-26. (a) Spatial distribution of bedform height across flume channel averaged over all surveys. (b) Temporal change in bedform height averaged over all surveys and profiles. Bedload-dominated, mixed and suspension-dominated transport stages are represented by blue, red and green line, respectively.

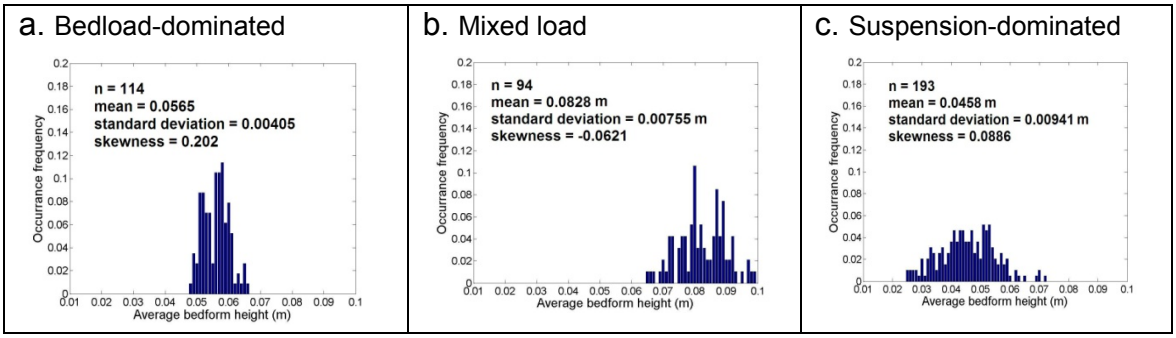

Figure 3-27. Histograms of averaged bedform height over all surveys and profiles.

3.3.3.2 Bedform length

The automated method tend to yield higher lengths than the conventional method (Figure 3-28). Comparing the two methods at sensor 17 (Figure 3-28 a,b,c), the automated method produced values 8%, 12% and 26% higher than the conventional method at bedload-dominated, mixed and suspension-dominated transport stage, respectively. The conventional method was only performed on Seatek® sensor 17(L_{m17}), so moving away from sensor 17 the

difference between the two methods increased (Figure 3-28 d,e,f). Comparison of bedform lengths averaged over all sensors obtained using the automated method (L_{Avg}) to data from the conventional method at sensor 17 (Figure 3-28 g,h,i) shows decreased accuracy and precision than when comparing the two methods at sensor 17 (Figure 3-28 a,b,c). The precision and accuracy of the automated method decreased at higher transport stages.

The correlation between the manual and automated methods is not as strong as for bedform height. The roughness function method is well defined and objective, but the bias relative to the manual method is not consistent. The bedform lengths produced by the roughness function do not appear to be a surrogate for the manual method. The results below should regarded with some caution.

Bedform lengths had a similar symmetrical pattern across the flume at all three transport stages (Figure 3-29a). Bedforms were longer 0.1 to 0.3m away from flume walls and were the shortest in the centre of the flume. Bedform length at the suspension-dominated transport stage did not display an obvious pattern across the channel.

Temporal change in bedform length (Figure 3-29b) showed patterns consistent with those for bedform height. Bedform lengths went through cycles of obvious increase and decrease at the bedload-dominated transport stage, but appeared to fluctuate randomly at suspension-dominated transport stage. Bedform lengths at the suspension-dominated transport stage decreased through time. This trend may have been part of a longer cycle or some non-equilibrium

effect in the flume. The difference in the trend was highlighted at the low transport stage where bedforms were more stable and evolved gradually. Bedforms at the higher transport stage were unstable and deformed more quickly and constantly. At the mixed transport stage, bedform height showed both cycles of obvious increase and decrease and fluctuated randomly because bedforms started to deform more quickly than at the bedload-dominated transport stage, but evolved more gradually than at the suspension-dominated flow.

The mean bedform length increased as transport stage increased (Figure 3-30). Data are positively skewed at all transport stages showing bedforms that were shorter than the average length occurred more frequently than bedforms that were longer than the average length. The coefficient of variation increased with higher transport stage (Table 3-9) showing bedforms became more unstable when suspension increased. The coefficient of variation (Table 3-9) shows bedform length fluctuated more than bedform height.

	Bedload-dominated	Mixed load	Suspension-dominated
Automated method on sensor 17(L_{17})	a 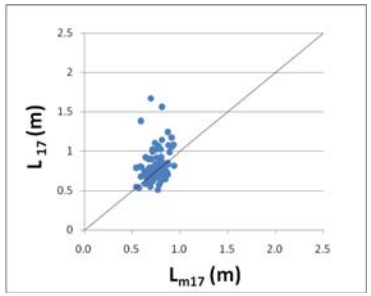	b 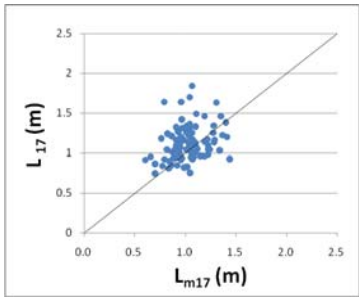	c 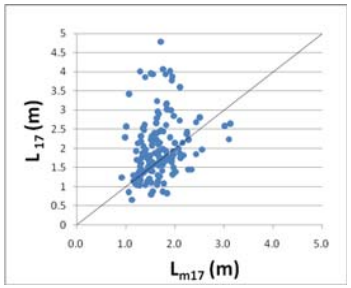
Automated method on sensor 17(L_{1})	d 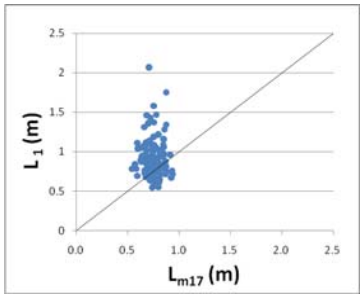	e 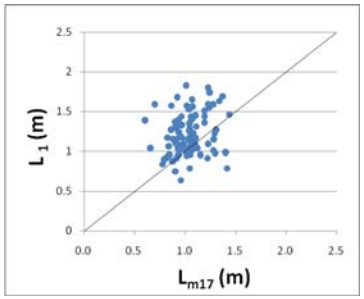	f 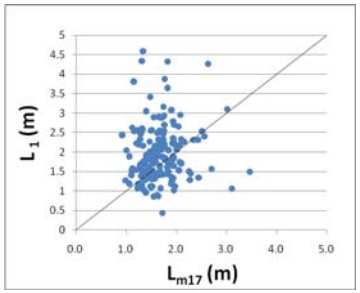
Automated method Averaged over all sensors (L_{Avg})	g 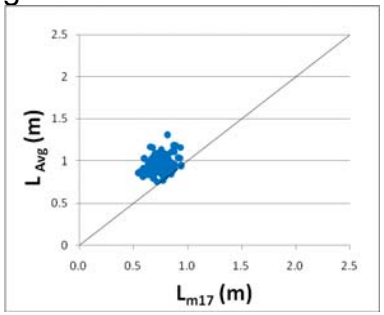	h 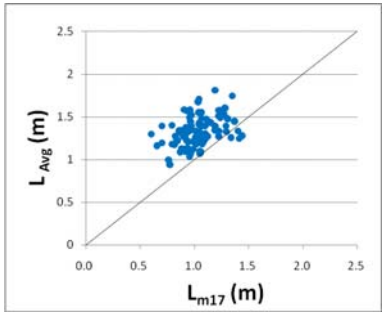	i 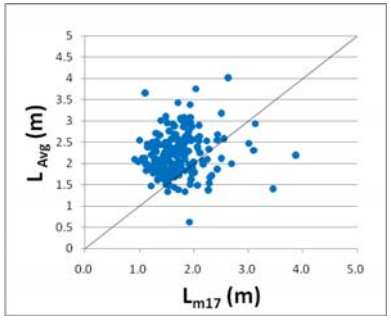

Figure 3-28. Bedform height obtained with conventional (L_{m17}) and automated method.

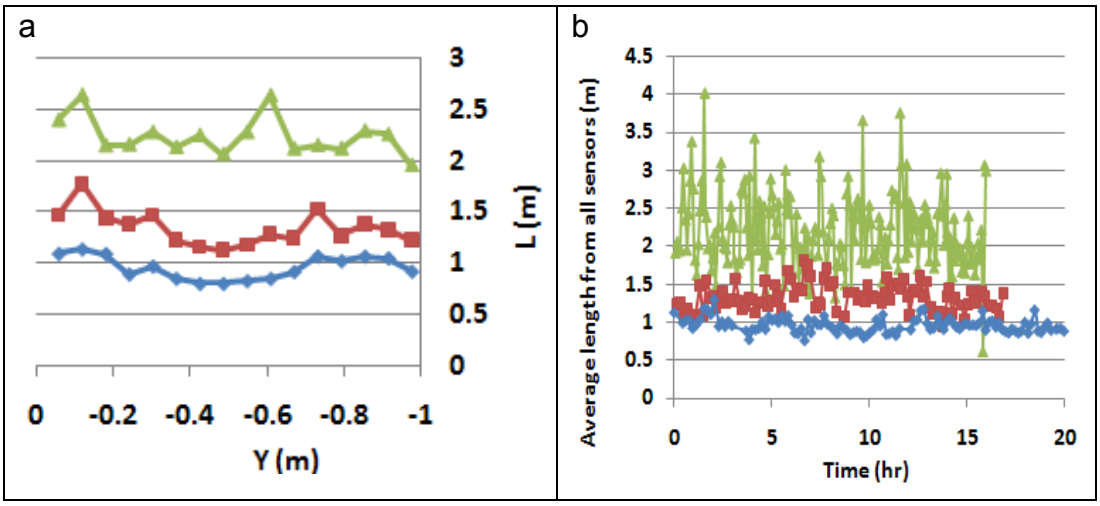

Figure 3-29. (a) Spatial distribution of bedform length across flume channel averaged over all surveys. (b) Temporal change in bedform length averaged over all surveys and profiles. Bedload-dominated, mixed and suspension-dominated transport stages are represented by blue, red and green line, respectively.

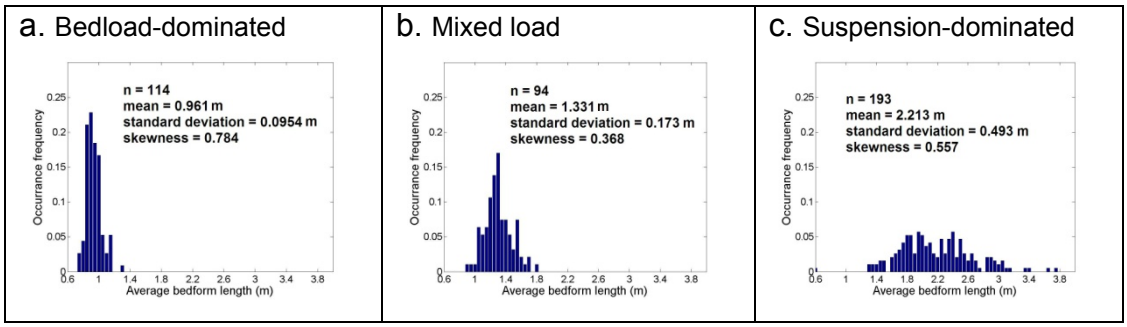

Figure 3-30. Histograms of averaged bedform length over all surveys and profiles.

3.3.3.3 Aspect ratio (H/L)

Bedform aspect ratio had similar symmetrical spatial patterns across the flume at the three transport stages (Figure 3-31a). Bedform aspect ratio reached a maximum in the centre of the channel and against the flume walls and had a minimum value 0.3m away from the walls. At the suspension-dominated transport stage, there was no obvious pattern in the bedform aspect ratio across the channel.

The temporal distribution of bedform aspect ratio (Figure 3-31b) shows similar patterns to bedform height. Aspect ratio went through cycles of obvious increase and decrease at bedload-dominated transport stage, but randomly fluctuated at suspension-dominated transport stage. Aspect ratio at the suspension-dominated transport stage also increased through time. At low transport stage, bedforms were more stable and evolved gradually, but became unstable and deformed quickly and constantly at high transport stage. At the mixed transport stage, bedforms started to deform but evolved gradually.

The mean bedform aspect ratio increased from bedload-dominated to mixed transport stage and decreased from mixed to suspension-dominated transport stage (Figure 3-32). This indicates that bedform became longer and flatter at the highest transport stage. However, distributions show positive skewness (steeper bedforms) at mixed and suspension-dominated transport stage and negative skewness (flatter bedforms) at bedload-dominated transport stage. Standard derivation remains constant regardless of the transport stage but the coefficient of variation (Table 3-9) increases with transport stage.

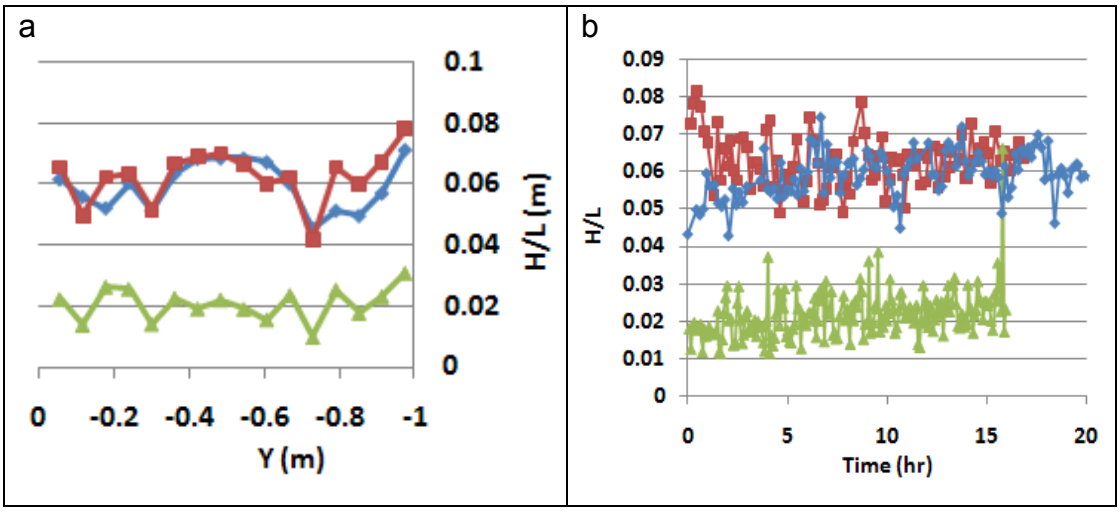

Figure 3-31. (a) Spatial distribution of bedform aspect ratio across flume channel averaged over all surveys. (b) Temporal change in bedform aspect ratio averaged over all surveys and profiles. Bedload-dominated, mixed and suspension-dominated transport stages are represented by blue, red and green line, respectively.

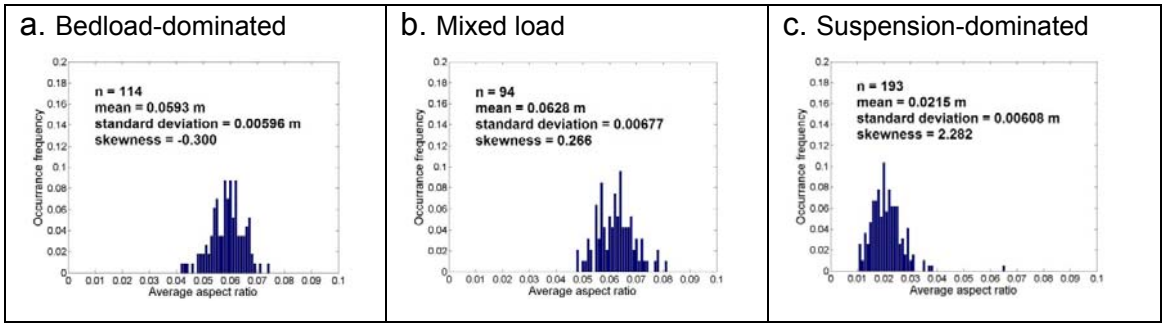

Figure 3-32. Histograms of averaged bedform aspect ratio over all surveys and profiles.

3.3.4 Bedform translation rate

The automated method tended to yield lower values at the bedload-dominated transport stage but higher value at the mixed transport stage (Figure 3-33). Comparing the two methods at sensor 17 (Figure 3-33 a,b), the automated method produced values 6% less than the conventional method at bedload-dominated transport stage but 20% higher at mixed transport stage. The bias at the mixed transport stage is misleading because most of the data are clustered around the 1:1 line. No comparison between the automated method and the conventional method at suspension-dominated transport stage is available because there was too much uncertainty in manually tracking bedforms. The accuracy and precision of the automated decreased away from sensor 17 (Figure 3-33 c,d) and at higher transport stages. Comparison of bedform translation rates averaged over all sensors using the automated method ($V_{b\ Avg}$) to data from the conventional bedform tracking method (Figure 3-33 e,f) shows the automated method is less accurate but has similar precision than when comparing the two methods at sensor 17 (V_{bm17})(Figure 3-33 a,b).

The observed difference between the manual and automated methods suggests that the automated method was biased toward lower translation rates because it tracked different aspects of the bed. In other words, the automated method tracked the entire bed whereas the manual method tracked selected individual bedforms. Evidently, the selected bedforms moved faster than the entire bed at the bedload transport stage and slower at the mixed transport stage. The automated method is not a surrogate for the dune tracking method, but can

be regarded as better defined and more objective and consistent method for determining bedform translation.

The bedform translation rate had a symmetrical pattern across the channel at the bedload-dominated and mixed transport stages (Figure 3-34a). At the bedload-dominated transport stage, bedform translation rates increased away from the flume walls toward the centre of the channel and reached a maximum at the centre. At the mixed transport stage, bedform translation rate reached a minimum at the centre of the channel and reached a maximum 0.25m away from the flume walls. At suspension-dominated transport stage, bedform translation rate was the fastest in the centre of channel and displayed no other patterns.

Bedforms translation rate went through obvious cycles of faster and slower translation at bedload-dominated transport stage (Figure 3-34b) and randomly fluctuated at suspension-dominated transport stage. The variability in fluctuations also increased at higher transport stages. The difference in temporal distribution suggests translation became a less important mechanism of bedform migration at higher transport stage where a large increase in suspension led to greater deformation of bedforms.

The mean bedform translation rate increased as transport stage increased (Figure 3-35). The coefficient of variation of bedform translation rates increased at the higher transport stage (Table 3-9) showing bedform translation became more variable when suspension increased. The distribution broadens a higher transport stage because at greater component of the transport stages happened by deformation.

	Bedload-dominated	Mixed load
Automated method on sensor 17($V_{b\ 17}$)	a 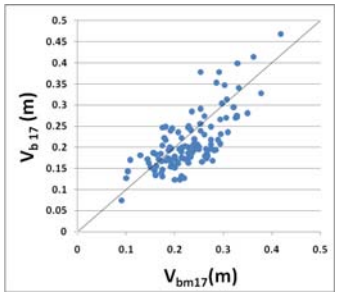	b 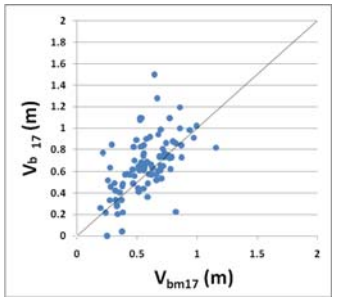
Automated method on sensor 1($V_{b\ 1}$)	c 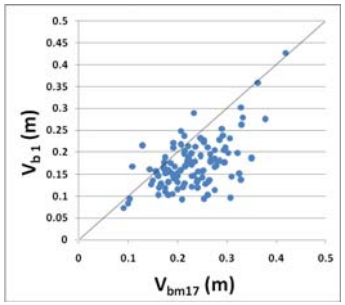	d 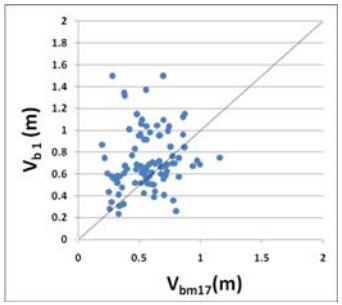
Automated method averaged over all sensors ($V_{b\ Avg}$)	e 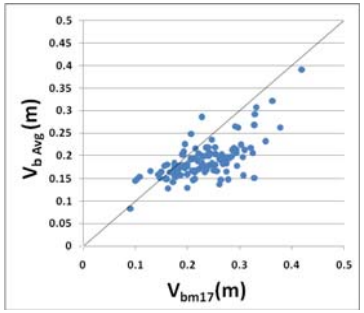	f 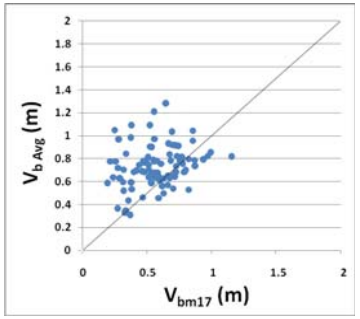

Figure 3-33. Bedform translation distances obtained with conventional (V_{bm17}) and automated method.

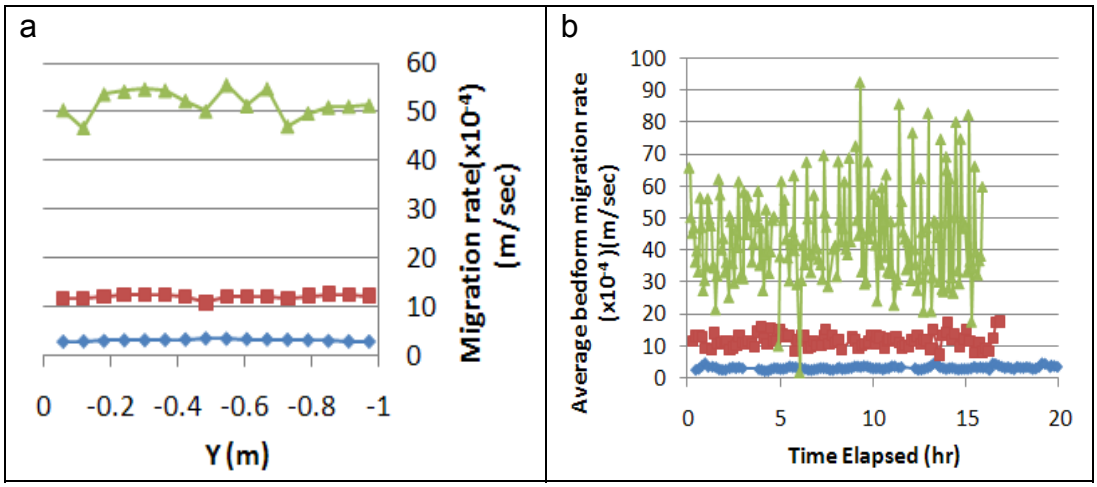

Figure 3-34. (a) Spatial distribution of bedform translation rate across flume channel averaged over all surveys. (b) Temporal change in bedform translation rate averaged over all surveys and profiles. Bedload-dominated, mixed and suspension-dominated transport stages are represented by blue, red and green line, respectively.

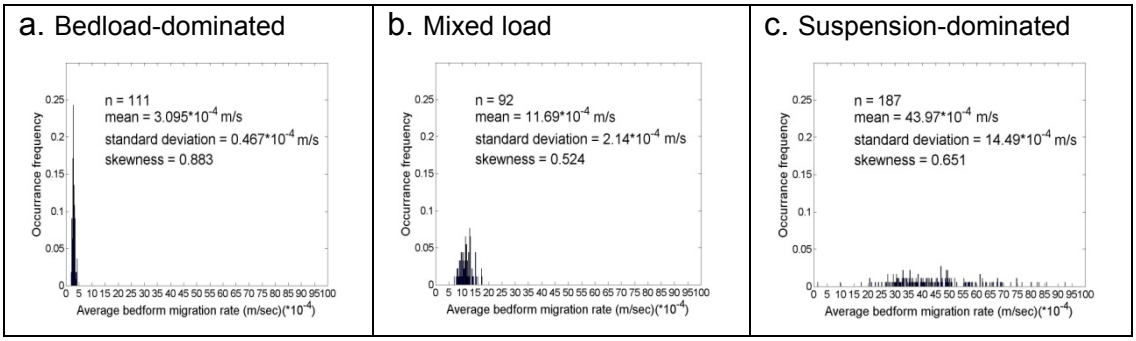

Figure 3-35. Histograms of averages bedform translation rate over all surveys and profiles.

3.3.5 Bedform translation and deformation

I calculated the bedform translation load using the bedform migration data. Translation load per unit width (q_{st}) was calculated from the *Simons et al.* [1965] equation (Equation 1-5) expressed in the form:

$$q_{st} = H V_b \beta_s (1 - P) \quad (3\text{-}12)$$

where β_s is the bedform shape factor and equals to 0.56 for angle of repose bedforms [*Venditti et al.*, 2005b], P is the porosity of sand (~0.4 for 550μm sand [*Van Rijn*, 1993]).

The bedform deformation rate was calculated as the difference between the total load and the translation load (Table 3-11). The total load was calculated as the sum of the bedload and the suspended bed-material load measurements in Table 3-11 at each transport stage. The proportion of total load being transported as translation load or deformation load is also shown in Table 3-11.

McElroy and Mohrig [2009] argued that the bedload transport rate is equivalent to the bedform translation load and that the bed material suspended sediment flux is equivalent to the bedform deformation rate in rivers. Our measurements of bedload and suspended-load transport need to be adjusted so that the measurements are consistent with the transport mechanism inferred by *McElroy and Mohrig* [2009] argument.

The bedload transport measurements in Table 3-11 are consistently greater than the suspended-load transport measurements because the bedload sampler collected suspended sediment above the bedload transport layer. I

attempted to separate suspended bed-material load from the bedload measurement between z = 0m and z = 0.02m by assuming a linear profile between 0 and 0.02m and calculating the proportion of the load captured in the sampler that was moving as bedload. I used the empirical relations by *van Rijn* [1984] to calculate the thickness of the bedload layer (d_{bl})

$$d_{bl} = 0.3{D_*}^{0.7}T^{0.5}D \tag{3-13}$$

where

$$D_* = D[\frac{g(\frac{\rho_S}{\rho_W}-1)}{\nu^2}]^{1/3} \tag{3-14}$$

and

$$T = \frac{\tau - \tau_c}{\tau_c} \tag{3-15}$$

where τ_c is the critical boundary shear stress. The thickness of the bedload layer was 0.0024m, 0.0039m, and 0.005m at the bedload-dominated, mixed and suspension-dominated transport stages, respectively. I also calculated the thickness of the bedload layer using the relations by *Bagnold* [1973], but the results did not conform to my observation during the experiments.

I used the Rouse equation [*Rouse*, 1939] (Equation 3-7) to calculate the suspended load transport between z = 0.02m and z = 0.04m using my measurements of suspended sediment concentration at 0.04m above the bed. Using the bedload measurement between z = 0m to z = 0.02m and the suspended load estimate from z = 0.02m to z = 0.04m, I constructed a sediment transport profile assuming a linear profile between 0 and 0.02m. Then I

partitioned the measured bedload transport into portions of the flux profile above and below the bedload layer. The modified bedload transport includes all the sediment transported within the bedload layer. The modified suspended bed-material load includes all the sediment transported from the top of the bedload layer to the water surface. The modified bedload and suspended bed-material load increase with transport stage (Table 3-12) and the modified suspended bed-material load is always greater than the modified bedload transport. However, the proportion of the bedload transport to the total load still increases with transport stage. Translation load was calculated from the bedform translation rate, so the proportion of the translation load to the total load and the proportion of the deformation load to the total load were not affected by the modification.

Translation load was greater than the modified bedload transport rate and the ratio of translation load to modified bedload decreased with increasing transport stage. Deformation load was less than the suspended bed-material transport rate for all flows. However, translation load and bedload were approximately equal at the suspension-dominated transport stage as were the deformation load and the suspended bed-material transport rate.

Table 3-11. Translation load and total load (unmodified values)

Transport stage	Bedload (g/sec/m)	SSBM load (g/sec/m)	Total load (g/sec/m)	Translation load (g/sec/m)	Deformation load (g/sec/m)	$\frac{\text{Translation}}{\text{Bedload}}$	$\frac{\text{Deformation}}{\text{SSBM load}}$	$\frac{\text{Translation}}{\text{Total load}}$	$\frac{\text{Deformation}}{\text{Total load}}$
Bedload	25.8	0	25.8	15.6	10.3	0.602	n/a	0.602	0.398
Mixed	111	7.34	119	86.2	32.6	0.773	4.44	0.726	0.274
Suspension	459	75.9	535	179	356	0.390	4.69	0.335	0.665

Note: SSBM load = Suspended bed-material load. n/a = not available.

Table 3-12. Translation load and total load (values modified by assuming linear profile)

Transport stage	Bedload (g/sec/m)	SSBM load (g/sec/m)	Total load (g/sec/m)	Translation load (g/sec/m)	Deformation load (g/sec/m)	$\frac{\text{Translation}}{\text{Bedload}}$	$\frac{\text{Deformation}}{\text{SSBM load}}$	$\frac{\text{Translation}}{\text{Total load}}$	$\frac{\text{Deformation}}{\text{Total load}}$
Bedload	4.65	21.2	25.8	15.6	10.3	3.35	0.485	0.602	0.398
Mixed	32.2	86.6	119	86.2	32.6	2.68	0.376	0.726	0.274
Suspension	164	371	535	179	356	1.10	0.958	0.335	0.665

Note: SSBM load = Suspended bed-material load. n/a = not available.

3.4 Discussion

3.4.1 Effect of transport stage on bedform geometry

Previous works show bedform geometry is influenced by transport stage [*Simons and Richardson*, 1966; *Guy et al.*, 1966; *Van Rijn*, 1993] and bedform aspect ratio increases from bedload-dominated to mixed transport stage then decreases from mixed to suspension-dominated transport stage (Figure 1-5) [*Yalin* ,1972; *Yalin and Karahan*, 1979a].

My experimental observations are in agreement with this idea and confirm the relation between dune aspect ratio proposed by *Yalin* [1972]. Figure 3-36 shows bedform height (Figure 3-36a) and aspect ratio (Figure 3-36b) increased from the bedload-dominated to the mixed transport stage then decreased from the mixed to the suspension-dominated transport stage. Bedform lengths were smallest at the thresholds of particle motion and increased with transport stage (Figure 3-36c). As suspended-sediment became a larger proportion of the load, the bedforms lengthened and began to wash out.

The increase in the variability of bedform height, length and aspect ratio with transport stage implies we would expect wider distribution of bedform sizes and less uniform bedform fields at higher transport stage. The bed topography maps appear to bear out this pattern across transport stages (Figure 3-12, Figure 3-20 and Figure 3-21).

3.4.2 Effect of transport stage on bedform migration

The relation between transport stage and bedform migration has not been defined in previous works. Results in Chapter 2 suggest a linear-power-law empirical relation between transport stage and bedform migration rate. My experimental observations in Figure 3-36d do not conform to Equation 2-5. This is because Equation 2-5 was derived from regression analysis that assumes all errors reside in the dependent variable. Since both translation rate and the Shields number contain errors, the data in Figure 3-36d would fit better to the functional form of Equation 2-5. However, performing functional analysis on data deriving Equation 2-5 requires the data to be normally distributed and the errors in both variables are equal. I cannot justify both assumptions.

As with the bedform geometry, the level of variability in the migration rate increased with transport stage. At the suspension-dominated transport stage, the level of variability in the data cloud is so large that defining a single migration rate is only possible by examine the central tendencies of data. The high level of variability at high transport stage may explain the wide scatter in the data from the literature (Figure 2-4). The results suggest that observations of bedform migration rates based on tracking a small population of bedforms or a single bedform in a larger bedform field should be regarded with caution. This is especially the case at the suspended transport stage where observed migration rates vary by two orders of magnitude at constant flow.

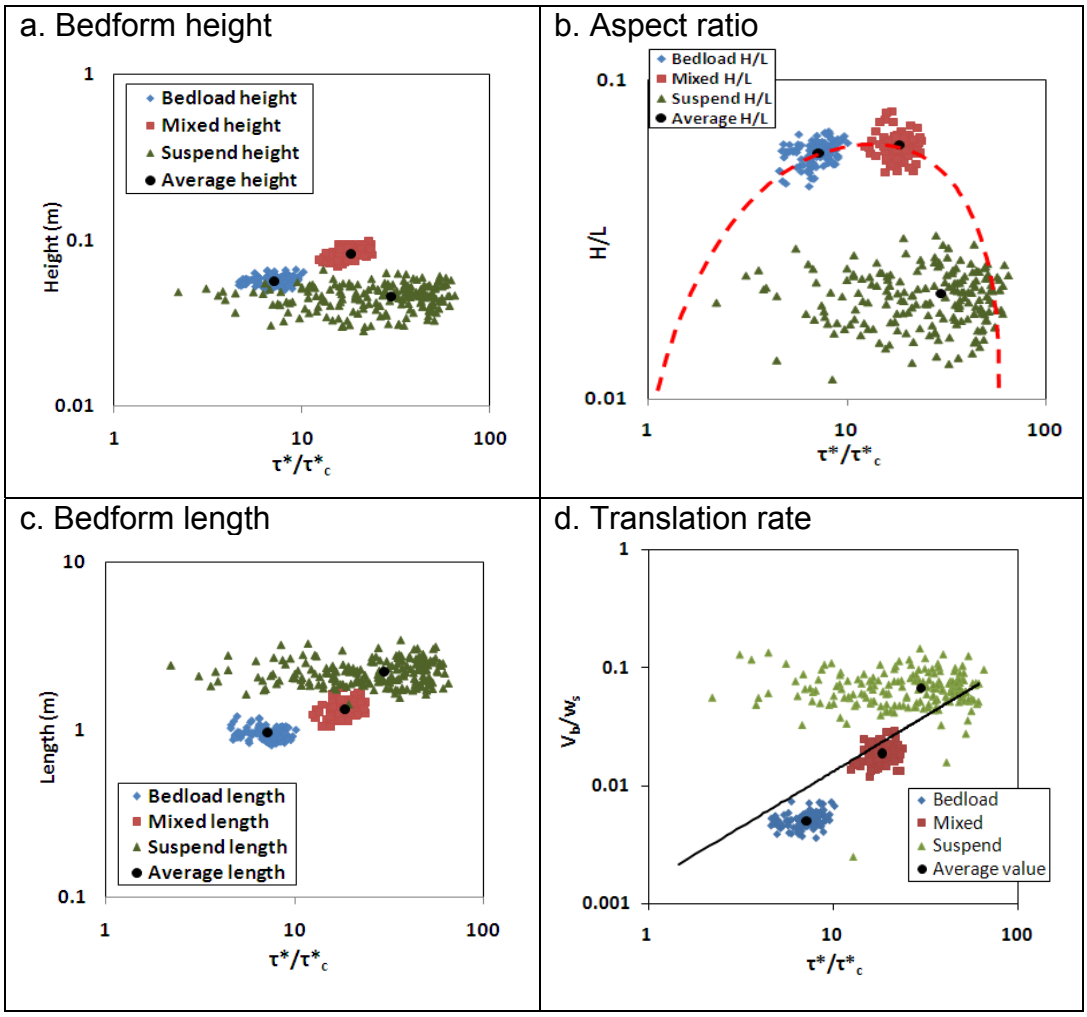

Figure 3-36. Bedform (a) height, (b) aspect ratio, (c) bedform length and (d) dimensionless translation rate versus transport strength. Black line in (d) is Equation 2-5.

3.4.3 Translation and deformation

McElroy and Mohrig [2009] argue that bedform shape deformation contributes significantly to the sediment flux in rivers and that its contribution is largely unrecognized. They suggest that bedform tracking exercises only characterize the translational component of bedform migration, which can be regarded as the bedload component of the total load. They also indicate that bedform deformation is caused by sediment suspension, so there should be an increase in deformation rate as the transport stage increases. This suggests that

$$\text{Bedload} + \text{Suspended bed material load} + \text{Washload} = \text{Translation load} + \text{Deformation load} + \text{Washload} \quad (3\text{-}16)$$

My results partially support the arguments of *McElroy and Mohrig* [2009]. Qualitatively, the bed topography showed changes in bedform morphology (deformation) were greater over a given time frame as transport stage increased (Figure 3-12; Figure 3-20; Figure 3-21). The increase in deformation coincided with the increase in suspended bed-material load (Table 3-12). However, my observations show deformation was 49%, 38% and 96% of the suspended bed-material transport at the bedload-dominated, mixed and suspension-dominated transport stage, respectively (Table 3-12). Bedform translation load increased with transport stage (Table 3-12). The portion of the total load moved by bedform translation increased from bedload-dominated to mixed transport stage, but decreased from mixed to suspension-dominated transport stage (Table 3-12; Figure 3-37c). This pattern is similar to that of bedform height versus transport

stage (Figure 3-37a). Since the translation load was calculated from the product of the bedform height and translation rate (Figure 3-37b), it is not surprising that the ratio of translation load to the total load displays the pattern in Figure 3-37c. The proportion of the total load related to deformation followed the opposite trend of the translation to total load ratio decreasing from bedload-dominated to mixed transport stage, but increasing from mixed to suspension-dominated transport stage (Table 3-12; Figure 3-37d).

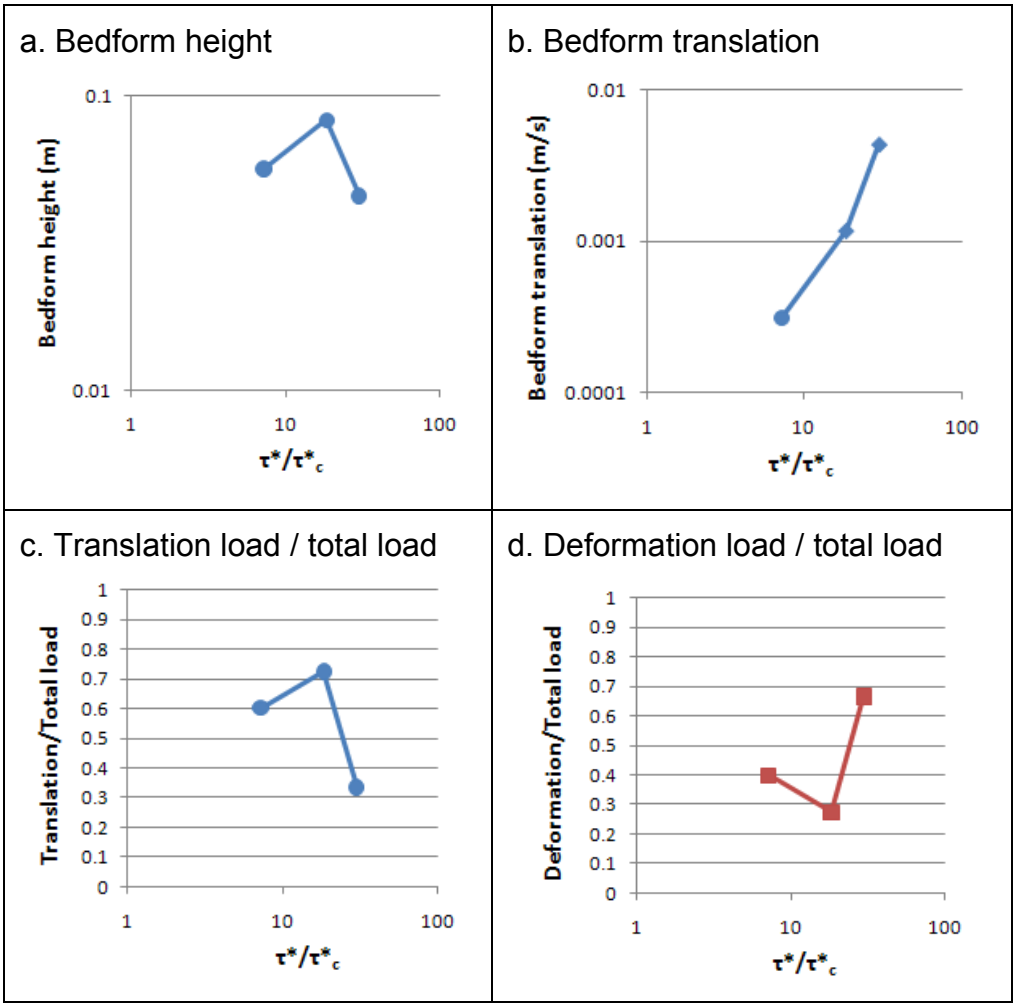

Figure 3-37. Patterns of the bedform height, bedform translation, translation load/total load, and deformation/total load under different transport stages.

The results presented here must be considered within the context of the measurements. There were uncertainties in the bedload and suspended load measurements. For example, bedload and suspended-load samplers disturbed the flow and caused wakes that perturbed bedforms at high flow. Similarly, sampler positioning on the bed or at the correct height above the bed was difficult when suspended-sediment concentration was high because of poor visibility.

My measurements of the bedload and the suspended bed-material load did not quantitatively demonstrate the equivalence of bedload and bedform translation or deformation and suspension at all flow stages. However, suspension was nearly equivalent to deformation at the suspension-dominated transport stage (Table 3-12) if I divided the bedload and the suspended bed-material load based on the calculated bedload transport-layer height. This suggests the fundamental concept may be correct.

Further observations designed to track actively deforming bedforms in a Lagrangian framework (that follows the bedforms) are required to resolve that relation.

4: CONCLUSION

The objective of this research is to examine the relation between transport stage and bedform migration (V_b) using literature data sets and a controlled laboratory experiment. The literature data sets were used to determine the nature of the relation between transport stage and bedform migration. The laboratory experiment was used to generate a detailed set of observations that lead to bedform migration under different transport stages.

Analysis of data sets from the literature reveals a positive relation between transport stage and bedform migration. Stratification of the dune migration data by flow depth (d) over grain size (D) yields a series of parallel positive linear relations between V_b and transport stage. This result shows grain size is an important control for bedform migration because at higher transport stages, more sediment is moved in suspension. Rendering non-dimensional the bedform migration rate by the grain settling velocity is able to partially collapse data onto a single curve that further highlights the important role sediment suspension plays in moderating the migration rate.

To further examine the relation discovered in the literature, laboratory experiments were conducted under bedload-dominated, mixed, and suspension-dominated transport stages. The results show average bedform height and aspect ratio increase when flow goes from bedload-dominated to mixed, then

decrease from mixed to suspension-dominated transport stage. Average bedform length and average migration rate increase with transport stage.

Qualitatively, bedform shape deformation increases with transport stage, which leads to greater variability in migration rate and bedform geometry. Sediment transport associated with bedform translation and deformation of the bedform morphology increases with transport stage. The proportion of the total load associated with bedform translation increases then decreases moving from bedload-dominated to mixed to suspension-dominated transport stages. The proportion of the total load associated with bedform deformation also decreases from bedload-dominated to mixed transport stage and increases from mixed to suspension-dominated transport stage. I did not find that bedform translation load was equivalent to the bedload transport rate or that the bedform deformation rate was equivalent to the suspended bed-material transport rate as has been suggested in the literature, but that may be related to the nature of the sediment transport observations.

Further work is required to couple my empirical bedform migration relation with a relation for bedform height to predict sediment flux associated with bedform translation. It is possible that such a transport model can be constructed. In this model, I can estimate bedform migration (V_b) from the Shields number, which also provides estimates of bedform height (H). Further work is also required to determine the most effective ways to estimate the contribution of deformation of bedforms to the total sediment flux in a channel.

APPENDICES

Appendix 1

Bedform data experiments

Table A-1. Values of experimental time, slope, flow depth, bedform height, bedform length, aspect ratio and translation rate at bedload-dominated transport stage. Bedform H, L, H/L and translation rates were measured with the automated methods.

Index	Time (hr)	S	d (m)	H (m)	L (m)	H/L	Translation rate (m/sec)
1	0.46	0.00122	0.149	0.0492	1.062	0.0463	0.000247
3	0.63	0.00125	0.148	0.0496	1.010	0.0491	0.000280
4	0.80	0.00130	0.148	0.0506	1.028	0.0492	0.000365
5	0.96	0.00165	0.148	0.0531	0.975	0.0545	0.000447
6	1.13	0.00171	0.148	0.0545	0.943	0.0578	0.000341
7	1.37	0.00124	0.148	0.0564	1.003	0.0563	0.000344
8	1.55	0.00109	0.149	0.0599	1.113	0.0538	0.000323
9	1.73	0.00120	0.150	0.0602	1.178	0.0511	0.000264
10	1.89	0.00110	0.150	0.0587	1.139	0.0516	0.000250
11	2.06	0.00093	0.149	0.0571	1.208	0.0473	0.000248
12	2.29	0.00090	0.148	0.0543	1.128	0.0482	0.000302
13	2.46	0.00107	0.147	0.0521	0.979	0.0532	0.000324
14	2.63	0.00123	0.149	0.0516	0.978	0.0527	0.000302
15	2.79	0.00126	0.148	0.0520	0.980	0.0531	0.000324
16	2.98	0.00145	0.147	0.0530	0.985	0.0538	0.000296
24	3.86	0.00146	0.152	0.0512	0.829	0.0617	0.000271
25	4.02	0.00164	0.151	0.0506	0.840	0.0603	0.000245
26	4.19	0.00150	0.150	0.0498	0.906	0.0549	0.000217
27	4.36	0.00126	0.150	0.0503	0.913	0.0551	0.000225
28	4.52	0.00113	0.150	0.0521	0.963	0.0541	0.000267
30	4.69	0.00122	0.150	0.0548	0.956	0.0573	0.000302
31	4.86	0.00147	0.151	0.0570	0.992	0.0575	0.000294
32	5.02	0.00157	0.153	0.0573	1.053	0.0544	0.000273
34	5.19	0.00155	0.153	0.0573	1.040	0.0551	0.000279
35	5.36	0.00149	0.151	0.0578	1.025	0.0564	0.000303
36	5.52	0.00157	0.149	0.0582	1.044	0.0558	0.000354
38	5.69	0.00149	0.150	0.0601	1.051	0.0572	0.000327
40	5.86	0.00164	0.153	0.0608	1.054	0.0577	0.000323
41	6.04	0.00165	0.154	0.0588	1.029	0.0571	0.000305
42	6.19	0.00158	0.154	0.0584	0.914	0.0639	0.000290
43	6.36	0.00148	0.156	0.0583	0.856	0.0681	0.000281

44	6.52	0.00120	0.157	0.0572	0.883	0.0648	0.000248
45	6.69	0.00103	0.156	0.0567	0.837	0.0677	0.000240
47	6.86	0.00094	0.154	0.0565	0.899	0.0628	0.000263
48	7.02	0.00097	0.153	0.0572	0.951	0.0602	0.000275
49	7.19	0.00118	0.154	0.0589	0.943	0.0624	0.000306
50	7.36	0.00131	0.155	0.0603	0.999	0.0604	0.000299
51	7.52	0.00131	0.154	0.0608	0.972	0.0626	0.000292
53	7.69	0.00118	0.154	0.0600	1.030	0.0582	0.000249
54	7.86	0.00117	0.154	0.0585	1.034	0.0565	0.000246
55	8.08	0.00151	0.154	0.0579	0.956	0.0606	0.000283
56	8.19	0.00147	0.155	0.0572	0.921	0.0621	0.000316
58	8.36	0.00124	0.154	0.0551	0.879	0.0626	0.000270
59	8.52	0.00091	0.153	0.0540	0.904	0.0597	0.000280
60	8.69	0.00089	0.153	0.0539	0.941	0.0573	0.000296
61	8.86	0.00092	0.152	0.0538	0.908	0.0593	0.000308
62	9.03	0.00106	0.151	0.0546	0.866	0.0630	0.000355
64	9.19	0.00131	0.151	0.0553	0.853	0.0649	0.000351
65	9.36	0.00144	0.150	0.0549	0.876	0.0627	0.000331
66	9.52	0.00158	0.150	0.0537	0.877	0.0612	0.000362
67	9.71	0.00136	0.150	0.0526	0.835	0.0630	0.000351
68	9.86	0.00142	0.149	0.0521	0.810	0.0643	0.000315
69	10.02	0.00140	0.150	0.0521	0.843	0.0618	0.000288
70	10.19	0.00132	0.149	0.0517	0.883	0.0586	0.000297
71	10.36	0.00125	0.149	0.0519	0.968	0.0536	0.000298
73	10.55	0.00118	0.151	0.0517	0.995	0.0520	0.000265
74	10.69	0.00126	0.151	0.0503	1.029	0.0489	0.000294
75	10.86	0.00121	0.151	0.0498	0.974	0.0512	0.000300
76	11.02	0.00145	0.150	0.0509	0.847	0.0601	0.000357
78	11.19	0.00160	0.151	0.0533	0.863	0.0618	0.000354
79	11.37	0.00156	0.151	0.0555	0.851	0.0652	0.000333
80	11.54	0.00167	0.151	0.0571	0.872	0.0655	0.000330
88	12.29	0.00153	0.153	0.0607	0.962	0.0631	0.000298
89	12.45	n/a	n/a	0.0608	1.028	0.0591	0.000249
90	12.62	n/a	n/a	0.0625	1.097	0.0569	0.000259
91	12.79	0.00118	0.154	0.0648	1.168	0.0555	0.000283
93	12.96	0.00119	0.153	0.0652	1.081	0.0603	0.000311
94	13.12	0.00150	0.153	0.0631	0.947	0.0666	0.000357
95	13.29	0.00179	0.152	0.0614	0.917	0.0669	0.000438
97	13.50	0.00186	0.152	0.0638	1.004	0.0636	0.000406
98	13.62	0.00168	0.154	0.0661	1.033	0.0639	0.000325
99	13.80	0.00148	0.154	0.0655	0.946	0.0692	0.000305

100	13.96	0.00129	0.154	0.0644	0.959	0.0671	0.000272
101	14.12	0.00103	0.152	0.0629	1.034	0.0608	0.000301
102	14.29	0.00125	0.153	0.0612	1.026	0.0597	0.000309
103	14.46	0.00138	0.155	0.0595	0.968	0.0615	0.000278
104	14.62	0.00141	0.154	0.0592	0.929	0.0638	0.000258
105	14.79	0.00133	0.153	0.0599	0.938	0.0638	0.000275
107	14.95	0.00104	0.154	0.0594	0.974	0.0610	0.000277
108	15.12	0.00091	0.153	0.0582	0.976	0.0597	0.000275
109	15.29	0.00094	0.152	0.0575	0.965	0.0595	0.000292
110	15.47	0.00099	0.153	0.0575	0.964	0.0596	0.000341
111	15.62	0.00102	0.154	0.0580	0.976	0.0594	0.000306
113	15.79	0.00128	0.153	0.0572	1.073	0.0533	0.000326
114	15.95	0.00126	0.152	0.0558	1.027	0.0544	0.000314
115	16.12	0.00117	0.151	0.0543	0.951	0.0571	0.000319
116	16.29	0.00122	0.150	0.0552	1.013	0.0544	0.000248
117	16.47	0.00157	0.149	0.0588	0.980	0.0600	0.000436
118	16.62	0.00163	0.147	0.0605	0.968	0.0625	0.000421
119	16.79	0.00167	0.149	0.0601	0.954	0.0630	0.000375
120	16.96	0.00176	0.151	0.0585	0.896	0.0653	0.000343
121	17.12	0.00174	0.153	0.0572	0.871	0.0656	0.000307
122	17.29	0.00167	0.154	0.0577	0.887	0.0650	0.000327
123	17.45	0.00154	0.153	0.0592	0.902	0.0656	0.000296
124	17.62	0.00142	0.153	0.0601	0.876	0.0686	0.000268
126	17.79	0.00142	0.154	0.0596	0.875	0.0681	0.000339
127	17.95	0.00133	0.154	0.0585	0.946	0.0619	0.000316
128	18.13	0.00109	0.153	0.0582	0.929	0.0626	0.000310
129	18.29	0.00089	0.151	0.0579	0.919	0.0630	0.000331
130	18.45	0.00085	0.151	0.0557	1.073	0.0519	0.000318
131	18.62	0.00085	0.150	0.0532	1.026	0.0519	0.000277
132	18.79	0.00088	0.150	0.0526	0.876	0.0601	0.000289
133	18.95	0.00091	0.149	0.0538	0.900	0.0598	0.000334
135	19.12	0.00111	0.149	0.0545	0.964	0.0565	0.000442
136	19.29	0.00140	0.147	0.0541	0.944	0.0573	0.000428
137	19.56	0.00132	0.146	0.0554	0.903	0.0613	0.000332
138	19.62	0.00143	0.146	0.0566	0.915	0.0618	0.000379
139	19.79	0.00153	0.147	0.0551	0.919	0.0600	0.000365
141	19.95	0.00157	0.149	0.0529	0.903	0.0586	0.000340
142	20.12	0.00144	0.149	0.0521	0.893	0.0584	0.000304
143	20.29	0.00132	0.149	0.0516	0.898	0.0574	0.000289

Note: n/a – data not available.

Table A-2. Values of experimental time, slope, flow depth, bedform height, bedform length, aspect ratio and translation rate at mixed transport stage. Bedform H, L, H/L and translation rates were measured with the automated methods.

Index	Time (hr)	S	d (m)	H (m)	L (m)	H/L	Translation rate (m/sec)
3	0.30	0.00280	0.156	0.0938	1.245	0.0754	0.00113
4	0.47	0.00304	0.154	0.0937	1.177	0.0796	0.00131
6	0.64	0.00294	0.151	0.0904	1.141	0.0792	0.00131
7	0.81	0.00270	0.152	0.0843	1.137	0.0741	0.00127
8	1.00	0.00255	0.153	0.0724	1.045	0.0693	0.00093
9	1.31	0.00312	0.152	0.0735	1.241	0.0593	0.00087
12	1.47	0.00406	0.152	0.0797	1.288	0.0618	0.00139
13	1.64	0.00419	0.151	0.0847	1.324	0.0639	0.00107
14	1.87	0.00376	0.153	0.0882	1.437	0.0614	0.00109
16	2.06	0.00394	0.155	0.0846	1.329	0.0636	0.00115
18	2.14	0.00380	0.156	0.0813	1.261	0.0645	0.00116
19	2.30	0.00297	0.156	0.0780	1.216	0.0641	0.00087
20	2.49	0.00236	0.155	0.0779	1.323	0.0589	0.00095
21	2.65	0.00280	0.153	0.0834	1.326	0.0629	0.00102
22	2.80	0.00349	0.149	0.0872	1.266	0.0689	0.00130
23	2.97	0.00332	0.150	0.0873	1.291	0.0677	0.00112
24	3.14	0.00296	0.156	0.0868	1.440	0.0603	0.00105
25	3.30	0.00326	0.154	0.0832	1.423	0.0585	0.00114
26	3.47	0.00296	0.151	0.0760	1.217	0.0625	0.00107
27	3.64	0.00240	0.150	0.0729	1.186	0.0615	0.00097
28	3.80	0.00303	0.148	0.0736	1.263	0.0583	0.00144
29	3.97	0.00411	0.149	0.0830	1.306	0.0636	0.00160
31	4.14	0.00391	0.151	0.0873	1.209	0.0722	0.00125
32	4.31	0.00297	0.150	0.0763	1.190	0.0641	0.00107
33	4.47	0.00342	0.150	0.0751	1.264	0.0594	0.00155
34	4.64	0.00354	0.149	0.0780	1.412	0.0553	0.00116
35	4.80	0.00298	0.146	0.0714	1.382	0.0516	0.00114
36	4.97	0.00309	0.147	0.0712	1.246	0.0571	0.00152
37	5.14	0.00377	0.150	0.0810	1.388	0.0583	0.00137
38	5.31	0.00430	0.152	0.0842	1.417	0.0594	0.00131
39	5.47	0.00437	0.151	0.0813	1.257	0.0646	0.00132
40	5.82	0.00409	0.152	0.0839	1.426	0.0589	0.00084
42	5.97	0.00411	0.152	0.0889	1.627	0.0546	0.00117
43	6.14	0.00427	0.153	0.0948	1.456	0.0651	0.00131
44	6.31	0.00401	0.158	0.0989	1.391	0.0711	0.00130

46	6.54	0.00328	0.156	0.0936	1.437	0.0652	0.00093
47	6.64	0.00294	0.151	0.0906	1.619	0.0560	0.00098
48	6.80	0.00335	0.151	0.0920	1.779	0.0517	0.00113
49	6.97	0.00312	0.149	0.0902	1.676	0.0538	0.00102
50	7.25	0.00266	0.147	0.0810	1.403	0.0577	0.00103
53	7.38	0.00303	0.146	0.0775	1.235	0.0627	0.00131
55	7.47	0.00329	0.145	0.0811	1.255	0.0646	0.00152
56	7.64	0.00357	0.145	0.0841	1.414	0.0595	0.00106
57	7.80	0.00408	0.148	0.0859	1.649	0.0521	0.00133
58	7.97	0.00375	0.153	0.0849	1.595	0.0532	0.00110
59	8.14	0.00355	0.153	0.0839	1.500	0.0560	0.00117
60	8.30	0.00324	0.151	0.0794	1.326	0.0599	0.00089
107	8.89	0.00306	0.156	0.0909	1.233	0.0737	0.00125
108	9.05	0.00364	0.156	0.0935	1.391	0.0672	0.00117
109	9.23	0.00322	0.157	0.0848	1.392	0.0609	0.00091
110	9.39	0.00296	0.156	0.0786	1.347	0.0583	0.00101
111	9.56	0.00301	0.150	0.0814	1.319	0.0617	0.00104
112	9.79	0.00386	0.150	0.0869	1.306	0.0666	0.00112
114	9.90	0.00407	0.154	0.0829	1.383	0.0599	0.00133
115	10.15	0.00316	0.154	0.0777	1.419	0.0548	0.00108
117	10.22	0.00325	0.152	0.0812	1.338	0.0607	0.00130
118	10.39	0.00383	0.155	0.0835	1.323	0.0631	0.00126
121	10.63	0.00346	0.154	0.0810	1.289	0.0628	0.00095
123	10.82	0.00308	0.152	0.0810	1.328	0.0610	0.00115
125	10.89	0.00303	0.155	0.0809	1.489	0.0544	0.00122
126	11.06	0.00333	0.151	0.0815	1.440	0.0566	0.00122
127	11.24	0.00362	0.150	0.0870	1.387	0.0628	0.00125
128	11.45	0.00335	0.153	0.0917	1.494	0.0614	0.00109
130	11.55	0.00330	0.153	0.0926	1.472	0.0629	0.00094
131	11.73	0.00319	0.154	0.0904	1.501	0.0602	0.00101
132	11.95	0.00289	0.152	0.0828	1.459	0.0567	0.00097
134	12.05	0.00286	0.153	0.0732	1.220	0.0600	0.00119
135	12.22	0.00315	0.153	0.0814	1.247	0.0653	0.00115
136	12.40	0.00372	0.153	0.0945	1.417	0.0667	0.00130
137	12.57	0.00387	0.155	0.0924	1.519	0.0609	0.00105
138	12.72	0.00375	0.155	0.0884	1.470	0.0601	0.00119
139	12.89	0.00408	0.154	0.0887	1.435	0.0618	0.00118
140	13.12	0.00349	0.155	0.0813	1.364	0.0596	0.00090
142	13.22	0.00265	0.155	0.0729	1.157	0.0630	0.00152
143	13.60	0.00288	0.153	0.0723	1.127	0.0641	0.00072
147	13.75	0.00286	0.151	0.0687	1.039	0.0661	0.00133

148	13.96	0.00298	0.150	0.0716	1.139	0.0629	0.00142
150	14.05	0.00379	0.149	0.0807	1.392	0.0580	0.00174
151	14.22	0.00370	0.149	0.0822	1.279	0.0643	0.00118
152	14.39	0.00369	0.149	0.0815	1.211	0.0673	0.00137
153	14.69	0.00396	0.152	0.0817	1.269	0.0644	0.00097
156	14.87	0.00314	0.154	0.0755	1.131	0.0668	0.00122
157	15.04	0.00316	0.156	0.0753	1.138	0.0662	0.00152
159	15.20	0.00352	0.155	0.0804	1.325	0.0606	0.00114
160	15.46	0.00427	0.151	0.0846	1.336	0.0634	0.00080
162	15.73	0.00424	0.153	0.0885	1.330	0.0665	0.00112
164	15.89	0.00284	0.157	0.0876	1.366	0.0641	0.00082
165	16.08	0.00239	0.156	0.0828	1.277	0.0648	0.00093
166	16.22	0.00223	0.155	0.0760	1.223	0.0621	0.00083
167	16.50	0.00281	0.154	0.0749	1.204	0.0622	0.00123
169	16.64	0.00355	0.151	0.0744	1.127	0.0660	0.00173
170	16.85	0.00399	0.151	0.0801	1.224	0.0654	0.00175

Table A-3. Values of experimental time, slope, flow depth, bedform height, bedform length, aspect ratio and translation rate at suspension-dominated transport stage. Bedform H, L, H/L and translation rates were measured with the automated methods.

Index		Time (hr)	Avg S (m)	Avg d (m)	Avg H (m)	Avg L (m)	Avg H/L	Translation Rate (m/sec)
2	1	0.13	0.00507	0.119	0.0301	1.996	0.0151	0.00659
2	2	0.21	0.00733	0.125	0.0313	2.010	0.0156	0.00502
2	3	0.30	0.01020	0.129	0.0376	1.962	0.0192	0.00453
2	4	0.38	0.01146	0.138	0.0426	2.245	0.0190	0.00470
2	5	0.46	0.00668	0.144	0.0501	2.774	0.0181	0.00363
2	6	0.55	0.00164	0.131	0.0487	2.693	0.0181	0.00397
2	7	0.63	0.00178	0.119	0.0407	2.157	0.0189	0.00332
2	8	0.71	0.00348	0.116	0.0329	2.194	0.0150	0.00565
2	9	0.80	0.00983	0.124	0.0398	2.647	0.0150	0.00471
2	10	0.88	0.01140	0.136	0.0525	3.124	0.0168	0.00273
2	11	0.96	0.00544	0.142	0.0498	3.073	0.0162	0.00306
2	12	1.05	0.00254	0.134	0.0397	2.295	0.0173	0.00352
2	13	1.13	0.00160	0.119	0.0307	1.729	0.0177	0.00561
2	14	1.22	0.00556	0.116	0.0305	1.832	0.0167	0.00497
2	15	1.30	0.01094	0.123	0.0373	2.253	0.0165	0.00476
2	16	1.38	0.01147	0.135	0.0448	2.672	0.0168	0.00349
2	17	1.49	0.00695	0.146	0.0526	2.685	0.0196	0.00345
2	18	1.55	0.00234	0.140	0.0517	3.260	0.0159	0.00214
2	19	1.63	0.00189	0.125	0.0368	3.205	0.0115	0.00320
2	20	1.72	0.00490	0.121	0.0283	2.184	0.0130	0.00622
2	21	1.80	0.01020	0.132	0.0372	2.002	0.0186	0.00573
2	22	1.88	0.01023	0.141	0.0445	1.857	0.0240	0.00401
2	23	1.96	0.00626	0.143	0.0494	1.772	0.0279	0.00437
2	24	2.05	0.00333	0.133	0.0491	2.020	0.0243	0.00330
2	25	2.13	0.00274	0.122	0.0373	1.836	0.0203	0.00361
2	26	2.27	0.00409	0.122	0.0308	1.877	0.0164	0.00252
2	27	2.31	0.00628	0.125	0.0352	2.596	0.0136	0.00507
2	28	2.38	0.00906	0.132	0.0420	3.018	0.0139	0.00489
2	29	2.46	0.00968	0.142	0.0481	2.609	0.0185	0.00359
2	30	2.55	0.00541	0.143	0.0553	2.055	0.0269	0.00298
2	31	2.64	0.00234	0.129	0.0492	1.989	0.0247	0.00462
2	32	2.72	0.00194	0.115	0.0325	1.886	0.0172	0.00409
2	33	2.80	0.00673	0.119	0.0313	2.042	0.0153	0.00614
2	34	2.88	0.01238	0.135	0.0460	2.414	0.0191	0.00314
2	35	2.96	0.00934	0.143	0.0537	2.438	0.0220	0.00326

2	36	3.05	0.00393	0.137	0.0467	2.299	0.0203	0.00311
2	37	3.08	0.00238	0.128	0.0364	2.043	0.0178	0.00582
2	38	3.18	0.00387	0.119	0.0304	1.745	0.0174	0.00450
2	39	3.27	0.00796	0.122	0.0306	1.726	0.0177	0.00570
2	40	3.35	0.00975	0.135	0.0349	1.810	0.0193	0.00520
2	41	3.43	0.00983	0.142	0.0404	2.291	0.0176	0.00510
2	42	3.51	0.00771	0.147	0.0487	2.731	0.0178	0.00363
2	43	3.60	0.00222	0.139	0.0535	2.798	0.0191	0.00421
2	44	3.68	0.00137	0.127	0.0476	2.570	0.0185	0.00490
2	45	3.78	0.00309	0.122	0.0344	2.072	0.0166	0.00509
2	46	3.85	0.00739	0.123	0.0310	2.411	0.0129	0.00585
2	47	3.93	0.01022	0.133	0.0386	2.517	0.0153	0.00353
2	48	4.01	0.00818	0.144	0.0459	1.720	0.0267	0.00470
2	49	4.10	0.00391	0.137	0.0443	2.384	0.0186	0.00274
2	50	4.18	0.00101	0.122	0.0366	2.775	0.0132	0.00387
2	51	4.26	0.00388	0.117	0.0302	2.040	0.0148	0.00528
2	52	4.35	0.01034	0.126	0.0332	2.280	0.0146	0.00397
2	53	4.43	0.01238	0.137	0.0462	2.494	0.0185	0.00328
2	54	4.51	0.00990	0.145	0.0510	2.069	0.0247	0.00396
2	55	4.60	0.00542	0.142	0.0486	2.141	0.0227	0.00494
2	56	4.69	0.00181	0.127	0.0426	1.971	0.0216	0.00505
2	57	4.80	0.00771	0.123	0.0412	1.654	0.0249	n/a
2	58	4.85	0.01285	0.135	0.0573	2.172	0.0264	n/a
2	59	4.93	0.00805	0.142	0.0579	2.670	0.0217	0.00100
2	60	5.01	0.00261	0.136	0.0463	2.790	0.0166	0.00379
2	61	5.10	0.00190	0.127	0.0418	2.604	0.0160	0.00615
2	62	5.18	0.00362	0.120	0.0337	2.345	0.0144	0.00493
2	63	5.27	0.00627	0.124	0.0363	2.254	0.0161	0.00558
2	64	5.35	0.00917	0.133	0.0455	2.460	0.0185	0.00434
2	65	5.43	0.00864	0.145	0.0536	2.274	0.0236	0.00376
2	66	5.52	0.00471	0.142	0.0527	2.002	0.0263	0.00304
2	67	5.61	0.00154	0.127	0.0409	1.762	0.0232	0.00421
2	68	5.69	0.00461	0.120	0.0362	2.250	0.0161	0.00459
2	69	5.76	0.01010	0.125	0.0450	2.747	0.0164	0.00634
2	70	5.79	0.01079	0.135	0.0531	2.588	0.0205	0.00398
2	71	5.85	0.00947	0.137	0.0526	2.565	0.0205	0.00431
2	72	5.93	0.00508	0.139	0.0507	2.552	0.0199	0.00293
2	73	6.07	0.00262	0.136	0.0435	2.162	0.0201	0.00016
2	74	6.18	0.00475	0.133	0.0413	1.862	0.0222	0.00305
2	75	6.26	0.00339	0.134	0.0474	2.248	0.0211	0.00416
2	76	6.36	0.00085	0.128	0.0437	1.952	0.0224	0.00355

2	77	6.45	0.00594	0.123	0.0348	1.732	0.0201	0.00676
2	78	6.52	0.01090	0.130	0.0328	1.856	0.0177	0.00498
2	79	6.60	0.00987	0.141	0.0412	1.718	0.0239	0.00384
2	80	6.68	0.00583	0.141	0.0525	1.982	0.0265	0.00331
2	81	6.76	0.00302	0.131	0.0504	1.879	0.0268	0.00385
2	82	6.85	0.00432	0.121	0.0372	1.816	0.0205	0.00573
2	83	6.93	0.00878	0.124	0.0366	1.754	0.0208	0.00409
2	84	7.01	0.01017	0.136	0.0422	1.634	0.0259	0.00405
2	85	7.10	0.00697	0.139	0.0437	1.985	0.0220	0.00371
2	86	7.21	0.00306	0.137	0.0541	2.170	0.0249	0.00355
2	87	7.29	0.00082	0.129	0.0492	2.226	0.0221	0.00309
2	88	7.37	0.00227	0.119	0.0338	2.044	0.0166	0.00696
2	89	7.43	0.00594	0.122	0.0402	2.536	0.0158	0.00519
2	90	7.51	0.00921	0.135	0.0467	3.055	0.0153	0.00473
2	91	7.61	0.00611	0.140	0.0460	2.566	0.0179	0.00286
12	1	7.90	0.00885	0.136	0.0429	1.866	0.0230	0.00403
12	2	8.00	0.00769	0.141	0.0479	2.208	0.0217	0.00415
12	3	8.07	0.00313	0.142	0.0527	2.409	0.0219	0.00318
12	4	8.15	0.00193	0.129	0.0426	2.460	0.0173	0.00678
14	1	8.24	0.00413	0.117	0.0328	1.875	0.0175	0.00496
14	2	8.32	0.00844	0.118	0.0341	1.560	0.0218	0.00425
14	3	8.40	0.01305	0.130	0.0402	1.772	0.0227	0.00469
14	4	8.49	0.01234	0.147	0.0465	1.899	0.0245	0.00614
16	1	8.57	0.00778	0.154	0.0507	2.022	0.0251	0.00403
16	2	8.65	0.00380	0.146	0.0541	1.885	0.0287	0.00386
16	3	8.74	0.00116	0.133	0.0486	1.636	0.0297	0.00689
18	1	8.82	0.00162	0.128	0.0414	2.103	0.0197	0.00427
18	2	8.91	0.00743	0.134	0.0484	2.813	0.0172	n/a
18	3	8.99	0.00910	0.145	0.0525	2.737	0.0192	n/a
18	4	9.09	0.00429	0.147	0.0504	1.992	0.0253	0.00726
20	1	9.16	0.00251	0.132	0.0461	1.932	0.0239	0.00494
20	2	9.24	0.00241	0.120	0.0387	2.256	0.0172	0.00446
20	3	9.32	0.00659	0.124	0.0431	2.310	0.0187	0.00926
22	1	9.40	0.01159	0.130	0.0564	2.582	0.0218	0.00332
22	2	9.49	0.01157	0.141	0.0594	2.504	0.0237	0.00453
22	3	9.57	0.00605	0.150	0.0629	2.107	0.0299	0.00294
22	4	9.65	0.00254	0.143	0.0664	2.748	0.0242	0.00302
22	5	9.74	0.00385	0.129	0.0551	2.967	0.0186	0.00677
24	1	9.82	0.00353	0.124	0.0404	2.035	0.0199	0.00436
24	2	9.94	0.00830	0.127	0.0453	2.092	0.0217	0.00460
24	3	9.99	0.01228	0.134	0.0543	2.468	0.0220	0.00474

24	4	10.07	0.00992	0.143	0.0511	2.429	0.0210	0.00576
26	1	10.16	0.00559	0.144	0.0545	2.089	0.0261	0.00416
28	1	10.24	0.00218	0.139	0.0523	1.847	0.0283	0.00240
28	2	10.32	0.00232	0.130	0.0449	1.845	0.0243	0.00553
28	3	10.40	0.00571	0.121	0.0381	1.914	0.0199	0.00356
28	4	10.49	0.00826	0.127	0.0383	2.177	0.0176	0.00596
30	1	10.57	0.00743	0.140	0.0479	2.339	0.0205	0.00490
30	2	10.65	0.00634	0.140	0.0471	1.917	0.0246	0.00378
30	3	10.74	0.00737	0.141	0.0475	1.733	0.0274	0.00637
32	1	10.82	0.00681	0.146	0.0523	2.023	0.0258	0.00333
32	2	10.91	0.00334	0.137	0.0443	1.949	0.0227	0.00329
32	3	10.99	0.00453	0.131	0.0407	1.928	0.0211	0.00489
32	4	11.08	0.00890	0.133	0.0471	2.186	0.0216	0.00329
34	1	11.15	0.01068	0.139	0.0574	2.515	0.0228	0.00228
34	2	11.28	0.00692	0.145	0.0623	2.688	0.0232	0.00293
34	3	11.35	0.00188	0.141	0.0559	2.660	0.0210	0.00308
34	4	11.43	0.00092	0.135	0.0479	2.274	0.0211	0.00858
36	1	11.49	0.00329	0.136	0.0424	1.785	0.0237	0.00493
36	2	11.57	0.00553	0.136	0.0465	2.731	0.0170	0.00554
36	3	11.65	0.00754	0.135	0.0459	3.420	0.0134	0.00456
36	4	11.74	0.00957	0.139	0.0463	2.827	0.0164	0.00435
36	5	11.83	0.01123	0.142	0.0536	2.216	0.0242	0.00339
36	6	11.91	0.00683	0.143	0.0573	2.475	0.0231	0.00425
38	1	11.99	0.00224	0.142	0.0540	2.508	0.0215	0.00355
38	2	12.07	0.00437	0.137	0.0479	2.258	0.0212	0.00305
38	3	12.15	0.00640	0.136	0.0487	2.329	0.0209	0.00767
40	1	12.26	0.00377	0.137	0.0528	2.250	0.0234	0.00402
40	2	12.32	0.00047	0.131	0.0487	2.426	0.0201	0.00356
40	3	12.40	0.00433	0.131	0.0437	2.336	0.0187	0.00274
40	4	12.50	0.00664	0.137	0.0448	1.984	0.0226	0.00310
40	5	12.58	0.00629	0.138	0.0458	1.969	0.0233	0.00625
42	1	12.66	0.00696	0.139	0.0504	2.292	0.0220	0.00457
42	2	12.74	0.00745	0.143	0.0525	2.217	0.0237	0.00208
42	3	12.84	0.00794	0.144	0.0465	2.312	0.0201	0.00339
42	4	12.91	0.00874	0.142	0.0489	2.508	0.0195	0.00469
42	5	12.99	0.00767	0.143	0.0588	2.417	0.0243	0.00829
44	1	13.03	0.00289	0.142	0.0585	2.340	0.0250	0.00377
44	2	13.07	0.00131	0.136	0.0548	2.063	0.0266	0.00367
44	3	13.16	0.00146	0.129	0.0505	1.969	0.0257	0.00208
44	4	13.24	0.00219	0.127	0.0511	2.159	0.0237	0.00316
46	1	13.32	0.00614	0.132	0.0529	1.961	0.0270	0.00492

46	2	13.40	0.00624	0.136	0.0542	1.772	0.0306	0.00487
46	3	13.49	0.00481	0.136	0.0584	2.129	0.0274	0.00441
46	4	13.57	0.00367	0.137	0.0526	2.449	0.0215	0.00300
46	5	13.67	0.00513	0.140	0.0497	2.712	0.0183	0.00747
48	1	13.75	0.00669	0.146	0.0531	2.688	0.0198	0.00278
48	2	13.82	0.00378	0.143	0.0481	2.217	0.0217	0.00270
48	3	13.90	0.00469	0.133	0.0455	2.292	0.0198	0.00487
48	4	13.96	0.00781	0.131	0.0533	2.759	0.0193	0.00692
48	5	13.99	0.00796	0.130	0.0507	2.575	0.0197	0.00650
48	6	14.07	0.00768	0.134	0.0414	1.785	0.0232	0.00280
48	7	14.15	0.00671	0.142	0.0442	1.740	0.0254	0.00623
50	1	14.24	0.00277	0.134	0.0426	1.858	0.0229	0.00314
50	2	14.34	0.00471	0.126	0.0387	1.996	0.0194	0.00266
50	3	14.40	0.01033	0.129	0.0396	2.099	0.0189	0.00503
50	4	14.49	0.01113	0.134	0.0429	1.923	0.0223	0.00801
52	1	14.57	0.01008	0.142	0.0523	1.966	0.0266	0.00335
52	2	14.66	0.00532	0.146	0.0543	1.942	0.0280	0.00295
52	3	14.74	0.00073	0.137	0.0464	1.828	0.0254	0.00748
54	1	14.83	0.00308	0.128	0.0403	1.775	0.0227	0.00469
54	2	14.91	0.00914	0.135	0.0398	1.766	0.0226	0.00489
54	3	14.99	0.00890	0.146	0.0466	1.851	0.0251	0.00473
54	4	15.08	0.00322	0.144	0.0548	2.226	0.0246	0.00331
54	5	15.16	0.00065	0.134	0.0511	2.092	0.0244	0.00824
56	1	15.24	0.00542	0.128	0.0421	1.887	0.0223	0.00365
56	2	15.32	0.01087	0.133	0.0365	1.940	0.0188	0.00176
56	3	15.41	0.01080	0.139	0.0386	1.758	0.0220	0.00344
56	4	15.50	0.00985	0.141	0.0455	1.740	0.0261	0.00663
58	1	15.57	0.00816	0.150	0.0597	1.947	0.0306	0.00393
58	2	15.65	0.00535	0.147	0.0634	1.941	0.0327	0.00322
58	3	15.74	0.00211	0.132	0.0522	2.028	0.0257	0.00367
58	4	15.82	0.00417	0.129	0.0456	1.423	0.0321	0.00382
58	5	15.91	0.00934	0.134	0.0469	1.848	0.0254	0.00598
60	1	15.99	0.01075	0.140	0.0607	3.034	0.0200	n/a

Note: n/a – data not available.

Appendix 2

Bedload transport measurements

Two miniaturized Helley-Smith samplers [*Helley and Smith*, 1971] were attached to a holding rod making it a sampler set (Figure 3-8). The 'top' sampler collected sediment moving within the bottom 0.02m of the flow while the 'bottom' sampler collected sediment between 0.02 and 0.04m above the bed. Sampler set 'A' was positioned at Y=0.75m. Sampler set 'B' was positioned at Y=0.5m. Sampler set 'C' was positioned at Y=0.25m. Some sampling trials do not contain samples from all three sampler sets because sampling conditions were poor and samples taken were considered unrepresentative.

Table A-4. Bedload transport measurements at bedload-dominated transport stage.

Index	Time (hr)	Samplers (g)						Average			
		A-top	A-bottom	B-top	B-bottom	C-top	C-bottom	Top	Bottom	Top (g/sec)	Bottom (g/sec)
1	0.15	0.056	10.302	0.030	22.303	n/a	n/a	0.043	16.303	0.001	0.272
2	1.08	n/a	n/a	0.171	20.387	n/a	n/a	0.171	20.387	0.003	0.340
3	2.00	0.305	20.637	0.202	10.360	0.191	11.056	0.233	14.018	0.004	0.234
4	2.24	0.158	33.144	0.105	19.297	0.094	23.649	0.119	25.363	0.002	0.423
5	4.43	n/a	n/a	0.385	13.755	0.091	28.889	0.238	21.322	0.004	0.355
6	5.12	0.134	10.794	0.134	5.644	0.079	12.331	0.116	9.590	0.002	0.160
7	5.80	0.204	15.980	n/a	n/a	n/a	n/a	0.204	15.980	0.003	0.266
8	6.28	0.091	26.209	0.188	20.306	n/a	n/a	0.140	23.258	0.002	0.388

9	7.08	n/a	n/a	0.176	13.165	0.072	21.347	0.124	17.256	0.002	0.288
10	8.08	0.167	56.685	0.485	27.610	0.269	27.043	0.307	37.113	0.005	0.619
11	9.08	n/a	n/a	0.864	29.937	0.134	42.351	0.134	42.351	0.002	0.706
12	9.73	0.313	25.934	0.183	15.363	0.297	30.471	0.264	23.923	0.004	0.399
13	10.03	0.594	79.920	0.470	16.380	n/a	n/a	0.532	48.150	0.009	0.803
14	10.69	0.274	45.160	n/a	n/a	n/a	n/a	0.274	45.160	0.005	0.753
15	11.21	0.365	47.246	1.600	65.686	n/a	n/a	0.983	56.466	0.016	0.941
16	12.04	n/a	n/a	0.215	36.465	0.210	43.321	0.213	39.893	0.004	0.665
17	12.86	0.124	16.108	n/a	n/a	0.192	34.516	0.158	25.312	0.003	0.422
18	13.87	0.192	28.730	n/a	n/a	n/a	n/a	0.192	28.730	0.003	0.479
19	14.37	0.607	53.966	0.566	20.268	0.944	38.696	0.706	37.643	0.012	0.627
20	14.89	0.597	48.578	0.550	31.284	0.225	44.203	0.457	41.355	0.008	0.689
21	15.68	0.700	74.433	0.175	31.015	0.280	51.751	0.385	52.400	0.006	0.873
22	16.19	0.127	43.367	0.185	31.937	n/a	n/a	0.156	37.652	0.003	0.628
23	17.04	0.280	30.372	0.343	20.851	0.289	60.444	0.312	25.612	0.005	0.427
24	17.70	0.185	30.492	0.119	41.141	0.402	36.707	0.261	38.924	0.004	0.649

Note: n/a – data not available.

Table A-5. Bedload transport measurements at mixed transport stage.

Index	Time (hr)	Samplers (g)						Average			
		A-top	A-bottom	B-top	B-bottom	C-top	C-bottom	Top	Bottom	Top (g/sec)	Bottom (g/sec)
1	1.38	n/a	n/a	n/a	n/a	26.34	154.98	26.343	154.977	0.439	2.583
2	1.54	6.640	146.712	12.220	125.924	2.965	186.107	4.803	166.410	0.080	2.773
3	2.20	2.659	85.374	3.748	46.992	3.226	82.044	3.211	71.470	0.054	1.191
4	2.86	3.669	153.010	13.722	125.806	2.918	136.268	6.770	138.361	0.113	2.306
5	3.38	4.867	116.691	52.103	14.576	19.804	99.580	25.591	76.949	0.427	1.282
6	4.06	3.501	162.667	10.375	131.847	7.088	70.690	6.988	121.735	0.116	2.029
7	4.92	6.947	170.847	4.535	69.875	5.145	44.279	5.542	95.000	0.092	1.583
8	5.36	3.358	189.343	9.444	77.403	4.083	95.949	5.628	120.898	0.094	2.015
9	6.03	6.184	182.449	3.119	116.676	18.802	174.411	9.368	157.845	0.156	2.631
10	6.71	9.326	199.372	52.202	52.263	n/a	n/a	30.764	125.818	0.513	2.097
11	7.87	4.739	113.208	16.323	112.558	5.514	43.843	8.859	89.870	0.148	1.498
12	8.52	3.191	175.667	4.676	82.342	3.997	64.679	3.955	107.563	0.066	1.793
13	8.95	30.697	202.214	10.392	207.659	n/a	n/a	20.545	204.937	0.342	3.416
14	9.63	2.919	122.528	5.236	102.068	4.263	87.377	4.078	112.298	0.068	1.872
17	10.69	n/a	n/a	2.571	145.043	n/a	n/a	2.571	145.043	0.043	2.417
18	12.79	3.658	126.497	12.165	109.803	48.439	233.057	21.421	156.452	0.357	2.608
19	13.66	30.440	190.053	4.802	54.467	31.420	120.914	22.221	121.811	0.370	2.030
20	14.11	31.990	239.085	2.468	88.405	60.318	123.245	31.592	150.245	0.527	2.504
21	15.54	5.127	201.787	n/a	n/a	4.698	198.944	4.913	200.366	0.082	3.339
22	16.14	19.277	106.611	38.187	6.468	151.401	61.550	69.622	58.210	1.160	0.970
23	16.58	29.112	68.958	n/a	n/a	43.898	232.014	43.898	232.014	0.732	3.867

Note: n/a – data not available.

Table A-6. Bedload transport measurements at suspension-dominated transport stage.

Index	Time (hr)	Samplers (g)						Average			
		A-top	A-bottom	B-top	B-bottom	C-top	C-bottom	Top	Bottom	Top (g/sec)	Bottom (g/sec)
1	0.13	8.673	150.785	21.182	116.000	n/a	n/a	14.928	133.393	1.493	13.339
2	0.41	5.595	84.212	n/a	n/a	n/a	n/a	5.595	84.212	0.560	8.421
3	1.16	8.717	22.426	89.018	14.912	14.143	162.002	37.293	66.447	3.729	6.645
4	1.66	12.920	36.135	n/a	n/a	15.351	108.971	14.136	72.553	1.414	7.255
5	2.14	6.010	93.833	56.280	101.202	89.690	178.263	50.660	124.433	5.066	12.443
6	2.91	5.433	49.988	n/a	n/a	41.541	163.878	23.487	106.933	2.349	10.693
7	3.31	6.538	143.533	n/a	n/a	n/a	n/a	6.538	143.533	0.654	14.353
8	3.71	10.128	78.310	n/a	n/a	n/a	n/a	10.128	78.310	1.013	7.831
9	4.13	5.999	99.840	n/a	n/a	4.491	97.396	5.245	98.618	0.525	9.862
10	4.46	9.753	122.220	n/a	n/a	n/a	n/a	9.753	122.220	0.975	12.222
11	4.81	10.225	119.111	106.426	110.425	30.281	37.013	48.977	88.850	4.898	8.885
12	5.81	4.180	76.213	60.982	62.308	14.422	51.185	26.528	63.235	2.653	6.324
13	6.64	6.369	113.718	7.418	193.062	27.768	152.194	13.852	152.991	1.385	15.299
14	7.31	4.226	56.701	4.391	75.144	n/a	n/a	4.309	65.923	0.431	6.592
15	8.14	6.671	97.528	108.006	6.898	n/a	n/a	57.339	52.213	5.734	5.221
16	8.81	11.267	119.303	n/a	n/a	n/a	n/a	11.267	119.303	1.127	11.930
17	9.64	5.987	127.913	n/a	n/a	11.057	38.037	8.522	82.975	0.852	8.298
18	10.31	3.502	64.762	n/a	n/a	5.429	89.480	4.466	77.121	0.447	7.712
19	11.14	n/a	n/a	n/a	n/a	14.845	77.931	14.845	77.931	1.485	7.793
20	11.81	3.805	69.152	51.709	35.533	6.755	57.077	20.756	53.921	2.076	5.392
21	12.64	4.894	159.268	85.453	36.979	103.387	87.940	64.578	94.729	6.458	9.473
23	13.31	5.208	40.798	223.460	46.593	82.390	170.396	43.799	105.597	4.380	10.560
24	14.14	11.455	45.558	n/a	n/a	34.920	49.343	23.188	47.451	2.319	4.745

Suspended-load transport measurements

Suspended-load transport was measured in grams per litre. The sampling method was described in section 3.2.3. Raw measurements were converted into concentration and the depth-averaged suspended-load transport measurements were calculated. The detail of the calculation was described in section 3.2.5.2.

Table A-7. Suspended-load transport measurements at bedload-dominated transport stage.

Index	Time (hr)	g/L @ 4cm	Concentration	Depth-averaged		
				Concentration	m^3/sec	g/sec/m
2	1.22	0.01	3.77×10^{-6}	4.46×10^{-6}	2.9×10^{-7}	0.769
4	1.51	0.011	4.15×10^{-6}	4.91×10^{-6}	3.19×10^{-7}	0.846
5	2.34	0.009	3.4×10^{-6}	4.02×10^{-6}	2.61×10^{-7}	0.692
6	3.24	0.008	3.02×10^{-6}	3.57×10^{-6}	2.32×10^{-7}	0.615
7	4.87	0.009	3.4×10^{-6}	4.02×10^{-6}	2.61×10^{-7}	0.692
8	6.50	0.009	3.4×10^{-6}	4.02×10^{-6}	2.61×10^{-7}	0.692
9	8.13	0.009	3.4×10^{-6}	4.02×10^{-6}	2.61×10^{-7}	0.692
10	9.76	0.006	2.26×10^{-6}	2.68×10^{-6}	1.74×10^{-7}	0.461
12	11.40	0.008	3.02×10^{-6}	3.57×10^{-6}	2.32×10^{-7}	0.615
13	13.03	0.012	4.53×10^{-6}	5.36×10^{-6}	3.48×10^{-7}	0.923
14	14.03	0.011	4.15×10^{-6}	4.91×10^{-6}	3.19×10^{-7}	0.846
15	14.54	0.01	3.77×10^{-6}	4.46×10^{-6}	2.9×10^{-7}	0.769
16	15.06	0.017	6.42×10^{-6}	7.59×10^{-6}	4.93×10^{-7}	1.307
18	16.36	0.009	3.4×10^{-6}	4.02×10^{-6}	2.61×10^{-7}	0.692
19	17.06	0.01	3.77×10^{-6}	4.46×10^{-6}	2.9×10^{-7}	0.769

Table A-8. Suspended-load sediment transport measurements at mixed transport stage.

Index	Time (hr)	g/L @ 4cm	Concentration	Depth-averaged		
				Concentration	m^3/sec	g/sec/m
1	1.22	0.206	7.77×10^{-5}	4.19×10^{-5}	3.68×10^{-6}	9.764
2	2.12	0.068	2.57×10^{-5}	1.38×10^{-5}	1.22×10^{-6}	3.223
3	3.03	0.139	5.25×10^{-5}	2.83×10^{-5}	2.49×10^{-6}	6.588

4	3.54	0.057	2.15×10^{-5}	1.16×10^{-5}	1.02×10^{-6}	2.702
6	4.75	0.136	5.13×10^{-5}	2.76×10^{-5}	2.43×10^{-6}	6.446
7	5.87	0.098	3.7×10^{-5}	1.99×10^{-5}	1.75×10^{-6}	4.645
8	6.99	0.218	8.23×10^{-5}	4.43×10^{-5}	3.9×10^{-6}	10.333
9	8.11	0.202	7.62×10^{-5}	4.11×10^{-5}	3.61×10^{-6}	9.574
10	9.23	0.257	9.7×10^{-5}	5.22×10^{-5}	4.6×10^{-6}	12.181
11	10.35	0.094	3.55×10^{-5}	1.91×10^{-5}	1.68×10^{-6}	4.455
12	11.48	0.239	9.02×10^{-5}	4.86×10^{-5}	4.27×10^{-6}	11.328
13	12.60	0.185	6.98×10^{-5}	3.76×10^{-5}	3.31×10^{-6}	8.768
14	13.72	0.052	1.96×10^{-5}	1.06×10^{-5}	9.3×10^{-7}	2.465
15	14.84	0.113	4.26×10^{-5}	2.3×10^{-5}	2.02×10^{-6}	5.356
16	15.96	0.188	7.09×10^{-5}	3.82×10^{-5}	3.36×10^{-6}	8.911
17	17.08	0.481	1.82×10^{-4}	9.78×10^{-5}	8.6×10^{-6}	22.798

Table A-9. Suspended-load sediment transport measurements at suspension-dominated transport stage.

Index	Time (hr)	g/L @ 4cm	Concentration	Depth-averaged		
				Concentration	m^3/sec	g/sec/m
1	1.22	1.324	0.0005	0.000258	3.35×10^{-5}	88.866
2	2.15	2.518	0.00095	0.000491	6.38×10^{-5}	169.007
3	3.08	0.699	0.000264	0.000136	1.77×10^{-5}	46.917
4	4.01	0.727	0.000274	0.000142	1.84×10^{-5}	48.796
5	4.94	0.970	0.000366	0.000189	2.46×10^{-5}	65.106
6	5.87	1.021	0.000385	0.000199	2.59×10^{-5}	68.529
7	6.80	0.528	0.000199	0.000103	1.34×10^{-5}	35.439
8	7.73	0.528	0.000199	0.000103	1.34×10^{-5}	35.439
9	8.66	0.676	0.000255	0.000132	1.71×10^{-5}	45.373
10	9.58	0.590	0.000223	0.000115	1.49×10^{-5}	39.601
11	10.51	0.872	0.000329	0.00017	2.21×10^{-5}	58.528
12	11.44	1.122	0.000423	0.000219	2.84×10^{-5}	75.308
13	12.37	4.822	0.00182	0.000939	1.22×10^{-4}	323.651
14	13.30	0.628	0.000237	0.000122	1.59×10^{-5}	42.151
15	14.23	0.781	0.000295	0.000152	1.98×10^{-5}	52.420
16	15.16	1.557	0.000588	0.000303	3.94×10^{-5}	104.505
17	16.09	0.665	0.000251	0.00013	1.68×10^{-5}	44.635
18	17.02	0.540	0.000204	0.000105	1.37×10^{-5}	36.245

REFERENCE LIST

Allen, J.R.L. (1973), Features of cross-stratified units due to random and other changes in bed forms, *Sedimentology*, *20*(2), 189–202, doi:10.1111/j.1365-3091.1973.tb02044.x.

Allen, J.R.L. (1974), Reaction, relaxation and lag in natural sedimentary systems: general principles, examples and lessons, *Earth-Science Reviews*, *10*(4), 263-342.

Allen, J.R.L. (1982), *Sedimentary Structures: Their Character and Physical Basis*, Elsevier, New York, NY.

Bagnold, R.A. (1973), The nature of saltation and bed-load transport in water, *Proc. R. Soc. London*, *332*, 473– 504

Barekyan, A., Sh. (1962), Discharge of channel forming sediments and elements of sand waves, in S*oviet Hydrology: Selected Papers (2nd Issue)*, pp. 128-130, AGU, Washington, D.C.

Bridge, J. S. (2003), *Rivers and Floodplains: Forms, Processes, and Sedimentary Record*, Blackwell Sci., Malden, MA.

Brownlie, W. R., (1981), Prediction of flow depth and sediment discharge in open channels, *Report No. KH-R-43A*, W. M. Keck Laboratory of Hydraulics and Water Resources, California Institute of Technology, Pasadena, California, USA.

Best, J. (2005), The fluid dynamics of river dunes: A review and some future research directions, *J. Geophys. Res.*, *110*, F04S02, doi: 10.1029/2004JF000218.

Buffington, J. M. and Montgomery, D. R. (1997), A systematic analysis of eight decades of incipient motion studies, with special reference to gravel-bedded rivers, *Water Resour. Res.*, *33*, 1993-2029, doi:10.1029/96WR03190.

Church, M. (2006), Bed material transport and the morphology of alluvial river channels, *Annu. Rev. Earth Planet. Sci, 34*, 325-354, doi:10.1146/annurev. earth.33.092203.122721.

Coleman, S. E. and Melville, B. W. (1994), Bed-form development, *J. Hydr. Engng.*, *120*(4), 544-560.

Dietrich, W. E. (1982), Settling velocity of natural particles, *Water Resour. Res.*, *18*(6), 1615–1626, doi:10.1029/WR018i006p01615.

Dietrich, W. E., and J. D. Smith (1984), Bed load transport in river meander, *Water Resour. Res.*, *20*, 1355-1380, doi:10.1029/WR020i010p01355.

Gabel, S. L. (1993), Geometry and kinematics of dunes during steady and unsteady flows in the Calamus River, Nebraska, USA, *Sedimentology*, *40*, 237-269, doi:10.1111/j.1365-3091. 1993.tb01763.x.

Guy, H. P., D. B. Simons, and E. V. Richardson (1966), Summary of alluvial channel data from flume experiments, 1956-61, *U.S. Geol. Surv. Prof. Pap*. 462-I, 1-96.

Helley, E. J. and Smith, W. (1971), Development and calibration of a pressure-difference bedload sampler, *U.S. Geol. Surv. Open-File Report,* 1-18.

Hickin, E. J. (1986), Concave-bank benches in the floodplains of Muskwa and Fort Nelson Rivers, British Columbia, *The Canadian Geographer*, *30*(2), 111-122.

Horowitz, A. J., Elrick, K. A. and Smith, J. J. (2001), Annual suspended sediment and trace element fluxes in the Mississippi, Columbia, Colorado, and Rio Grande drainage basins, *Hydrol. Process., 15*, 1169–1207, doi: 10.1002/hyp.209.

Jerolmack, D. J., and D. Mohrig (2005a), A unified model for subaqueous bed form dynamics, *Water Resour. Res.*, *41*, W12421, doi:10.1029/2005WR004329.

Jerolmack, D. J., and D. Mohrig (2005b), Frozen dynamics of migrating bedforms, *Geology*, *33*, 57-61, doi:10.1130/G20987.1.

Kostaschuk, R., and Best, J., (2005), Response of sand dunes to variations in tidal flow: Fraser Estuary, Canada. *J. Geophys. Res.*, *110*, F04S04, doi:10.1029/2004JF000176.

Kostaschuk, R., and Villard, P. (1996), Flow and sediment transport over large subaqueous dunes: Fraser River, Canada, *Sedimentology*, *43*(5), 849-863, doi:10.1111/j.1365-3091.1996. tb01506.x

Leclair, S. F. (2002), Preservation of cross-strata due to the migration of subaqueous dunes: an experimental investigation, *Sedimentology*, *49*,1157-1180, doi:10.1046/j.1365-3091. 2002.00482.x.

Leopold, L. B., Wolman, M. G., and Miller, J. P. (1964), *Fluvial Processes in Geomorphology*, Dover Publications, Inc., Mineola, N.Y.

Mark, D. M, and Church, M. (1977), On the misuse of regression in earth science, *Mathematical Geology, 9*(1), 63-75.

McElroy, B. J. (2009), Expressions and Implications of Sediment Transport Variability in Sandy Rivers, Ph.D. dissertation, Dep. of Geological Sciences, Jackson School of Geosciences, University of Texas, Austin, Texas, Texas, USA.

McElroy, B., and D. Mohrig (2009), Nature of deformation of sandy bed forms, *J. Geophys. Res.*, *114*, F00A04, doi:10.1029/2008JF001220.

McLean, S. R., and J. D. Smith (1986), A model for flow over two-dimensional bed forms, *J. Hydr. Engng*., *112*, 300-317, doi:10.1061/(ASCE)0733-9429(1986)112:4(300).

McLean, S. R. (1990), The stability of ripples and dunes, *Earth-Sci. Rev.*, *29*, 131-144, doi:10.1016/0012-8252(0)90032-Q.

Mohrig, D., and J. D. Smith (1996), Predicting the migration rates of subaqueous dune, *Water Resour. Res.*, *32*(10), 3207-3217.

Nittrouer, J. A., M. A. Allison, and R. Campanella (2008), Bedform transport rates for the lowermost Mississippi River, *J. Geophys. Res.*, *113*, F03004, doi:10.1029/2007JF000795.

Raudkivi, A. J. (1967), *Loose Boundary Hydraulics*, Pergamon, Oxford.

Ritter, D. F., Kochel, R. C, and Miller, J. R. (2002), *Process Geomorphology* (*4th ed*)., McGraw-Hill Companies, New York, N.Y.

Rouse, H. (1939), Experiments on the mechanics of sediment suspension, in *Proceedings 5th International Congress on Applied Mechanics*, pp. 550-554, Cambridge, Mass.

Shields, A. (1936), *Application of the Theory of Similarity and Turbulence Research to the Bedload Movement*. Transl. QM Saleh. Mitt. Preuss. Vers. Wasserbau Schiffbau, 26th, Berlin.

Shugar, D. H., Kostaschuk, R., Best, J. L., Lane, S. N., Parsons, D. R., Orfeo, O., and Hardy, R.J. (2010). On the relationship between flow and suspended sediment transport over the crest of a sand dune, Río Paraná, Argentina, *Sedimentology*, *57*, 252-272, doi: 10.1111/j.1365-3091.2009.01110.x.

Simons, D. B. and E. V. Richardson (1966), Resistance to flow in alluvial channels. *U.S. Geol. Surv. Prof. Pap.*, 422-J, 1-61.

Simons, D. B., E. V. Richardson, and W. L. Haushild, (1963), Some effects of fine sediment on flow phenomena, *U.S. Geol. Surv. Prof. Pap.*, 1489-G, 1-47.

Simons, D. B., E. V. Richardson, and C. F. Nordin Jr. (1965), Bedload equation for ripples and dunes, *U.S. Geol. Surv. Prof. Pap.*, 462-H, 1-9.

Smith, L. D. (1970), Stability of a sand bed subjected to a shear flow of low Froude number, *J. Geophys. Res.*, *75*, 5928-5940, doi:10.1029/JC075i030p05928.

Southard, J. B., and Boguchwal, L. A. (1990), Bed configurations in steady unidirectional flows. Part 2. Synthesis of flume data. *J. Sed. Pet.*, *60*, 658-679.

Stein, R. A. (1965), Laboratory studies of total load and apparent bed load, *J. Geophys. Res.*, *70*(8), 1831-1842, doi:10.1029/JZ070i008p01831.

Ten Brinke, W. B. M., A. W. E. Wilbers, , and C. Wesseling (1999), Dune growth, decay and migration rates during a large-magnitude flood at a sand and mixed-gravel bed in the Dutch Rhine river system, In *Fluvial Sedimentology VI*, edited by N. D. Smith and J. Rogers, *Spec*. *Publ*. *Int*. *Assoc*. *Sedimentol*., *28*, , 15-32, Blackwell Sci., Malden, MA.

Van den Berg, J. H. (1987), Bedform migration and bed-load transport in some rivers and tidal environments, *Sedimentology*, 34, 681-698, doi:10.1111/j.1365-3091.1987.tb00794.x.

Van Rijn, L. C. (1984), Sediment transport, part III: Bed forms and alluvial roughness, *J. Hydraul. Eng.*, *110*, 1733–1754.

Van Rijn, L. C. (1993), *Principle of Fluid Flow and Surface Waves in Rivers, Estuaries, Seas, and Ocean*, Aqua, Amsterdam, The Netherlands.

Venditti, J. G. (2007), Turbulent flow and drag over fixed two- and three-dimensional dunes, *J. Geophys. Res*, *112*, F04008, doi:10.1029/2006JF000605.

Venditti, J.G. (in press), Bedforms in sand-bedded rivers, in *Treatise on Geomorphology*, edited by J. Shroder, Jr., and E. Wohl, Academic Press, San Diego, Calif.

Venditti, J.G., Church, M. and Bennett, S.J. (2005a), On the transition between 2D and 3D dunes, *Sedimentology*, *52*, 1343–1359, doi:10.1111/j.1365-3091.2005.00748.x.

Venditti, J. G., M. Church, and S. J. Bennett (2005b), Morphodynamics of small-scale superimposed sand waves over migrating dune bed forms, *Water Resour. Res.*, *41*, W10423, doi:10.1029/2004WR003461.

Villard, P. V. and Church, M. A. (2003), Dunes and associated sand transport in a tidally influenced sand-bed channel: Fraser River, British Columbia, *Canadian Journal of Earth Sciences*, *40*, 115-130, doi:10.1139/e02-102.

Wan, Z. (1982), Bed material movement in hyperconcentrated flow, *Ser. Pap.* 31, Inst. of Hydrodyn. and Hydraul. Eng., Tech. Univ. of Den., Lyngby, Denmark.

Wan, Z., and Z. Wang (1994), *Hyperconcentrated Flow*, A. A. Balkema, Rotterdam, The Netherlands.

Wilcock, P. R. and Crowe, J. C. (2003), Surface-based transport model for mixed-size sediment, *J. of Hydr. Engng.*, *129*(2), 120-128, doi:10.1061/(ASCE)0733-9429(2003)129:2 (120).

Williams, G. P. (1967), Flume experiments on the transport of a coarse sand, *U.S. Geol. Surv. Prof. Pap*., 562-B, 1-31.

Williams, G. P. (1970), Flume width and water depth effects in sediment-transport experiments, *U.S. Geol. Surv. Prof. Pap*., 562-H, 1-37.

Yalin, M. S. (1972), *Mechanics of Sediment Transport*, Pergamon Press, Oxford.

Yalin, M. S., and Karahan, E. (1979a), Steepness of sedimentary dunes, *J. Hydr. Div., 105*(4), 381-392.

Yalin, M. S., and Karahan, E. (1979b), Inception of sediment transport, *J. Hydr. Div., 105*(11), 1433-1443.

Znamenskaya, H. S. (1962), Calculation of dimensions and speed of shifting channel formations, in *Soviet Hydrology: Selected Papers (2nd Issue)*, pp. 111-116, AGU, Washington, D.C.